From Living Fossils to Adaptive Radiations:
Examining Phenotypic Evolution in Lobe-Finned Fishes

by

Rafael A. Rivero Vega

A dissertation submitted in partial fulfillment
of the requirements for the degree of
Doctor of Philosophy
(Earth and Environmental Sciences)
in the University of Michigan
2024

Doctoral Committee:

Professor Matt Friedman, Chair
Professor Jeffrey Wilson Mantilla
Associate Professor Selena Smith
Professor Stephen A. Smith

Rafael A. Rivero Vega

rarivero@umich.edu

ORCID iD: 0000-0001-5937-6377

Dedication

This dissertation is dedicated with all the love in the world to those who have provided it to me over my life: my mom, my dad, and my brother.

Acknowledgements

The work in this dissertation was funded in part by the Earth and Environmental Sciences Scott Turner Student Research Grant Award and by the Rackham Graduate School. All research herein was performed in collaboration with my advisor Matt Friedman. Helpful comments on varying versions of the manuscripts were provided by Hadeel H. Saad, James V. Andrews, Rodrigo T. Figueroa, Sanaa El-Sayed, Lindsey DeHaan, and Jacob S. Berv (aka The Friedman Lab, minus one Alessio Capobianco who has moved on to bigger and better things). Additionally, the research in chapter 2 was a collaboration with Jacob S. Berv and John T. Clarke; the research in chapter 3 was a collaboration with Edward (Ted) B. Daeschler, Neil H. Shubin, and undergraduate research assistant Emma Archer; and the research in chapter 4 was a collaboration with Hadeel H. Saad, James V. Andrews, Rodrigo T. Figueroa, Xindong Cui, Min Zhu, Alice M. Clement, and undergraduate research assistants Janel Lapalm and Matthew Palumbo. I am indebted to those that provided additional datasets, troubleshooting assistance, back and forths on the minutia of scientific figuring in exchange for granola bars, and comprehensive answers to uninformed emails: Adam Rountrey, Carol Abraczinskas, Roger Close, Julien Clavel, Graeme T. Lloyd. Chapters 2 and 3 would not exist without the worldwide network of museums and collaborators that either graciously opened their doors to me or were able facilitate the acquisition of their digitized specimens. A special thanks goes out to my committee members—Jeffrey A. Wilson Mantilla, Selena Smith, Stephen A. Smith—for the

active discussions they had with me both individually and during our committee meetings over my time in Michigan.

I'm also grateful for the innumerable UMMP, EES, and EEB faculty, lecturers, staff, and grad students that have made my time here amazing. Literally too many to count, but I know from so much personal experience that they will, whether loudly or quietly, support me through thick and thin. Within that bubble are the two cohorts that welcomed me as I slinked in mid-school year, the BSB office gang (which will always have meme-mas), and the aforementioned Friedman Lab. I won't name the latter crew again or else risk sounding like I'm picking favorites, but I've cherished every moment I've spent with you all even though this statement will never leave the confines of this dissertation. Much like with the people from this university, I have a number of other 'corillos' scattered around the world, and they have been and will continue to be my greatest cheerleaders. I can't thank them enough, but I also won't name them individually as that would make this section unreasonably long. However, I *am* excited to finally have the free time to see them again after this is all done! This dissertation is, of course, dedicated to my family, who have supported me ever since the admittedly rushed decision I made to become a scientist the moment I grabbed a lizard as a three-year-old. Their never-ending love and support are what has kept me and my curiosity alive—literally and figuratively, respectively. Last but certainly not least, I cannot fully express how grateful I am that Matt was as patient as he was with me during these years as well as his incessant nudging in the right direction academically. I was told that when I interviewed, he was giddy with excitement over me to joining the lab (shh don't tell him that someone snitched) and I don't think I could ever live up to that expectation! I just hope that I only slightly disappointed him with my shenanigans.

Table of Contents

List of Tables

List of Figures

List of Appendices

Abstract

Vertebrates have experienced diverse eras that shaped their evolutionary trajectory, from the development of jaws to the transition from water to land. However, the patterns of morphological evolution in deep time that underlie macroevolutionary changes such as these remain not well understood. In this dissertation, I investigate the early success and subsequent decline of lobe-finned fishes, a now mostly extinct assemblage of bony fishes at the base of the vertebrate tree of life, by considering vignettes at varying time scales to assess the tempo of their evolutionary history. First, I use two independent types of trait data to assess if, across a span of hundreds of millions of years of evolution, three fish lineages identified as iconic "living fossils" share common patterns as implied by this title. I find that there are marked differences in patterns recovered among and within groups and traits, implying a variety of unique evolutionary trajectories at the largest timescales and urging the reassessment of the use of qualitative descriptors like "living fossils" without forming the proper quantitative foundation. Then, I adjust to a smaller scale by describing a 'phaneropleurid' lungfish from Late Devonian fluvial deposits in the Canadian Arctic. The articulated fossil represents a new species that possesses characters that intimate a transitional nature, such as skeletal adaptations for buccal pumping as well as the elongation of the base of the second dorsal fin. I show how this structurally intermediate lungfish can elucidate the conditions punctuating the lungfish transition from Devonian, generalized lobe-finned anatomy, to a more modern, post-Devonian one. Finally, I step back to examine the Devonian as a period of changing macroevolutionary patterns in lobe-finned fishes using their jaws as a robust, ecologically informative system to interrogate whether this early diversification bears the hallmarks of an adaptive radiation. I detect patterns fitting the hypothesized expectations of high initial evolutionary rates followed by a deceleration, with clades within the group showing more diffusive patterns and more extensive or restricted exploration of shape space early in their evolutionary history. This dissertation offers new perspectives on hundreds of millions of years of evolution in sarcopterygian and "living fossil" lineages, and further underscores how paleontological data can provide insights into the

intricacies of macroevolutionary patterns at varying scales, including during periods of accelerating or decelerating phenotypic change.

Chapter 1 – Introduction

1.1 Sarcopterygians as a System for Exploring the Tempo and Mode of Evolution

The early evolution of jawed vertebrates reflects multiple episodes of diversification and extinction, with many once prominent lineages going extinct entirely while a few survivors diversified into the modern day (Romer 1966; Hecht et al. 1977; Jarvik 1980; Friedman and Sallan 2012; Donoghue and Keating 2014). Originating in the late Silurian (ca. 420 Ma), the lobe-finned fishes (Sarcopterygii) represent one of the most prominent examples of the shifting fortunes of certain groups during this interval (Zhu et al. 2009; Friedman and Sallan 2012). Named due to their distinctive fleshy fins attached by one bone directly to a supporting girdle (setting them apart from other fishes), they inhabited a range of environmental settings—from coral reefs to lakes to newly emergent fluvial ecosystems (Forster-Cooper 1937; Trewin 1986; Cressler et al. 2010; Long and Trinajstic 2010; Daeschler and Cressler 2011)—and occupy a central place in vertebrate evolution as the group that would eventually dominate the land (Cloutier and Ahlberg 1996; Clack 2012; Friedman and Sallan 2012; Clement 2019).

More sarcopterygians are known from the Devonian (419.2–358.9 Ma) than any subsequent interval of their history (Klug et al. 2010; Blieck 2011; Friedman and Sallan 2012; Clement 2019), a time which is marked by the emergence of several major groups, including lungfishes and their closest relatives (Dipnomorpha), coelacanths (Actinistia), and early representatives of the tetrapods (Tetrapodomorpha) (**Figure 1.1**). These are joined by less well-understood groups, including latest Silurian and earliest Devonian species that are likely early-diverging extinct members of the sarcopterygian total group (stem Sarcopterygii) and enigmatic

lineages like the tooth-whorled onychodonts (Onychodontida) (Cloutier and Ahlberg 1995; Zhu et al. 1999, 2001, 2009; Mondéjar-Fernández 2020; Ciudad Real et al. 2022). Remarkably, many of these lineages appear within a short interval (~30 myr) between the last few million years of the Silurian and the end of the Early Devonian. Despite this early explosion of diversity, only the tetrapods, emerging after the initial burst, gave rise to tens of thousands of surviving lineages (Ruta et al. 2006; Alfaro et al. 2009; Sahney et al. 2010; Clack 2012). For all of their early success, living coelacanths and lungfishes have narrow environmental distributions and collectively number four genera (<10 species) (Forey 1998; Jørgensen and Joss 2011; Clack 2012)—an order of magnitude fewer genera compared to their extinct Devonian ancestors (Cloutier and Ahlberg 1996; Sallan and Coates 2010; Clack et al. 2011). These patterns in ancient and modern evolutionary history have led to the designation of today's surviving lobe-finned fishes as "living fossil" (Eldredge and Stanley 1984; Forey 1984; Lloyd et al. 2011).

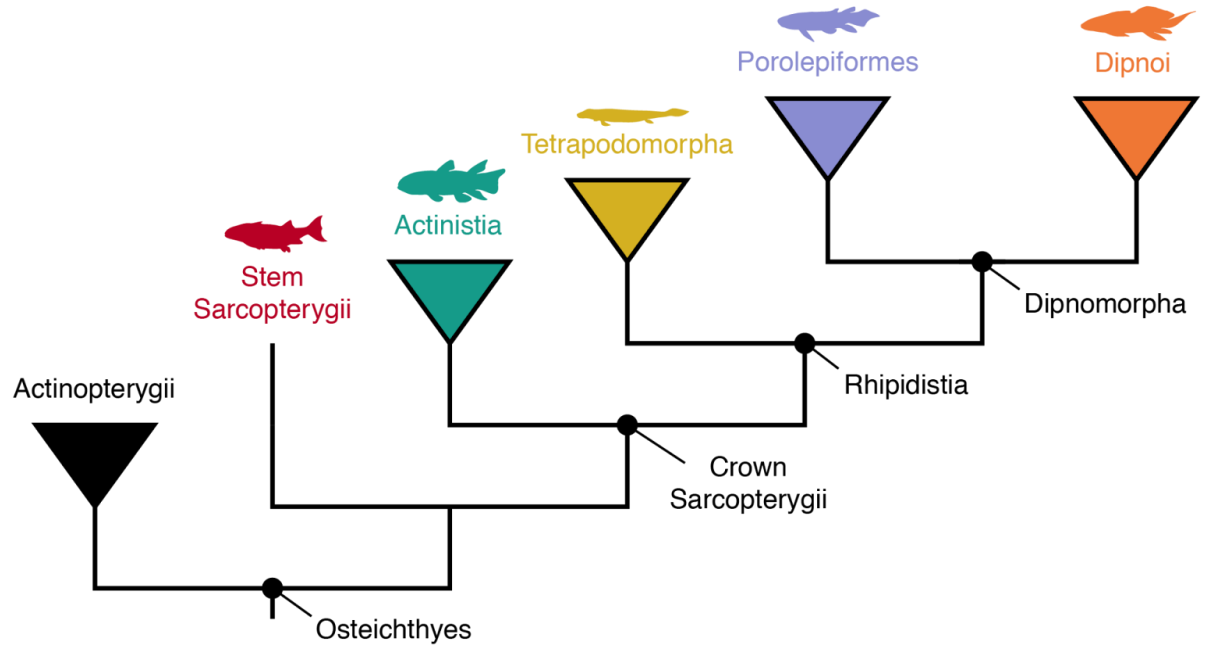

Figure 1.1. Cladogram of Osteichthyes (bony fishes) showing the five principal assemblages of sarcopterygians (lobe-finned fishes, labeled with different colors) referenced throughout this dissertation. Nodes denote clades (labeled in black), which are

groups that include a common ancestor and all of its descendants (also known as a monophyletic group). Actinopterygii (ray-finned fishes) make up the overwhelming diversity of fishes in the modern day and are sister to all sarcopterygians. Stem Sarcopterygii (red) are a paraphyletic grade of early-diverging sarcopterygians, meaning all lineages within the group share a common ancestor, but no lineages further up the tree are included (e.g., Actinistia). An exemplar from this grade is one of the oldest osteichthyans, *Guiyu*. Actinistia (blue) is the coelacanth total group, including the only extant genus, *Latimeria*. Tetrapodomorpha (yellow) is the tetrapod total group, containing water-to-land transitional forms like *Tiktaalik* as well as all four-legged animals that exist today, including humans. Porolepiformes (purple) are an extinct group of bony fishes that includes the eponymous *Porolepis*. Similar to Stem Sarcopterygii, they are likely paraphyletic; however, for the purposes of this dissertation, they will be defined as monophyletic. This arrangement makes Porolepiformes the sister group to Dipnoi (orange), the lungfishes, a group with three extant genera. For the purposes of this dissertation, Dipnoi will be defined as all lungfishes beginning with *Youngolepis* and including all crownward lineages. Together, Actinopterygii and all Sarcopterygii make up Osteichthyes; Actinistia, Tetrapodomorpha, Poroloepiformes, and Dipnoi form Crown Sarcopterygii (a monophyletic group encompassing the common ancestor of the extant representatives in the group and its descendants); Tetrapodomorpha, Poroloepiformes, and Dipnoi are called Rhipidistia; and Porolepiformes and Dipnoi are all Dipnomorpha. Silhouettes from PhyloPic, *Tiktaalik* silhouette by *Nobu Tamura* (CC BY-SA 3.0).

One sarcopterygian clade, the lungfishes, represents a central example of a "living fossil." This began when Darwin (1859) defined the "living fossil" concept and cited lungfishes as an example, only to later be amplified by other 19th century researchers who noted the distinctive boom and bust evolutionary trajectory of the group (Woodward 1891; Dollo 1895). Subsequent work also showed lungfish once occupied both marine and continental habitats (Campbell and Barwick 1986; Cloutier and Ahlberg 1996; Clement and Long 2010), with many specializations that would come to define the group—such as tooth plates (Cui et al. 2022), cranial ribs and other adaptations for air gulping (Long 1993; Clement and Long 2010; Clement et al. 2016), and a long-based dorsal fin (**Figure 1.2**) (Dollo 1895; Friedman 2010)—evolving rapidly in the Devonian. They were also among the earliest jawed vertebrates to specialize on hard prey, with major changes to their skulls and teeth arising in the earliest Devonian (Cui et al. 2022). However, after this period, they experienced a decline in diversity as they became more closely associated with freshwater systems (Günther 1871; Daeschler et al. 2006; Friedman and Daeschler 2006; Downs et al. 2011, 2019). It is at this same time that lungfishes appear to show substantial declines in rates of morphological evolution (Westoll 1949; Lloyd et al. 2011). This history reinforces the Devonian as a key moment for the transition of lungfishes from an

apparent Devonian heyday to their less diverse, and environmentally more restricted, post-Devonian history (Dollo 1895; Cloutier and Ahlberg 1996; Friedman 2010; Jørgensen and Joss 2011; Lloyd et al. 2011; Smithson et al. 2016).

1.2 "Living Fossils" as a Gateway to Understanding Shared Evolutionary Patterns

"*. . . Lepidosiren, which, like fossils, connect to a certain extent orders now widely separated in the natural scale. These anomalous forms may almost be called living fossils . . .*"

Darwin (1859: p. 107)

Conspicuous contrasts in apparent rates of phenotypic evolution among different branches of the Tree of Life have been the subject of investigation from the early days of evolutionary biology (Simpson 1944, 1953; Westoll 1949; Stanley 1985; Hunt and Rabosky 2014). Such stark differences in rates of change are claimed to separate so-called "living fossil" lineages from others showing more accelerated diversification (Fisher 1990; Musick and Thomson 1993; Lee et al. 2006; Bennett et al. 2018). This concept has a long history dating back to when Darwin first coined the term (Darwin 1859) and extending to the present. In the modern literature, most assert that extant lobe-finned fishes are "living fossil" while others argue vehemently against that designation, or against the living fossil concept more generally (Casane and Laurenti 2013; Cavin and Guinot 2014; Lidgard and Love 2018).

Although recent work goes so far as to propose genetic mechanisms for low rates of change in some groups (Brownstein et al. 2024), an outstanding problem remains: identification and characterization of patterns of anatomical change within putative living fossil lineages

remains idiosyncratic. Markedly, researchers often utilize disparate measures of phenotype and assess rates of evolution in key "living fossil" groups in ways that preclude comparisons across datasets (Westoll 1949; Schaeffer 1952; Forey 1988, 1998; Cloutier 1991; Lloyd et al. 2011; Clarke and Friedman 2018). This inconsistency has resulted in a weak foundation upon which to build the frameworks required to interrogate shared evolutionary patterns (see discussion in Harmon et al. 2010).

To address this problem, the second chapter will take a comparative approach using Darwin's initial conception of "living fossil." I will use both discrete morphological and continuous shape data from extant and extinct members of three iconic "living fossil" lineages—the lobe-finned coelacanths and lungfishes, plus the ray-finned holosteans—to probe for similarities in their patterns of phenotypic change through time. In doing so, I aim to determine what, if any, aspects of evolutionary change over long timescales are shared in common by these three key groups of "living fossil."

1.3 A New 'Phaneropleurid' Lungfish as a Link Between Two Eras of Lungfish Evolution

"*So long ago as the Devonian period, there were members of the subclass agreeing precisely with the existing* Ceratodus *[Australian lungfish] in the development of the fins and the axial skeleton of the trunk. . . . The typical Dipnoi of the Devonian period had, indeed, already become more specialized than any known in later times . . .*"

Woodward (1891: p. xx)

The latter half of the Devonian has been identified as a critical evolutionary stage due to anatomical changes occurring in vertebrates concurrently with the proliferation of new continental aquatic environments (Daeschler and Cressler 2011). Fossil deposits from this period reflect the expansion of terrestrial flora and the consequent alterations of their ecological settings (Algeo et al. 2001; Davies and Gibling 2010; Morris et al. 2018). Notably, the Upper Devonian Fram Formation in Canada's Ellesmere Island records one such early fluvial ecosystem that emerged during this time (Daeschler et al. 2006; Downs et al. 2011, 2019).

Among the diverse array of vertebrates from the Late Devonian, 'phaneropleurid' lungfishes represent a distinctive group with unique anatomical developments (Cloutier and Ahlberg 1996; Challands and den Blaauwen 2017). Characterized primarily by the elongation of the base of the second dorsal fin, 'phaneropleurids' present an intriguing evolutionary step and members of this grade provide crucial clues about the transitions in lungfish evolution during this epoch (**Figure 1.2**) (Cloutier and Ahlberg 1996; Friedman 2010; Challands and den Blaauwen 2017). Indeed, these morphological characteristics foreshadow traits retained and lost in post-Devonian lungfishes, linking derived characters such as a continuous median fin fringe to adaptations that arose in the Devonian (Cloutier and Ahlberg 1996; Friedman 2010; Pardo et al. 2014). It is also because of traits such as reduction in ossification and taphonomy (e.g., flattened specimens) limiting available character data that the phylogenetic relationships within 'phaneropleurids' remain unstable (Cloutier and Ahlberg 1995; Lloyd et al. 2011; Luo et al. 2021).

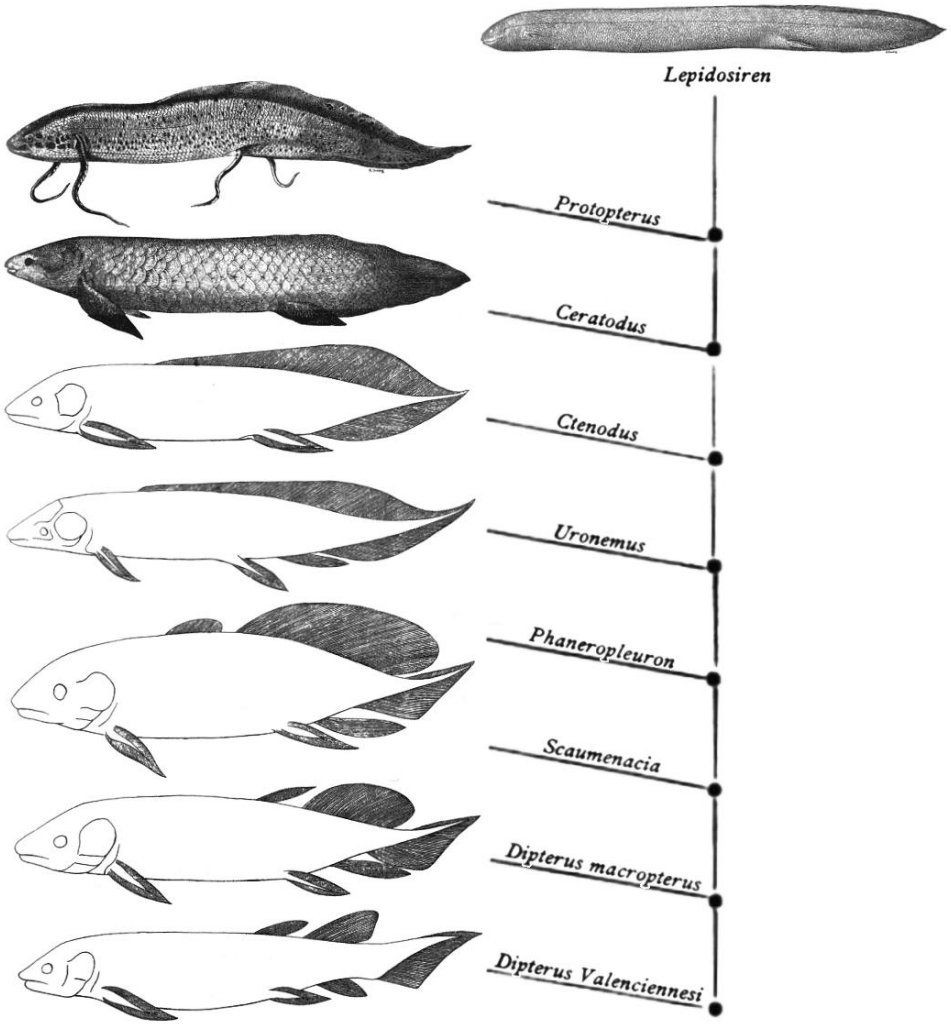

Figure 1.2. Lungfish cladogram showing the stepwise evolution of the median fins in lungfishes from the Devonian to the recent. The lower three images depict taxa restricted to the last ~30 million years of the Devonian. This represents less than 10% of the entire chronological range illustrated by the diagram, emphasizing the relatively rapid change in lungfish body form early in the group's history. Adapted version of two figures from Dollo (1895: p. 89 and Pl. V.).

Although lungfishes are abundant in many other ecologically and contemporaneous fossil localities (Sallan and Coates 2010; Schultze 2010; Cloutier et al. 2011), to date, they have not been formally described from the Late Devonian Fram Formation. The third chapter will focus on the three-dimensionally preserved cranial and post-cranial remains of a 'phaneropleurid'-grade lungfish found at this locality. I will describe the new species with a focus on anatomy

typically observed in transitional lungfishes, such as the skull and median fins, and use this exceptionally rare, articulated fossil to provide insights into the evolutionary changes taking place at the end of this period.

1.4 Sarcopterygian Jaws as Indicators of Morphological Innovation and Adaptive Radiation

> "*. . . dipnoans in the structure of the lower jaw differ fundamentally from the rhipidistids [porolepiforms and osteolepiforms] and other crossopterygians [sarcopterygians] . . .*"
>
> Jarvik (1967: p. 179)

The Devonian—colloquially referred to as the "Age of Fishes"—was a period of major change in vertebrate diversity as jawed fishes such as lobe-fins and placoderms radiated ecologically, taxonomically, and morphologically, while jawless fishes entered a long period of decline (Klug et al. 2010; Anderson et al. 2011; Friedman and Sallan 2012). Not only did sarcopterygians exhibit substantial taxonomic diversity (over 200 species), but in just the span from the latest Silurian and Early Devonian, they had already split into the principal groups shown in Fig. 1 (Cloutier and Ahlberg 1996; Anderson et al. 2011; Friedman and Sallan 2012; Clement 2019). This divergence happened so rapidly that it presented early difficulties in resolving the relationships among the three living sarcopterygian lineages (coelacanths, lungfishes, and tetrapods) using molecular datasets (Brinkmann et al. 2004; Rokas and Carroll 2006). However, the predominance of sarcopterygians would not last, as it transitioned to a decline characterized by reduced morphological disparity and taxonomic diversity, perhaps

modulated by the end-Devonian extinction (Forey 1998; Sallan and Coates 2010; Clack et al. 2011; Friedman and Sallan 2012). Today, the only survivors are six lungfish and two coelacanth species, occupying niches in slow moving freshwater and deep-sea marine ecosystems, respectively (Forey 1998; Jørgensen and Joss 2011). This low ecological diversity in modern species, coupled with rapid early divergence followed by limited anatomical change over hundreds of millions of years, represents a pattern that has been hotly debated in the adaptive radiation and "living fossil" literature (Alfaro et al. 2009; Lloyd et al. 2011; Casane and Laurenti 2013; Bennett et al. 2018).

Although well-preserved body fossils provide a wealth of data for comparative analyses, previous macroevolutionary studies on this group have relied on qualitative descriptions or taxonomic counts of highly incomplete fossils, including ones known only from fragments (Westoll 1949; Cloutier 1991; Forey 1998; Blieck 2011; Lloyd et al. 2011; Friedman and Sallan 2012). To mitigate these issues, some researchers have turned to lower jaws, as they are more commonly found than complete body fossils, can be identified at the generic or species level, and exhibit classic adaptations related to their ecological niches (e.g., dental plates, size and shape variations, and specialized features like fangs) (Ahlberg and Clack 1998; Brazeau and Friedman 2014; Hill et al. 2018). Over time, jaws have become a model system for examining feeding and ecology across disparate groups (Ahlberg and Clack 1998, 1998; Wainwright et al. 2000; Westneat 2003, 2004; Botella et al. 2007; Anderson et al. 2011; Brazeau and Friedman 2014; Klug et al. 2017; Hill et al. 2018; Deakin et al. 2022), since they not only preserve dental information but also fossa in the mandibles crucial for understanding biomechanics and function (Westneat 2004; Hill et al. 2018).

To quantitatively analyze the diversification of lobe-finned fishes, the fourth chapter aims to explore whether sarcopterygians underwent an evolutionary radiation early in their history. I will test the hypothesis that observed evolution in mandible morphology from the late Silurian to the end of the Devonian period most closely aligns with models of evolutionary change traditionally associated with putative adaptive radiations (Todd Streelman and Danley 2003; Gavrilets and Losos 2009; Anderson et al. 2011, 2013; Simões et al. 2016; Stroud and Losos 2016; Deakin et al. 2022).

1.5 Future Directions

Due to their status as structural intermediates and their intriguing evolutionary patterns, the study of sarcopterygians provides valuable insights into the history of early changes in vertebrate lineages. In light of this, I will review the key takeaways from the previous chapters in the conclusion, focusing on the implications for understanding patterns of vertebrate evolution. I will also highlight potential future avenues of research using comparative approaches, as well as the revising and coalescing of independent discrete morphological data into more robust, cross-clade datasets.

1.6 References

Ahlberg, P.E., Clack, J.A., 1998. Lower jaws, lower tetrapods–a review based on the Devonian genus Acanthostega. Trans. R. Soc. Edinb. Earth Sci. 89, 11–46. https://doi.org/10.1017/S0263593300002340

Alfaro, M.E., Santini, F., Brock, C., Alamillo, H., Dornburg, A., Rabosky, D.L., Carnevale, G., Harmon, L.J., 2009. Nine exceptional radiations plus high turnover explain species diversity in jawed vertebrates. Proc. Natl. Acad. Sci. 106, 13410–13414. https://doi.org/10.1073/pnas.0811087106

Algeo, T.J., Scheckler, S.E., Maynard, J.B., 2001. 12. Effects of the Middle to Late Devonian Spread of Vascular Land Plants on Weathering Regimes, Marine Biotas, and Global Climate, in: Gensel, P.G., Edwards, D. (Eds.), Plants Invade the Land. Columbia University Press, pp. 213–236. https://doi.org/10.7312/gens11160-013

Anderson, P.S.L., Friedman, M., Brazeau, M.D., Rayfield, E.J., 2011. Initial radiation of jaws demonstrated stability despite faunal and environmental change. Nature 476, 206–209. https://doi.org/10.1038/nature10207

Anderson, P.S.L., Friedman, M., Ruta, M., 2013. Late to the Table: Diversification of Tetrapod Mandibular Biomechanics Lagged Behind the Evolution of Terrestriality. Integr. Comp. Biol. 53, 197–208. https://doi.org/10.1093/icb/ict006

Bennett, D.J., Sutton, M.D., Turvey, S.T., 2018. Quantifying the living fossil concept. Palaeontol. Electron. 21. https://doi.org/10.26879/750

Blieck, A., 2011. The André Dumont medallist lecture: From adaptive radiations to biotic crises in Palaeozoic vertebrates: a geobiological approach. Geol. Belg. 14, 203–2027.

Botella, H., Blom, H., Dorka, M., Ahlberg, P.E., Janvier, P., 2007. Jaws and teeth of the earliest bony fishes. Nature 448, 583–586. https://doi.org/10.1038/nature05989

Brazeau, M.D., Friedman, M., 2014. The characters of Palaeozoic jawed vertebrates. Zool. J. Linn. Soc. 170, 779–821. https://doi.org/10.1111/zoj.12111

Brinkmann, H., Venkatesh, B., Brenner, S., Meyer, A., 2004. Nuclear protein-coding genes support lungfish and not the coelacanth as the closest living relatives of land vertebrates. Proc. Natl. Acad. Sci. 101, 4900–4905. https://doi.org/10.1073/pnas.0400609101

Brownstein, C.D., MacGuigan, D.J., Kim, D., Orr, O., Yang, L., David, S.R., Kreiser, B., Near, T.J., 2024. The genomic signatures of evolutionary stasis. Evolution 78, 821–834. https://doi.org/10.1093/evolut/qpae028

Campbell, K.S.W., Barwick, R.E., 1986. Paleozoic lungfishes—a review. J. Morphol. 190, 93–131. https://doi.org/10.1002/jmor.1051900409

Casane, D., Laurenti, P., 2013. Why coelacanths are not 'living fossils.' BioEssays 35, 332–338. https://doi.org/10.1002/bies.201200145

Cavin, L., Guinot, G., 2014. Coelacanths as "almost living fossils." Front. Ecol. Evol. 2, 1–5. https://doi.org/10.3389/fevo.2014.00049

Challands, T., den Blaauwen, J., 2017. A redescription of the Middle Devonian dipnoan *Pentlandia macroptera* Traquair, 1889, and an assessment of the Phaneropleuridae. Zool. J. Linn. Soc. 180, 414–460. https://doi.org/10.1111/zoj.12491

Ciudad Real, M., Mondéjar-Fernández, J., Vidal, D., Botella, H., 2022. Is Onychodontida (Osteichthyes, Sarcopterygii) monophyletic? Assessing discordant phylogenies with quantitative comparative cladistics. Span. J. Palaeontol. https://doi.org/10.7203/sjp.24256

Clack, J.A., 2012. Gaining Ground: The Origin and Evolution of Tetrapods. Indiana University Press, Bloomington & Indianapolis.

Clack, J.A., Sharp, E.L., Long, J.A., 2011. The Fossil Record of Lungfishes, in: Jørgensen, J.M., Joss, J. (Eds.), The Biology of Lungfishes. CRC Press, Enfield, N.H., pp. 1–42.

Clarke, J.T., Friedman, M., 2018. Body-shape diversity in Triassic–Early Cretaceous neopterygian fishes: sustained holostean disparity and predominantly gradual increases in teleost phenotypic variety. Paleobiology 44, 402–433. https://doi.org/10.1017/pab.2018.8

Clement, A.M., 2019. Sarcopterygian Fishes, the "Lobe-Fins," in: Ziermann, J.M., Diaz Jr, R.E., Diogo, R. (Eds.), Heads, Jaws, and Muscles, Fascinating Life Sciences. Springer International Publishing, Cham, pp. 119–142. https://doi.org/10.1007/978-3-319-93560-7_6

Clement, A.M., Long, J.A., 2010. Air-breathing adaptation in a marine Devonian lungfish. Biol. Lett. 6, 509–512. https://doi.org/10.1098/rsbl.2009.1033

Clement, A.M., Long, J.A., Tafforeau, P., Ahlberg, P.E., 2016. The dipnoan buccal pump reconstructed in 3D and implications for air breathing in Devonian lungfishes. Paleobiology 42, 289–304. https://doi.org/10.1017/pab.2015.41

Cloutier, R., 1991. Patterns, trends, and rates of evolution within the Actinistia. Environ. Biol. Fishes 32, 23–58. https://doi.org/10.1007/BF00007444

Cloutier, R., Ahlberg, P.E., 1996. Morphology, characters, and the interrelationships of basal sarcopterygians, in: Stiassny, M.L.J., Parenti, L.R., Johnson, G.D. (Eds.), Interrelationships of Fishes. Academic Press, Inc., New York, pp. 445–479. https://doi.org/10.1016/B978-012670950-6/50018-7

Cloutier, R., Ahlberg, P.E., 1995. Sarcopterygian interrelationships: How far are we from a phylogenetic consensus? Geobios 28, 241–248. https://doi.org/10.1016/S0016-6995(95)80121-9

Cloutier, R., Proust, J.-N., Tessier, B., 2011. The Miguasha Fossil-Fish-Lagerstätte: a consequence of the Devonian land–sea interactions. Palaeobiodiversity Palaeoenvironments 91, 293–323. https://doi.org/10.1007/s12549-011-0058-0

Cressler, W.L., Daeschler, E.B., Slingerland, R., Peterson, D.A., 2010. Terrestrialization in the Late Devonian: a palaeoecological overview of the Red Hill site, Pennsylvania, USA. Geol. Soc. Lond. Spec. Publ. 339, 111–128. https://doi.org/10.1144/SP339.10

Cui, X., Friedman, M., Qiao, T., Yu, Y., Zhu, M., 2022. The rapid evolution of lungfish durophagy. Nat. Commun. 13, 2390. https://doi.org/10.1038/s41467-022-30091-3

Daeschler, E.B., Cressler, W.L., 2011. Late Devonian paleontology and paleoenvironments at Red Hill and other fossil sites in the Catskill Formation of north-central Pennsylvania, in: From the Shield to the Sea: Geological Field Trips from the 2011 Joint Meeting of the GSA Northeastern and North-Central Sections. Geological Society of America, pp. 1–16. https://doi.org/10.1130/2011.0020(01)

Daeschler, E.B., Shubin, N.H., Jenkins Jr, F.A., 2006. A Devonian tetrapod-like fish and the evolution of the tetrapod body plan. Nature 440, 757–763. https://doi.org/10.1038/nature04639

Darwin, C.R., 1859. On the Origin of Species by Means of Natural Selection, or the Preservation of Favoured Races in the Struggle for Life. John Murray, London.

Davies, N.S., Gibling, M.R., 2010. Paleozoic vegetation and the Siluro-Devonian rise of fluvial lateral accretion sets. Geology 38, 51–54. https://doi.org/10.1130/G30443.1

Deakin, W.J., Anderson, P.S.L., Den Boer, W., Smith, T.J., Hill, J.J., Rücklin, M., Donoghue, P.C.J., Rayfield, E.J., 2022. Increasing morphological disparity and decreasing optimality for jaw speed and strength during the radiation of jawed vertebrates. Sci. Adv. 8, eabl3644. https://doi.org/10.1126/sciadv.abl3644

Dollo, L., 1895. Sur la phylogénie des Dipneustes. Bull. Société Belge Géologie Paléontol. Hydrol. 9, 79–128.

Donoghue, P.C.J., Keating, J.N., 2014. Early vertebrate evolution. Palaeontology 57, 879–893. https://doi.org/10.1111/pala.12125

Downs, J.P., Daeschler, E.B., Jenkins, F.A., Shubin, N.H., 2011. A new species of *Laccognathus* (Sarcopterygii, Porolepiformes) from the Late Devonian of Ellesmere Island, Nunavut, Canada. J. Vertebr. Paleontol. 31, 981–996. https://doi.org/10.1080/02724634.2011.599462

Downs, J.P., Daeschler, E.B., Lo, N., Carey, E.N., Shubin, N.H., 2019. *Asterolepis alticristata* n. sp. (Antiarchi) from the Upper Devonian (Frasnian) of Nunavut, Canada, and a report on the antiarch diversity of the Fram Formation. Geodiversitas 41, 679. https://doi.org/10.5252/geodiversitas2019v41a19

Eldredge, N., Stanley, S.M., 1984. Living Fossils. Springer Verlag, New York.

Fisher, D.C., 1990. Rates of Evolution – Living Fossils, in: Briggs, D.E.G., Crowther, P.R. (Eds.), Paleobiology: A Synthesis. Blackwell Scientific, London, UK, pp. 152–159.

Forey, P., 1984. The Coelacanth as a Living Fossil, in: Living Fossils. Springer Verlag, pp. 166–169. https://doi.org/10.1007/978-1-4613-8271-3_18

Forey, P.L., 1998. History of the Coelacanth Fishes. Chapman & Hall.

Forey, P.L., 1988. Golden jubilee for the coelacanth *Latimeria chalumnae*. Nat. Rev. 336, 727–732.

Forster-Cooper, C., 1937. The Middle Devonian fish fauna of Achanarras. Trans. R. Soc. Edinb. 59, 223–239.

Friedman, M., 2010. Postcranial evolution in early lungfishes (Dipnoi: Sarcopterygii): new insights from *Soederberghia groenlandica*, in: Elliott, D.K., Maisey, J.G., Yu, X., Miao, D. (Eds.), Morphology, Phylogeny and Paleobiogeography of Fossil Fishes: Honoring Meemann Chang. Verlag Dr. Friedrich Pfeil, München, Germany, pp. 299–324.

Friedman, M., Daeschler, E.B., 2006. Late Devonian (Famennian) lungfishes from the Catskill Formation of Pennsylvania, USA. Palaeontology 49, 1167–1183. https://doi.org/10.1111/j.1475-4983.2006.00594.x

Friedman, M., Sallan, L.C., 2012. Five hundred million years of extinction and recovery: A phanerozoic survey of large-scale diversity patterns in fishes. Palaeontology 55, 707–742. https://doi.org/10.1111/j.1475-4983.2012.01165.x

Gavrilets, S., Losos, J.B., 2009. Adaptive Radiation: Contrasting Theory with Data. Science 323, 732–737. https://doi.org/10.1126/science.1157966

Günther, A.C.L.G., 1871. XIX. Description of ceratodus, a genus of ganoid fishes, recently discovered in rivers of Queensland, Australia. Philos. Trans. R. Soc. Lond. 161, 511–571. https://doi.org/10.1098/rstl.1871.0020

Harmon, L.J., Losos, J.B., Jonathan Davies, T., Gillespie, R.G., Gittleman, J.L., Bryan Jennings, W., Kozak, K.H., McPeek, M.A., Moreno-Roark, F., Near, T.J., Purvis, A., Ricklefs, R.E., Schluter, D., Schulte, J.A., Seehausen, O., Sidlauskas, B.L., Torres-Carvajal, O.,

Weir, J.T., Mooers, A.T., 2010. Early bursts of body size and shape evolution are rare in comparative data. Evolution. https://doi.org/10.1111/j.1558-5646.2010.01025.x

Hecht, M.K., Goody, P.C., Hecht, B.M. (Eds.), 1977. Major Patterns in Vertebrate Evolution. Plenum Publishing Company, New York & London. https://doi.org/10.1007/978-1-4684-8851-7

Hill, J.J., Puttick, M.N., Stubbs, T.L., Rayfield, E.J., Donoghue, P.C.J., 2018. Evolution of jaw disparity in fishes. Palaeontology 61, 847–854. https://doi.org/10.1111/pala.12371

Hunt, G., Rabosky, D.L., 2014. Phenotypic Evolution in Fossil Species: Pattern and Process. Annu. Rev. Earth Planet. Sci. 42, 421–441. https://doi.org/10.1146/annurev-earth-040809-152524

Jarvik, E., 1980. Basic Structure and Evolution of Vertebrates. Academic Press, Inc., New York.

Jarvik, E., 1967. On the structure of the lower jaw in dipnoans: with a description of an early Devonian dipnoan from Canada, *Melanognathus canadenis* gen. et sp. nov. J. Linn. Soc. Lond. Zool. 47, 155–183. https://doi.org/10.1111/j.1096-3642.1967.tb01401.x

Jørgensen, J.M., Joss, J., 2011. The Biology of Lungfishes. CRC Press, Enfield, N.H.

Klug, C., Frey, L., Pohle, A., De Baets, K., Korn, D., 2017. Palaeozoic evolution of animal mouthparts. Bull. Geosci. 511–524. https://doi.org/10.3140/bull.geosci.1648

Klug, C., Kröger, B., Kiessling, W., Mullins, G.L., Servais, T., Frýda, J., Korn, D., Turner, S., 2010. The Devonian nekton revolution. Lethaia 43, 465–477. https://doi.org/10.1111/j.1502-3931.2009.00206.x

Lee, J., Alrubaian, J., Dores, R.M., 2006. Are lungfish living fossils? Observation on the evolution of the opioid/orphanin gene family. Gen. Comp. Endocrinol. 148, 306–314. https://doi.org/10.1016/j.ygcen.2006.07.010

Lidgard, S., Love, A.C., 2018. Rethinking Living Fossils. BioScience 68, 760–770. https://doi.org/10.1093/biosci/biy084

Lloyd, G.T., Wang, S.C., Brusatte, S.L., 2011. Identifying heterogeneity in rates of morphological evolution: discrete character change in the evolution of lungfish (Sarcopterygii; Dipnoi). Evolution 66, 330–348. https://doi.org/10.1111/j.1558-5646.2011.01460.x

Long, J.A., 1993. Cranial ribs in Devonian lungfishes and the origin of air-breathing. Mem. Assoc. Australas. Palaeontol. 15, 199–209.

Long, J.A., Trinajstic, K., 2010. The Late Devonian Gogo Formation Lägerstatte of Western Australia: Exceptional Early Vertebrate Preservation and Diversity. Annu. Rev. Earth Planet. Sci. 38, 255–279. https://doi.org/10.1146/annurev-earth-040809-152416

Luo, Y., Cui, X., Qiao, T., Zhu, M., 2021. A new dipnoan genus from the Middle Devonian of Huize, Yunnan, China. J. Syst. Palaeontol. 19, 1303–1315. https://doi.org/10.1080/14772019.2022.2042409

Mondéjar-Fernández, J., 2020. A new onychodont (Osteichthyes; Sarcopterygii) from the Middle Devonian of Morocco and its bearing on early osteichthyan evolution. J. Syst. Palaeontol. 18, 573–606. https://doi.org/10.1080/14772019.2019.1655495

Morris, J.L., Puttick, M.N., Clark, J.W., Edwards, D., Kenrick, P., Pressel, S., Wellman, C.H., Yang, Z., Schneider, H., Donoghue, P.C.J., 2018. The timescale of early land plant evolution. Proc. Natl. Acad. Sci. 115. https://doi.org/10.1073/pnas.1719588115

Musick, J.A., Thomson, K.S., 1993. Living Fossil: The Story of the Coelacanth, Copeia. https://doi.org/10.2307/1447265

Pardo, J.D., Huttenlocker, A.K., Small, B.J., 2014. An exceptionally preserved transitional lungfish from the lower permian of Nebraska, USA, and the origin of modern lungfishes. PLoS ONE 9, e108542. https://doi.org/10.1371/journal.pone.0108542

Rokas, A., Carroll, S.B., 2006. Bushes in the tree of life. PLoS Biol. 4, e352. https://doi.org/10.1371/journal.pbio.0040352

Romer, A.S., 1966. Vertebrate Paleontology. University of Chicago Press.

Ruta, M., Wagner, P.J., Coates, M.I., 2006. Evolutionary patterns in early tetrapods. I. Rapid initial diversification followed by decrease in rates of character change. Proc. R. Soc. B Biol. Sci. 273, 2107–2111. https://doi.org/10.1098/rspb.2006.3577

Sahney, S., Benton, M.J., Ferry, P.A., 2010. Links between global taxonomic diversity, ecological diversity and the expansion of vertebrates on land. Biol. Lett. 6, 544–547. https://doi.org/10.1098/rsbl.2009.1024

Sallan, L.C., Coates, M.I., 2010. End-Devonian extinction and a bottleneck in the early evolution of modern jawed vertebrates. Proc. Natl. Acad. Sci. 107, 10131–10135. https://doi.org/10.1073/pnas.0914000107

Schaeffer, B., 1952. Rates of Evolution in the Coelacanth and Dipnoan Fishes. Evolution 6, 101. https://doi.org/10.2307/2405507

Schultze, H.-P., 2010. The late Middle Devonian fauna of Red Hill I, Nevada, and its paleobiogeographic implications. Foss. Rec. 13, 285–295. https://doi.org/10.1002/mmng.201000001

Simões, M., Breitkreuz, L., Alvarado, M., Baca, S., Cooper, J.C., Heins, L., Herzog, K., Lieberman, B.S., 2016. The Evolving Theory of Evolutionary Radiations. Trends Ecol. Evol. 31, 27–34. https://doi.org/10.1016/j.tree.2015.10.007

Simpson, G.G., 1953. The Major Features of Evolution. Columbia University Press. https://doi.org/10.7312/simp93764

Simpson, G.G., 1944. Tempo and Mode in Evolution. Columbia University Press, New York, NY. https://doi.org/10.7312/simp93040

Smithson, T.R., Richards, K.R., Clack, J.A., 2016. Lungfish diversity in Romer's Gap: reaction to the end-Devonian extinction. Palaeontology 59, 29–44. https://doi.org/10.1111/pala.12203

Stanley, S.M., 1985. Rates of evolution. Paleobiology 11, 13–26.

Stroud, J.T., Losos, J.B., 2016. Ecological Opportunity and Adaptive Radiation. Annu. Rev. Ecol. Evol. Syst. 47, 507–532. https://doi.org/10.1146/annurev-ecolsys-121415-032254

Todd Streelman, J., Danley, P.D., 2003. The stages of vertebrate evolutionary radiation. Trends Ecol. Evol. 18, 126–131. https://doi.org/10.1016/S0169-5347(02)00036-8

Trewin, N.H., 1986. Palaeoecology and sedimentology of the Achanarras fish bed of the Middle Old Red Sandstone, Scotland. Trans. R. Soc. Edinb. Earth Sci. 77, 21–46. https://doi.org/10.1017/S0263593300010737

Wainwright, P.C., Westneat, M.W., Bellwood, D.R., 2000. Linking feeding behaviour and jaw mechanics in fishes, in: Blake, R.W., Domenici, P. (Eds.), Biomechanics in Animal Behaviour. Garland Science, London, pp. 207–221.

Westneat, M.W., 2004. Evolution of Levers and Linkages in the Feeding Mechanisms of Fishes. Integr. Comp. Biol. 44, 378–389. https://doi.org/10.1093/icb/44.5.378

Westneat, M.W., 2003. A biomechanical model for analysis of muscle force, power output and lower jaw motion in fishes. J. Theor. Biol. 223, 269–281. https://doi.org/10.1016/S0022-5193(03)00058-4

Westoll, T.S., 1949. On the evolution of the Dipnoi, in: Jepsen, G.L., Mayr, E., Simpson, G.G. (Eds.), Genetics, Paleontology and Evolution. Princeton University Press, Princeton, NJ, pp. 121–184.

Woodward, A.S., 1891. Catalogue of the Fossil Fishes in the British Museum (Natural History). Part II. Taylor & Francis, London.

Zhu, M., Yu, X., Ahlberg, P.E., 2001. A primitive sarcopterygian fish with an eyestalk. Nat. Lett. 410, 81–84. https://doi.org/10.1038/35065078

Zhu, M., Yu, X., Janvier, P., 1999. A primitive fossil fish sheds light on the origin of bony fishes. Nat. Lett. 397, 607–610. https://doi.org/10.1038/17594

Zhu, M., Zhao, W., Jia, L., Lu, J., Qiao, T., Qu, Q., 2009. The oldest articulated osteichthyan reveals mosaic gnathostome characters. Nature 458, 469–474. https://doi.org/10.1038/nature07855

Chapter 2 – Variable Patterns of Phenotypic Evolution Among Canonical 'Living Fossil' Lineages

Note: The contents of this chapter are under review for publication.

2.1 Abstract

Coelacanths, lungfishes, and holosteans represent three emblematic living fossil lineages, thought to be united by similar patterns of phenotypic change through time. Past work suggests a variety of evolutionary patterns for these groups, but it is unclear whether these reflect biological differences or stem from contrasting analytical approaches. Here, we examine these lineages under a common framework to assess variation in the evolution of discrete and morphometric shape data and test whether living fossils show comparable patterns of phenotypic evolution. Our results show different evolutionary modes both among and within these lineages as a function of data type. For lungfishes, rates in discrete characters are highest in the Devonian and monotonically decline over time. Coelacanth rates show multiple early rate peaks followed by a decline toward the recent. Holostean rates show modest peaks but are broadly consistent over time. Patterns of body shape evolution also differ among clades, with overwhelming support for declining rates over time for coelacanths but mixed evidence for similar dynamics in the other groups. Our results imply idiosyncratic processes of evolutionary change among traditional examples of living fossils and indicate a need to explicitly quantify patterns of change rather than apply informal, often qualitative, macroevolutionary classifications.

2.2 Introduction

"Living fossil"—a term coined by Darwin [1]—is one of the most evocative ideas in evolutionary biology. Like many concepts first articulated in *On the Origin of Species*, the initial account of living fossils combined careful natural history observations with hypotheses of their origins. Darwin provided three examples of living fossils: ganoid fishes (bichirs, sturgeons, paddlefishes, gars, and the bowfin), *Ornithorynchus* (platypus), and *Lepidosiren* (South American lungfish) ([1]: p. 107). These groups were, Darwin argued, united by a set of common features. First, each contained the last survivors of lineages that the fossil record indicates were once much more diverse. Second, all three represented structural intermediates between more species-rich groups (chondrichthyans and teleosts in the case of 'ganoids', reptiles and mammals in the case of *Ornithorhynchus*, and fishes and tetrapods in the case of *Lepidosiren*). Third, all are restricted to specific, often spatially limited habitats. Darwin saw in this final observation a potential explanation for the first two features of living fossils: endurance of such lineages might reflect reduced competition encountered in geographically or environmentally restricted settings.

Since Darwin's proposal, the concept of living fossils has been widely applied across the tree of life [2]. As the set of lineages interpreted as living fossils has expanded, the concept's meaning has grown so diffuse that its utility is hotly debated [3–9]. Investigations of the dynamics of phenotypic evolution reflect a shift from Darwin's original formulation of living fossils to more recent conceptualisations [10,11]. Although Darwin only indirectly addressed processes of morphological change in these groups, aspects of evolutionary tempo and mode responsible for patterns of phenotypic variation are central to many of today's applications of the living fossil concept (e.g., see criteria in [7]). Generally, the phenotypic variation in these groups is interpreted as either uniformly low [12], declining over time [13], or subject to strong

evolutionary constraint [14]. With some exceptions [15], quantitative investigations of phenotypic evolution in putative living fossil lineages are restricted to isolated examples. While some aspects of tempo and mode may be shared, assessing these lineages independently challenges comparisons among them [13,16–20].

To assess the degree of macroevolutionary convergence in aspects of phenotypic evolution among the most prominent examples of living fossils, we combined existing and newly collected morphological data and analysed our dataset in a consistent framework. Our goal is to establish whether there is any coherence among the most prominent examples of the phenomenon beyond the three defining characteristics outlined by Darwin. Our methodological approach is inspired by cross-clade comparative approaches used to evaluate adaptive radiations [21,22], another macroevolutionary concept that has come to be broadly—and at times imprecisely—applied since it was first articulated [21,23–27]. We take a restricted approach, emphasising two of the lineages first identified by Darwin: lungfishes and holosteans. Darwin's third example, monotremes, are too scarce in the fossil record [28] to offer a helpful comparison, so we examine coelacanths instead. Though obviously not considered by Darwin because eight decades separate the publication of *Origin* from the naming of the living *Latimeria*, coelacanths conform to the original definition of living fossils. Features common to these three groups make them ideal for the comparative study of phenotypic evolution: a long history of systematic and paleontological examination, established phylogenetic frameworks, and articulated fossils that provide perspectives on changes in gross morphology over time. Prior studies of evolutionary rates in holosteans [29], lungfishes [13,16,30], and coelacanths [17–19,30] focus on different aspects of phenotype using contrasting analytical tools that limit comparisons. Here, we examine the evolution of discrete (i.e., cladistic characters) and continuous (i.e., body shape) traits in

these three groups in a common framework to address whether the least controversial examples of living fossils show similar patterns of phenotypic change over time.

2.3 Materials and Methods

2.3.1 Discrete Character Matrices

We used published morphological character matrices to simultaneously infer time-scaled phylogenetic hypotheses and rates of discrete-trait evolution in coelacanths, lungfishes, and holosteans (see Phylogenetic Analyses). Our analyses of shape evolution within a model-fitting framework then used these phylogenetic hypotheses. The source character matrices are described below. For all matrices, we collapsed ambiguous or polymorphic character states to question marks (?) prior to running new phylogenetic analyses.

For coelacanths, we used the matrix from Toriño et al. [43], a descendant of the matrix presented by Forey [17] and one which has been used, with modest modifications, in a series of additional studies [38,44,45]. The matrix contains 50 taxa (48 coelacanths) scored for 110 unordered characters.

For lungfishes, most character matrices focus on either Devonian [46,47] or post-Devonian [48,49] taxa, with few offering dense taxonomic sampling over the entire evolutionary history of the group [13,20,31,50]. From the available matrices, we selected Lloyd et al. [13], which represents a ‘supermatrix’ combining datasets from several studies [46–48,51]. This matrix formed the basis of a relatively recent assessment of evolutionary rates in lungfishes [13], permitting direct comparison with our results obtained from a different analytical approach. This matrix contains 86 taxa (85 lungfishes) scored for 91 characters.

For holosteans, we used the dataset from López-Arbarello and Sferco [52] that includes a broad sample of holosteans and other crown neopterygians. It contains 70 taxa (39 holosteans) scored for 339 characters.

2.3.2 Phylogenetic Analyses

Bayesian phylogenetic analyses for the lungfish, coelacanth, and holostean morphological datasets were performed in BEAST v2.6.5 [53,54]. The Fossilized Birth-Death (FBD) approach was used, which uses extinct taxa as informative tips and simultaneously estimates relationships, branch durations, and rates of morphological change through time [55,56]. Empirical studies and simulations show that use of the FBD prior generally results in estimated divergence times that are more closely in agreement with the fossil record than with node- and tip-dating analyses [57–60]. A Lewis MK model [61] with 4-category gamma distributions and a relaxed lognormal clock was used for morphological traits. Relative to the default settings in BEAST, we changed two priors for coelacanths specifically: (1) *diversificationRateFBD* (Log Normal; upper = 10) and (2) *ucldMean* (Log Normal distribution; initial = 0.1; M = 1.0; S = 1.25). The only other change was the *originFBD* prior. For both sarcopterygian lineages, we set the initial search to 425 Ma (upper bound of 440 Ma), which we selected based on the age range estimates of the most recent common ancestor (MRCA) between sarcopterygians and actinopterygians (*Guiyu* from the late Silurian [62]). For holosteans, we set the initial search to 260 Ma (upper bound of 423 Ma), which we selected based on the MRCA for the group. All remaining FBD priors were left in their default settings—Uniform for the *diversificationRateFBD* (initial = 0.01; upper = infinity), *samplingProportionFBD* (initial = 0.5; upper = 1.0), *turnoverFBD* (initial = 0.5; upper = 1.0), and *ucldMean* (initial = 1.0; upper = infinity); Exponential for the *gammaShape* (initial = 1.0; mean = 1.0); and Gamma for the

ucldStdev (initial = 0.1; alpha = 0.5396; beta = 0.3819). This was done to reduce biases associated with the *ad hoc* adjustment of informative priors by limiting their use to "realistic" mechanistic models at the root search [63].

We applied a small set of constraints to our analyses. Topological constraints included: (1) rooting using a designated outgroup (actinopterygians for coelacanths, *Psarolepis* for lungfishes, and *Pteronisculus* for holosteans), (2) monophyly of the apomorphic Paleozoic coelacanths *Allenypterus* and *Holopterygius* [38], (3) monophyly of a well-supported subset of total-group Lepidosireniformes for lungfishes (*Gosfordia truncata*, *Lepidosiren paradoxa*, *Protopterus annectens*, and *Ptychoceratodus serratus*) [49]. Temporal constraints included: (1) a fossil calibration minimum at 100 Ma for the node representing the MRCA of *Lepidosiren paradoxa* and *Protopterus annectens* based on the breakup of Gondwana [64–66] and (2) a calibration setting a minimum age of divergence between *Lepiososteus* and *Atractosteus* at 93 Ma, based on the first occurrence of fossil *Atractosteus* in the early Late Cretaceous [67]. Phylogenetic analyses were run for 500 million generations, with trees sampled every 100,000 generations. Tracer v1.7 [68] was used to assess convergence visually via the trace plot and with effective sample size values greater than 200. The first 10% of the trees sampled were discarded as burn-in fraction, with post burn-in trees used to generate MCC consensus trees and used as posterior samples for other analyses. These latter analyses using the posterior trees considered only those tips assigned to the total group of interest in the MCC tree.

Age constraints for fossil taxa were compiled at the finest level possible (typically geologic stage [69–71]), drawing from a combination of original descriptions, revisions, and other resources (e.g., The Paleobiology Database, https://paleobiodb.org/). In BEAUTi v. 2.6.5 [54], the age prior for each extinct taxon was set as a uniform distribution. The upper and lower

boundaries are defined by the age estimates for the most restrictive stratigraphic bin identified for each fossil taxon. Likewise, if there was more than one fossil from different deposits or localities representing the taxon, we used the most restrictive bin that accounted for its overall stratigraphic extent. We then linked age priors for taxa deriving from the same geological horizon (typically a well-known fossil site or formation) using the R package *palaeo* [72] to generate an XML code block that would be appended manually to the BEAUTi input file used to initialise BEAST. This enforced matching ages for fossils from the same deposits when running phylogenetic analyses.

2.3.3 Evolution in Discrete Characters

Any outgroup taxa used to root the trees during the BEAST runs (including all Teleostei for the holostean tree) were excluded from summaries of evolutionary rate in discrete characters. All subsequent steps in the rate analysis pipeline used the packages *phytools* [73] and *ape* [74], along with an adjusted script from Close et al. [75] calling an additional function from *OutbreakTools* [76] in R v3.6.1 [77]. The code and data used to run this and subsequent analyses can be found on Deep Blue. Per-branch estimates of rates of phenotypic evolution were taken from a random sample of 100 trees from the posterior distribution generated by the BEAST analysis. Per-branch rates were plotted on a natural log scale over a span equaling their temporal duration to create a "rate cloud". This was overlain with a loess line generalised from the MCC tree by calculating a moving average using million-year timesteps. This delivered a rate through time (percent change per lineage per million years) plot for the entire clade ([75]: figure 4).

In addition to variation in rates of change over time, we evaluated character saturation levels within all three groups using their respective morphological matrices. The measure has been established to estimate if convergence in character states is more likely than the generation

of new character states [78–81]. This was achieved by comparing pairwise character-state dissimilarity and plotting it against patristic morphological distance (distance_metric = "mord") [82]. In these analyses, if the average value (loess curve) increases linearly, it indicates persistent generation of novel traits. However, if the average value asymptotes, it signals lineages reaching character exhaustion with increased incidence of homoplasy. These analyses illustrate the relative contributions of innovation and homoplasy to overall change.

2.3.4 Morphological Landmarking Schemes

Landmarks were selected based on previous publications with adjustments made on a per-clade basis to capture homologous aspects of cranial and postcranial anatomy (see clade information below). All semi-landmarks were spread out evenly beginning at the rostrum, following the dorsal body line including the fleshy part of any fins, curving at the fleshy posterior end of the caudal fin, and then proceeding ventrally while tracing the fleshy part of any additional fins, and then ending at the posteriormost contact of the lower jaw with the ventral body line. We did not use a consistent number of semi-landmark points between fixed landmarks; rather, the total semi-landmarks varied depending on the topological complexity of the region they were outlining. Non-identical constellations of fixed landmarks for the three lineages reflected important differences in the number and arrangement of median fins. The full landmarking schemes for each clade are discussed below and figured in the Appendices.

The arrangement of fixed landmarks for coelacanths matches that used by Friedman and Coates [38], with 8 landmarks capturing fin position and 6 landmarks capturing cranial features (14 total, Supplement to Chapter 2, **Figure A4**). 155 additional semi-landmarks were placed to capture the outline of the body along segments beginning at the anteriormost tip of the skull and tracing the head (one curve, 25 semi-landmarks); the dorsal region, including tracing around the

fleshy area of each fin lobe (four curves, 35 semi-landmarks); the fleshy dorsal and ventral regions of the caudal fin (two curves, 60 semi-landmarks); and the entire ventral region, including tracing around the fleshy area of each ventral midline fin, ending posteriorly at the lower jaw (two curves, 35 semi-landmarks).

The landmarking scheme for lungfishes was built to closely match the configuration of the coelacanth scheme, resulting in 5 landmarks capturing fin position and 6 landmarks capturing variations in skull morphology (11 total, Supplement to Chapter 2, **Figure A5**). The reduced number of fixed cranial landmarks reflects the absence of median fin divisions in all lungfishes; these divisions remain apparent in coelacanths with the most divergent postcranial anatomy [38]. 115 additional semi-landmarks were placed to capture the outline of the body along segments beginning at the anteriormost tip of the skull and tracing the head (one curve, 15 semi-landmarks), the entire dorsal region, including tracing around the fleshy area of each fin lobe, extending to the posterior tip of caudal fin (two curves, 50 semi-landmarks), the entire ventral region, including tracing around the fleshy area of each ventral midline fin, ending at the lower jaw (two curves, 50 semi-landmarks).

The landmarking scheme for holosteans descends from that used in Clarke et al. [39] and Clarke and Friedman [29], with 8 landmarks capturing fin position and 6 landmarks capturing variation in skull morphology (14 total, Supplement to Chapter 2, **Figure A6**). 120 additional semi-landmarks were placed to capture the outline of the body along segments beginning at the anteriormost tip of the skull and tracing the head (one curve, 25 semi-landmarks); the dorsal region, including tracing around the fleshy area of each fin (four curves, 55 semi-landmarks); the fleshy dorsal and ventral regions of the caudal fin (two curves, 20 semi-landmarks), and the

entire ventral region, including tracing around the fleshy area of each ventral midline fin, ending posteriorly at the lower jaw (one curve, 20 semi-landmarks).

2.3.5 Body Shape Analysis

We landmarked a combination of original specimen photographs, published fossil images, and technical illustrations for species that were present in our phylogenetic analyses. The final dataset consisted of 27 coelacanths, 16 lungfishes, and 62 holosteans. Each taxon was then landmarked according to the schemes outlined above and their body shape was traced with spline curves in R v3.6.1 [77] using the package *StereoMorph* (*digitizeImages*) [83]. The unaligned landmark and semi-landmark coordinates were imported using the package *geomorph* [84,85] (*readland.shapes*, adapting the total semilandmarks on a per-curve basis to be dense enough to capture fin details as detailed above), adjusted with a Procrustes transformation (*gpagen*), and transformed using a principal components analysis (PCA) and phylogenetically-aligned components analysis (PaCA) (both via *gm.prcomp*). Morphospace plots for all taxa can be found in the Supplement to Chapter 2.

2.3.6 Fitting Evolutionary Models of Continuous Trait Evolution

We fit three alternative models of continuous trait evolution to body shape datasets for each clade using the R package mvMORPH [86], taking advantage of new approaches for investigating highly dimensional morphometric datasets [34]. For each clade, we fit: (1) Brownian Motion (BM), (2) Ornstein-Uhlenbeck (OU), and (3) Accelerating-Decelerating (ACDC) models. BM reflects a constant accumulation of shape disparity over time; OU models a central tendency, which is interpreted biologically as an adaptive peak or evolutionary constraint [87,88]; and ACDC reflects accelerating or decelerating exponential rates of change over the

history of a clade [86,89]. Early Burst (EB) is a special case within the ACDC framework where rates exclusively decelerate [21,86,89]. EB was originally formulated as a model of adaptive radiation [21], but it also matches patterns sometimes inferred for living fossils [13,16]. For the purposes of our analyses, we refer to the exponential models inferring declining rates as EB.

We optimised the three models using the *mvgls* function in mvMORPH. We opted for the penalised likelihood approach in *mvgls* because it has been shown to generate more accurate inferences for rich multivariate datasets [34]. Using other likelihood models can lead to, for example, exaggerated estimates of the exponential parameter *b* in likelihood (e.g., *mvEB*) versus penalised likelihood (e.g., *mvgls*) model fitting analyses [34]. The *mvgls* flags we used across all analyses were *scale.height* = F, *method* = "PL-LOOCV", *penalty* = "RidgeArch", *target* = "unitVariance", and *error* = T. The error option estimates an extra nuisance parameter intended to account for variation not explained by the model (e.g., measurement error) and is recommended for empirical datasets [34,90].

To run the analyses, we used the MCC tree as an initial phylogenetic framework and all PC axes—those explaining 100% of the variation—for each taxon (24, 15, and 60 total axes for coelacanths, lungfishes, and holosteans, respectively). To account for variation in model fit as a function of uncertainty in tree topology and evolutionary timescale, we repeated the procedure using a sample of 100 trees from the posterior distribution of trees generated by the BEAST analyses. We calculated GIC scores [32–34] and weights for each model fit across all sampled trees, and visualised the resulting distributions (**Figure 2.1**, **Figure 2.2**, **Figure 2.3**; GIC scores in the Supplement to Chapter 2).

We also performed parametric bootstrapping—using only the parameters from the best fit model per clade—to explore our results more thoroughly. The empirical parameters for the

mvSIM function were thus derived from *mvgls* model fitting using the unit-scaled MCC tree and the PC axes explaining 100% of the variance. Due to optimization issues, holosteans required the *mvgls* parameter under *model* = "EB" to be estimated using *REML* = FALSE throughout. Coelacanths and lungfishes showed no optimization issues and used the default *REML* = TRUE. We then performed bootstrapping on 100 *mvSIM* replicates, with the upper and lower bounds of parameter search space iteratively increased if model fitting reached the default parameter limits. We plotted the distribution of the parameter for each best fit model estimated from these bootstrapped datasets per group (Supplement to Chapter 2, **Figure A8**) and calculated the 95% confidence interval.

2.4 Results

2.4.1 Phylogenetic Relationships and Evolutionary Timescales

The topologies of the phylogenies inferred using Bayesian analyses with a Fossilised Birth-Death prior correspond closely to those reported from prior analyses of the same matrices. Our estimated ages of last common ancestor of all sampled lineages for each of our groups are: Silurian for coelacanths (428 Ma; 95% HPD: 415–446 Ma; Supplement to Chapter 2, **Figure A1**) and lungfishes (432 Ma; 95% HPD: 425–435 Ma; Supplement to Chapter 2, **Figure A2**), and early Permian for holosteans (288 Ma; 95% HPD: 272–307 Ma; Supplement to Chapter 2, **Figure A3**). Most nodes within the holostean and coelacanth phylogenies have relatively high clade credibility values (>75%). Posterior support for most nodes in the lungfish tree is considerably lower, reflecting a longstanding pattern of heterogeneous topologies recovered in phylogenetic studies of the group (e.g., [31]). Further discussion and complete maximum clade credibility (MCC) trees can be found in the Appendices.

2.4.2 Discrete Character Evolution

For coelacanths, rates of discrete character evolution show an overall decline from the origin of the clade to the present (**Figure 2.1**). Modest peaks in evolutionary rates occur during the Early Devonian, Permian, and Early Triassic, with rates dropping substantially by the end of the Triassic. Rates plateau during the Jurassic before dropping precipitously by the end of the Cretaceous. A nearly linear relationship between morphological disparity and patristic distances indicates little character saturation.

For lungfishes, rates of discrete character evolution show an overall decline from the origin of the clade to the present (**Figure 2.2**). The highest rates occur in the Silurian and Early Devonian, but these decline into the Late Devonian. At this point, they stabilise for the duration of the Paleozoic. Rates decline monotonically throughout the Mesozoic and Cenozoic. An apparent asymptote in values of morphological dissimilarity with increasing patristic distance indicates some saturation of character states.

For holosteans, rates of discrete character evolution show irregular but modest fluctuations about a relatively constant rate over time (**Figure 2.3**). Distinct peaks in rates of morphological evolution were recovered in the Triassic and Early Cretaceous, each followed by a nearly equal and opposite decrease in rates. From the Late Cretaceous onward, rates remain approximately constant. Dissimilarity increases sharply as the patristic distance increases at relatively low patristic distances. Slower accumulation at higher patristic distances indicates some character saturation. Discrete patterns are summarised for all three lineages in the Supplement to Chapter 2, **Table A1**.

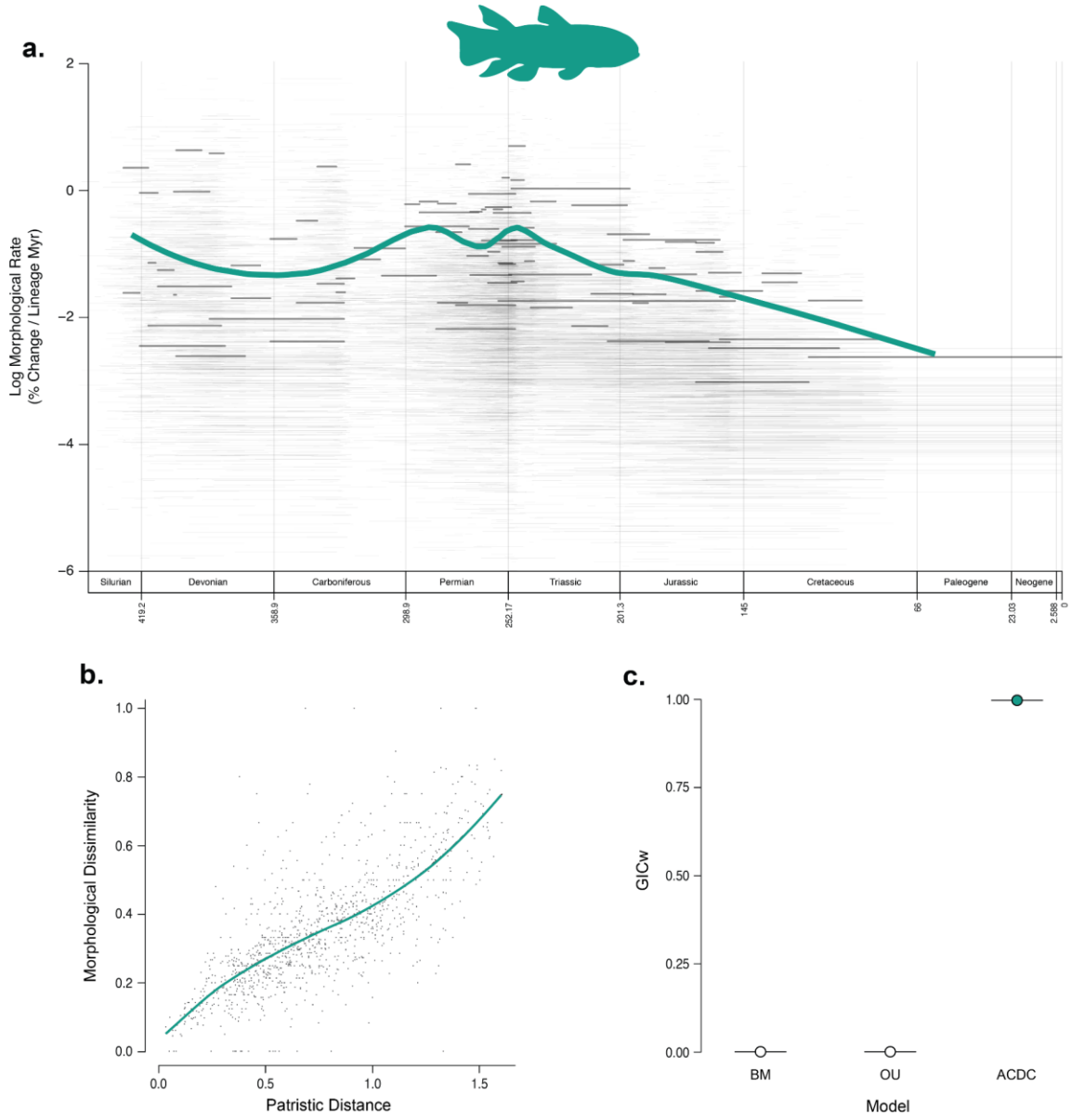

Figure 2.1. Patterns of phenotypic evolution in coelacanths. (a) rate-through-time plot for discrete characters, derived from the MCC tree and a random sampling of 100 trees from the posterior generated using morphological data in BEAST v2.6.5 with the Fossilized Birth-Death model. The thicker, solid green line is the average rate across the MCC tree; the thinner, solid black lines are the MCC per-branch rates; and the semi-transparent gray lines forming a "cloud" behind the plot are the per-branch rates from each tree sampled from the posterior. (b) character saturation, generated using the discrete character matrix to calculate pairwise character-state dissimilarity and plot it against patristic morphological distance. (c) support for competing models of body-shape evolution (GICw) derived from the MCC tree (circles), a sample of 100 posterior trees (violin plot distribution), and the PC axes that summarized 100% of the variability for each clade. Models and *mvMORPH* methods are discussed in the text. Silhouette of *Miguashaia* by Steven Coombs (Public Domain) via PhyloPic.

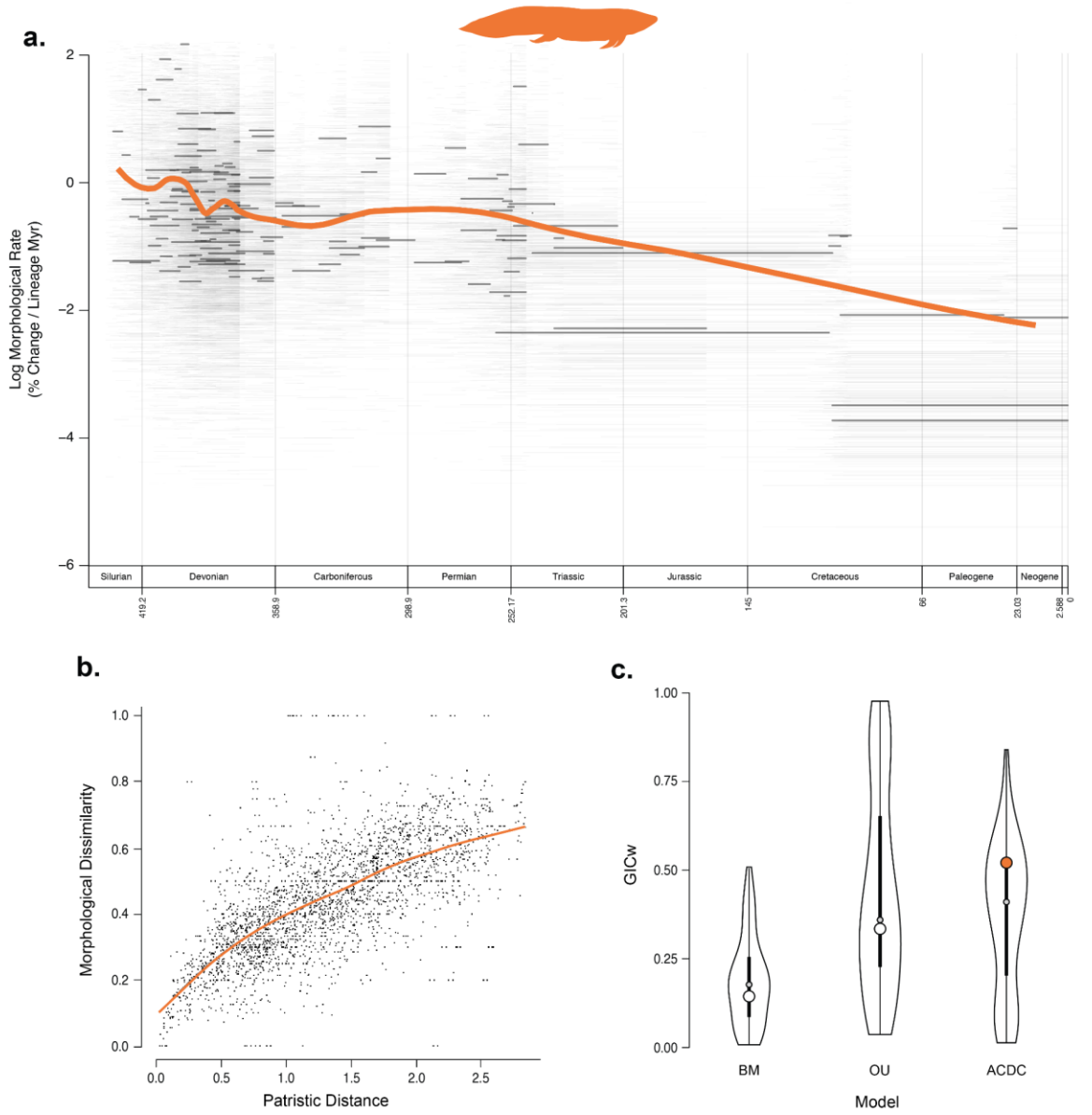

Figure 2.2. Patterns of phenotypic evolution in lungfishes. (a) rate-through-time plot for discrete characters, derived from the MCC tree and a random sampling of 100 trees from the posterior generated using morphological data in BEAST v2.6.5 with the Fossilized Birth-Death model. The thicker, solid orange line is the average rate across the MCC tree; the thinner, solid black lines are the MCC per-branch rates; and the semi-transparent gray lines forming a "cloud" behind the plot are the per-branch rates from each tree sampled from the posterior. (b) character saturation, generated using the discrete character matrix to calculate pairwise character-state dissimilarity and plot it against patristic morphological distance. (c) support for competing models of body-shape evolution (GICw) derived from the MCC tree (circles), a sample of 100 posterior trees (violin plot distribution), and the PC axes that summarized 100% of the variability for each clade. Models and *mvMORPH* methods are discussed in the text. Silhouette of *Ceratodus* by T. Michael Keesey (Public Domain) via PhyloPic.

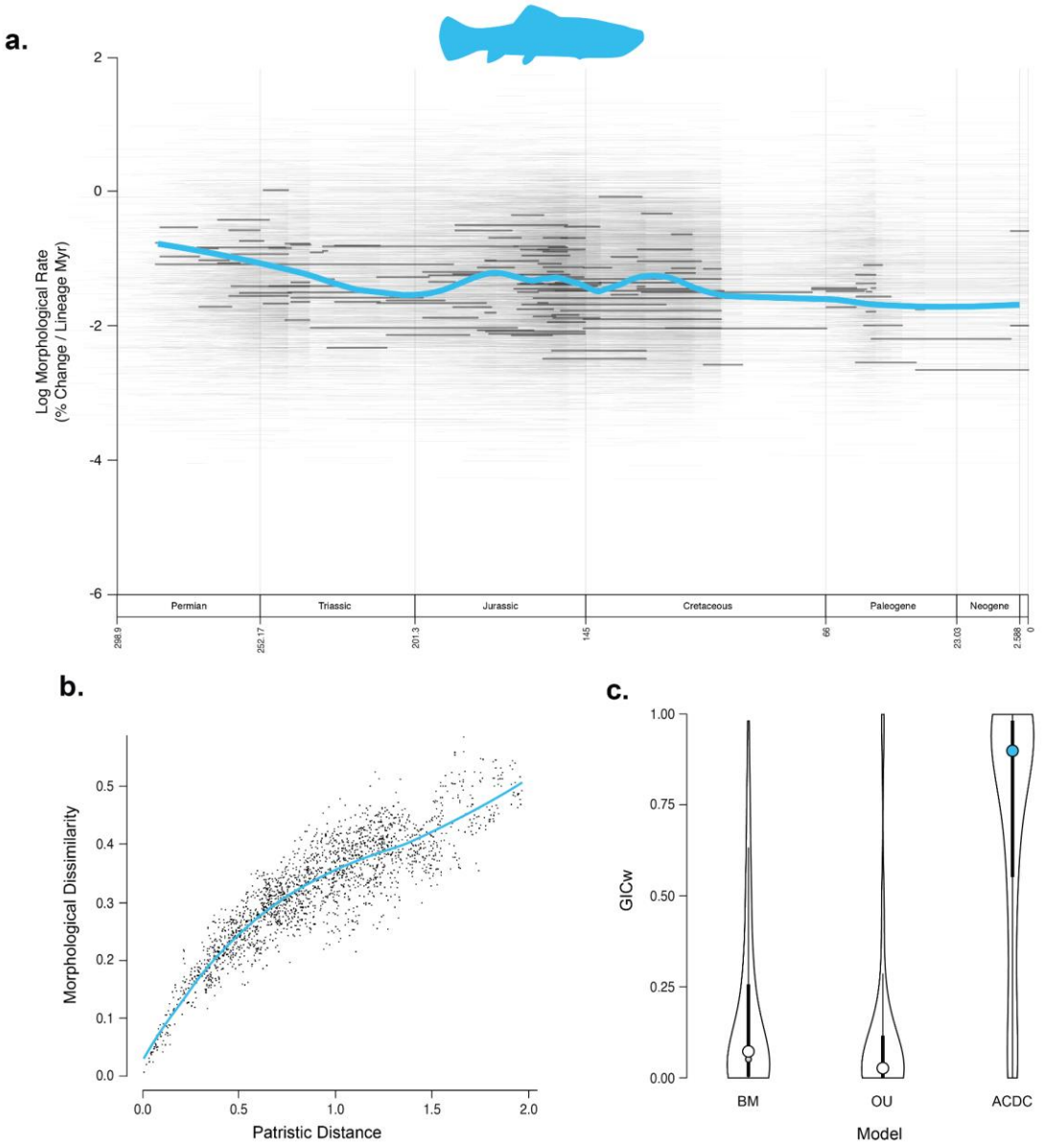

Figure 2.3. Patterns of phenotypic evolution in holosteans. (a) rate-through-time plot for discrete characters, derived from the MCC tree and a random sampling of 100 trees from the posterior generated using morphological data in BEAST v2.6.5 with the Fossilized Birth-Death model. The thicker, solid blue line is the average rate across the MCC tree; the thinner, solid black lines are the MCC per-branch rates; and the semi-transparent gray lines forming a "cloud" behind the plot are the per-branch rates from each tree sampled from the posterior. (b) character saturation, generated using the discrete character matrix to calculate pairwise character-state dissimilarity and plot it against patristic morphological distance. (c) support for competing models of body-shape evolution (GICw) derived from the MCC tree (circles), a sample of 100 posterior trees (violin plot distribution), and the PC axes that summarized 100% of the variability for each clade. Models and *mvMORPH* methods are discussed in the text. Silhouette of *Calamopleurus* by Aline M. Ghilardi (CC BY-NC 3.0) via PhyloPic.

2.4.3 Body Shape Evolution

Landmarking schemes and shape spaces for the three lineages are summarised in the Supplement to Chapter 2. For coelacanths, 24 principal component (PC) axes summarised 100% of body shape variance, with over 70% captured by the first two axes. PC1 reflects variation in the anterior extension of the epichordal/hypochordal lobes of the caudal fin (48% of total variance) and PC2 summarises differences in body depth (23% of total variance) (Supplement to Chapter 2, **Figure A4.** Landmarking scheme and shape space for coelacanths.). PC3 and PC4 capture head shape, pelvic fin placement, and posterior body shape (14% of total variance, cumulatively). All further axes summarise minor variations relating to the median fins. The best-fit model on the MCC tree was the Accelerating-Decelerating (ACDC) model with declining rates of change, corresponding to the Early Burst (EB) variant (Generalised Information Criterion [32–34] weight [GICw] = 1) (**Figure 2.1**; Supplement to Chapter 2, **Figure A7**, **Table A2**). Estimated *b*—representing the exponential change in evolutionary rate—for empirical data on the unit-scaled MCC tree was strongly negative ($b \sim -10.7$; 95% CI from parametric bootstrapping: -20.3, -8.99; Supplement to Chapter 2, **Figure A8**). This estimate implies a substantial decrease in rates of approximately four orders of magnitude at the tips compared to those at the root.

For lungfishes, 15 PC axes summarised 100% of body shape variance, with 69% captured by the first two axes. PC1 reflects differences in the dorsal extent and anterior reach of the epichordal lobe (52.6% of total variance) and PC2 indicates the anterior extension and separation of the dorsal fin or fins as well as the extent of the anal fin (16.5% of variance) (Supplement to Chapter 2, **Figure A5**). PC3 and PC4 capture two aspects of body depth (extension and compression, respectively; 18% of total variance, cumulatively). Subsequent axes summarised more subtle differences between fin placement, head length, and body length. The best-fit

evolutionary model was ACDC (GICw ~ 0.52), although this is not decisive due to alternative models we evaluated receiving non-trivial support (Ornstein-Uhlenbeck [OU]: GICw ~ 0.34; Brownian motion [BM]: GICw ~ 0.14) (**Figure 2.2**; Supplement to Chapter 2,

Table A3). Additionally, some of our results show slightly higher support for OU in fitted posterior trees when ACDC was not the preferred model (**Figure 2.2**). Estimated *b* was negative (*b* ~ -3.85; 95% CI from parametric bootstrapping: -24.3, -0.91; Supplement to Chapter 2, **Figure A8**), corresponding to the EB case of ACDC. This value represents an order of magnitude decline in rates, with those at the youngest tips 2% of that at the root. Although the confidence interval for the bootstrapped values does not include zero, some replicates estimated a positive *b*, indicating an inability to distinguish EB from BM (Supplement to Chapter 2, **Figure A8**).

For holosteans, 60 PC axes summarised 100% of body shape variation, with 63% of the variance summarised by the first two axes. PC1 captures the anterior-posterior position of the dorsal fin (35.6% of total variance), and PC2 reflects body depth (27.2% of variance) (Supplement to Chapter 2, **Figure A6**). PC3 and PC4 indicate dorsal and caudal fin form and placement, and dorsal or ventral body curves (together 16.9% of total variance). Further axes summarised differences in snout and head length, fin placement, and body shape. The best-fit evolutionary model was ACDC (GICw ~ 0.90) (**Figure 2.3**; Supplement to Chapter 2,

Table A4). Estimated *b* was very weakly negative (*b* ~ -0.27; 95% CI from parametric bootstrapping: -1.65, 0.44, Supplement to Chapter 2, **Figure A8**), indicating a minor decrease where the rates at the youngest tips are ~76% of those at the base of the tree. The distribution of b generated by parametric bootstrapping encompasses zero, which signifies difficulty

differentiating between changing versus constant rates (a pattern more readily apparent in the nearly identical plots of GIC scores for holosteans, Supplement to Chapter 2, **Figure A7**).

2.5 Discussion and Conclusions

2.5.1 Comparison With Previous Interpretations of Phenotypic Evolution in Living Fossil Lineages

Our results provide a reexamination of previous interpretations of phenotypic evolution in coelacanths, lungfishes, and holosteans. While these groups are commonly thought to exhibit specific types of morphological change, the degree to which these evolutionary trajectories have been quantified varies substantially. Patterns in lungfishes are perhaps the most well-established as they benefit from a long pedigree of research, beginning with Westoll's [16] formative study quantifying the accumulation of "modern" traits in fossil lungfishes. That study and those that followed [13,20,29] support high rates of change in discrete traits at the root of lungfish phylogeny followed by a pronounced decline over the group's history. Our results broadly corroborate these findings. In contrast to studies of evolutionary rate in discrete characters, there are no quantified assessments of body-shape evolution in lungfishes. Nevertheless, there is a strong informal argument in the literature—tracing back to at least Dollo [35]—that the most substantial changes to lungfish body shape occurred early in the group's Devonian history, associated with the origin of a single, continuous median fin [29,36,37]. However, we do not find overwhelmingly strong support for declining rates of body shape evolution in lungfishes, with constant-rate alternatives having a combined GICw ~0.48. The lungfish shape dataset is the smallest for the three lineages considered (n = 16, versus 27 coelacanths and 62 holosteans). This sample size is a limitation of the lungfish record [35–38] and it is possible additional discoveries

of articulated material could increase support for a model with high early rates of change (e.g., EB) for the group.

Quantitative investigation of phenotypic evolution in coelacanths began with Schaeffer's [30] comparative analysis of the group alongside lungfishes. Inspired by and building on Westoll's [16] approach, Schaeffer [30] identified similar patterns for lungfishes and coelacanths: a Devonian peak in rates of change followed by a rapid decay. Using a more extensive set of taxa and characters in an explicitly phylogenetic framework, Cloutier [19] reported a broadly similar pattern with three different measures of evolutionary rate. Forey [17] provided a coarse overview of accumulated changes across coelacanth phylogeny between arbitrary stratigraphic intervals, showing a net decline in steps over time. In line with these previous estimates, we find a decrease in rates of discrete character evolution in coelacanths, punctuated by modest increases in the latest Paleozoic and earliest Mesozoic. Interestingly, the most consistent interval of declining rates in coelacanths begins in the early Triassic, preceding their peak in lineage diversity later in that period [17] (**Figure A1.** Time-scaled maximum clade credibility tree for coelacanths.). Thus, it appears that the onset of low rates of change preceded a decline in taxonomic diversity. Our results add further detail to this picture by showing that coelacanths consistently developed new traits even as their overall rates of change declined over time. As with lungfishes, no quantitative assessments of coelacanth evolutionary rates are based on shape. However, Schaeffer ([30]: figure 1) implied extreme conservatism in body form consistent with low rates of change. Friedman and Coates [38] suggested that high morphological disparity early in coelacanth history could stem from elevated evolutionary rates that subsequently declined. Our comparative analyses strongly support this latter interpretation,

which indicates a substantial decline in rates of body-shape evolution in coelacanths over their history.

Holosteans are central to the concept of living fossils, but there are few quantitative assessments of phenotypic evolution in the group. Clarke et al. [39] compared patterns of body shape evolution between early holosteans and teleosts, finding no consistent differences in rate between the groups when considering phylogenetic uncertainty. This prior study did not test for variable evolutionary rates within holosteans, and there is no strong prior hypothesis for patterns within the group beyond qualitative assessments based on close phenotypic correspondence between living holosteans relative to their closest fossil relatives. Clarke et al. [39] did investigate the degree of constraint in holostean body shape relative to null models using Bloomberg's *K* and suggested that body shape evolution in holosteans is substantially more constrained than that expected under Brownian motion. Clarke and Friedman [29] later reported relatively static levels of morphological disparity over the first 150 million years of holostean history, consistent with many modes of phenotypic change, including evolutionary constraint [40]. Although our examination of character saturation for holosteans suggests some degree of constraint for discrete characters, we find that OU is the least well supported of the models considered for holostean shape data.

2.5.2 Inconsistent Evolutionary Patterns Among and Within Living Fossil Lineages

Systematic paleobiologists typically infer processes or modes of phenotypic evolution from subsets of an organism's overall anatomy. However, different aspects of morphology can show divergent macroevolutionary patterns, suggesting that mosaic evolution of phenotypes is widespread [27,40]. Therefore, we aim to summarise the overall anatomy of our focal lineages across two datasets—discrete characters and overall body shape—which has provided an

opportunity to examine the degree to which different aspects of phenotype show corresponding or divergent patterns of change. Our unified approach helps to understand the living fossil concept, which historically has been derived from independent evaluations of evolutionary mode using contrasting approaches. Two important conclusions emerge from our analyses. First, and directly addressing the question posed at the outset of this study, there is no single pattern of morphological evolution universally shared *among* these lineages. Although there is some evidence for declining rates in both discrete-trait and shape evolution for all three groups, both the support for, and magnitude of, this decline shows substantial differences among the lineages. Second, and perhaps equally important, different aspects of morphology (i.e., discrete characters and shape) do not necessarily show similar evolutionary patterns *within* each lineage even though both might be thought of as broadly summarising overall organismal morphology.

A close correspondence between discrete and continuous trait evolution is clearly demonstrated in coelacanths. Rates of discrete-character evolution show a first-order pattern of decline over time; body shape is likewise best fit by a declining-rates ACDC (i.e., EB) model, and parameter estimates imply a reduction of rates by several orders of magnitude over coelacanth history. Patterns of character saturation for coelacanths suggest continued innovation throughout the clade's history, suggesting few constraints on the evolution of discrete traits (consistent with persistent diffusion through trait space), although at ever-decreasing rates. Likewise, evolutionary patterns across both morphological datasets in holosteans are highly congruent. Rates of discrete-character evolution are remarkably constant over time, with only a modest decline over their entire history. Patterns of shape evolution broadly mirror this, with estimated values of *b* suggesting only minor changes in evolutionary rates throughout clade history.

Lungfishes present a contrasting case. Like coelacanths, their rates of discrete character evolution decline substantially over time but appear to evolve in a more constrained fashion with more pronounced character saturation. Although the EB case of ACDC is the favoured model for body shape evolution in lungfishes, this is not decisive given its weak support (GICw ~ 0.52) combined with parameter estimates that imply a modest rate reduction over time in comparison to coelacanths.

Phenotypically, lungfishes, coelacanths, and holosteans illustrate attributes commonly ascribed to living fossils [7]: extant species closely resemble ancient taxa and there is apparent conservation of morphology over long periods of geological time. However, it has long been clear that superficially similar patterns like these can arise from contrasting dynamics of evolutionary change [41]. Phylogenetic information is crucial for distinguishing between alternative mechanisms underlying otherwise comparable phenotypic patterns [42]. By employing a common phylogenetic comparative framework, we sought to determine whether the similarities among three canonical living fossil groups reflected shared aspects of phenotypic evolution or whether contrasting processes yielded superficially similar morphological patterns. We find noteworthy differences in the evolutionary processes inferred across—and in some cases within—these living fossil lineages. Thus, as with other quantitative assessments of phenotypic diversification across clades [21], we find that shared features ascribed to living fossils can arise from distinct histories of evolutionary change. We anticipate that a broader approach will lead to better characterization of such groups [26], contributing to a better understanding of the origin and persistence of living fossils and other phylogenetic relics [8].

2.6 References

1. Darwin CR. 1859 *On the Origin of Species by Means of Natural Selection, or the Preservation of Favoured Races in the Struggle for Life*. London: John Murray.
2. Eldredge N, Stanley SM. 1984 *Living Fossils*. New York: Springer Verlag.
3. Casane D, Laurenti P. 2013 Why coelacanths are not 'living fossils'. *BioEssays* **35**, 332–338. (doi:10.1002/bies.201200145)
4. Watkins A. 2021 The Epistemic Value of the Living Fossils Concept. *Philos. Sci.* **88**, 1221–1233. (doi:10.1086/714875)
5. Grandcolas P, Nattier R, Trewick S. 2014 Relict species: a relict concept? *Trends Ecol. Evol.* **29**, 655–663. (doi:10.1016/j.tree.2014.10.002)
6. Lidgard S, Love AC. 2018 Rethinking Living Fossils. *BioScience* **68**, 760–770. (doi:10.1093/biosci/biy084)
7. Lidgard S, Love AC. 2021 The living fossil concept: reply to Turner. *Biol. Philos.* **36**, 13. (doi:10.1007/s10539-021-09789-z)
8. Turner DD. 2019 In defense of living fossils. *Biol. Philos.* **34**, 23. (doi:10.1007/s10539-019-9678-y)
9. Werth AJ, Shear WA. 2014 The Evolutionary Truth About Living Fossils. *Am. Sci.* **102**, 434–443.
10. Schopf TJM. 1984 Rates of Evolution and the Notion of 'Living Fossils'. *Annu. Rev. Earth Planet. Sci.* **12**, 245–292. (doi:10.1146/annurev.ea.12.050184.001333)
11. Fisher DC. 1990 Rates of Evolution – Living Fossils. In *Paleobiology: a Synthesis* (eds DEG Briggs, PR Crowther), pp. 152–159. London, UK: Blackwell Scientific.
12. Cavin L, Guinot G. 2014 Coelacanths as 'almost living fossils'. *Front. Ecol. Evol.* **2**, 1–5.

(doi:10.3389/fevo.2014.00049)

13. Lloyd GT, Wang SC, Brusatte SL. 2011 Identifying heterogeneity in rates of morphological evolution: discrete character change in the evolution of lungfish (Sarcopterygii; Dipnoi). *Evolution* **66**, 330–348. (doi:10.1111/j.1558-5646.2011.01460.x)
14. Bicknell RDC *et al.* 2022 Habitat and developmental constraints drove 330 million years of horseshoe crab evolution. *Biol. J. Linn. Soc.* **136**, 155–172. (doi:10.1093/biolinnean/blab173)
15. Bennett DJ, Sutton MD, Turvey ST. 2018 Quantifying the living fossil concept. *Palaeontol. Electron.* **21**. (doi:10.26879/750)
16. Westoll TS. 1949 On the evolution of the Dipnoi. In *Genetics, Paleontology and Evolution* (eds GL Jepsen, E Mayr, GG Simpson), pp. 121–184. Princeton, NJ: Princeton University Press.
17. Forey PL. 1998 *History of the Coelacanth Fishes*. Chapman & Hall.
18. Forey PL. 1988 Golden jubilee for the coelacanth *Latimeria chalumnae*. *Nat. Rev.* **336**, 727–732.
19. Cloutier R. 1991 Patterns, trends, and rates of evolution within the Actinistia. *Environ. Biol. Fishes* **32**, 23–58. (doi:10.1007/BF00007444)
20. Cui X, Friedman M, Qiao T, Yu Y, Zhu M. 2022 The rapid evolution of lungfish durophagy. *Nat. Commun.* **13**, 2390. (doi:10.1038/s41467-022-30091-3)
21. Harmon LJ *et al.* 2010 Early bursts of body size and shape evolution are rare in comparative data. *Evolution* (doi:10.1111/j.1558-5646.2010.01025.x)
22. Miles DB, Ricklefs RE, Losos JB. 2023 How exceptional are the classic adaptive radiations of passerine birds? *Proc. Natl. Acad. Sci.* **120**, e1813976120. (doi:10.1073/pnas.1813976120)

23. Givnish TJ. 2015 Adaptive radiation versus ‘radiation’ and ‘explosive diversification’: why conceptual distinctions are fundamental to understanding evolution. *New Phytol.* **207**, 297–303. (doi:10.1111/nph.13482)
24. Osborn HF. 1902 The Law of Adaptive Radiation. *Am. Nat.* **36**, 353–363.
25. Schluter D. 2000 *The ecology of adaptive radiation*. Oxford: Oxford University Press.
26. Simões M, Breitkreuz L, Alvarado M, Baca S, Cooper JC, Heins L, Herzog K, Lieberman BS. 2016 The Evolving Theory of Evolutionary Radiations. *Trends Ecol. Evol.* **31**, 27–34. (doi:10.1016/j.tree.2015.10.007)
27. Slater GJ, Friscia AR. 2019 Hierarchy in adaptive radiation: A case study using the Carnivora (Mammalia). *Evolution* **73**, 524–539. (doi:10.1111/evo.13689)
28. Musser AM. 2003 Review of the monotreme fossil record and comparison of palaeontological and molecular data. *Comp. Biochem. Physiol. A. Mol. Integr. Physiol.* **136**, 927–942. (doi:10.1016/S1095-6433(03)00275-7)
29. Clarke JT, Friedman M. 2018 Body-shape diversity in Triassic–Early Cretaceous neopterygian fishes: sustained holostean disparity and predominantly gradual increases in teleost phenotypic variety. *Paleobiology* **44**, 402–433. (doi:10.1017/pab.2018.8)
30. Schaeffer B. 1952 Rates of Evolution in the Coelacanth and Dipnoan Fishes. *Evolution* **6**, 101. (doi:10.2307/2405507)
31. Challands TJ, Smithson TR, Clack JA, Bennett CE, Marshall JEA, Wallace-Johnson SM, Hill H. 2019 A lungfish survivor of the end-Devonian extinction and an Early Carboniferous dipnoan radiation. *J. Syst. Palaeontol.* **17**, 1825–1846. (doi:10.1080/14772019.2019.1572234)
32. Konishi S, Kitagawa, Genshiro. 1996 Generalised information criteria in model selection.

Biometrika **83**, 875–890. (doi:10.1093/biomet/83.4.875)

33. Konishi S, Kitagawa G. 2008 *Information Criteria and Statistical Modeling*. New York, NY: Springer New York. (doi:10.1007/978-0-387-71887-3)
34. Clavel J, Aristide L, Morlon H. 2019 A Penalized Likelihood Framework for High-Dimensional Phylogenetic Comparative Methods and an Application to New-World Monkeys Brain Evolution. *Syst. Biol.* **68**, 93–116. (doi:10.1093/sysbio/syy045)
35. Dollo L. 1895 Sur la phylogénie des Dipneustes. *Bull. Société Belge Géologie Paléontol. Hydrol.* **9**, 79–128.
36. Ahlberg PE, Trewin NH. 1994 The postcranial skeleton of the Middle Devonian lungfish *Dipterus valenciennesi*. *Trans. R. Soc. Edinb. Earth Sci.* **85**, 159–175. (doi:10.1017/S0263593300003588)
37. Friedman M, Daeschler EB. 2006 Late Devonian (Famennian) lungfishes from the Catskill Formation of Pennsylvania, USA. *Palaeontology* **49**, 1167–1183. (doi:10.1111/j.1475-4983.2006.00594.x)
38. Friedman M, Coates MI. 2006 A newly recognized fossil coelacanth highlights the early morphological diversification of the clade. *Proc. R. Soc. B Biol. Sci.* **273**, 245–250. (doi:10.1098/rspb.2005.3316)
39. Clarke JT, Lloyd GT, Friedman M. 2016 Little evidence for enhanced phenotypic evolution in early teleosts relative to their living fossil sister group. *Proc. Natl. Acad. Sci.* **113**, 11531–11536. (doi:10.1073/pnas.1607237113)
40. Hopkins MJ, Lidgard S. 2012 Evolutionary mode routinely varies among morphological traits within fossil species lineages. *Proc. Natl. Acad. Sci.* **109**, 20520–20525. (doi:10.1073/pnas.1209901109)

41. Foote M. 1997 The evolution of morphological diversity. *Annu. Rev. Ecol. Syst.* **28**, 129–152. (doi:10.1146/annurev.ecolsys.28.1.129)
42. Sidlauskas B. 2008 Continuous and arrested morphological diversification in sister clades of characiform fishes: a phylomorphospace approach. *Evolution* **62**, 3135–3156. (doi:10.1111/j.1558-5646.2008.00519.x)
43. Toriño P, Soto M, Perea D. 2021 A comprehensive phylogenetic analysis of coelacanth fishes (Sarcopterygii, Actinistia) with comments on the composition of the Mawsoniidae and Latimeriidae: evaluating old and new methodological challenges and constraints. *Hist. Biol.* **33**, 3423–3443. (doi:10.1080/08912963.2020.1867982)
44. Dutel H, Maisey JG, Schwimmer DR, Janvier P, Herbin M, Clément G. 2012 The Giant Cretaceous Coelacanth (Actinistia, Sarcopterygii) *Megalocoelacanthus dobiei* Schwimmer, Stewart & Williams, 1994, and Its Bearing on Latimerioidei Interrelationships. *PLoS ONE* **7**, e49911. (doi:10.1371/journal.pone.0049911)
45. Cavin L, Mennecart B, Obrist C, Costeur L, Furrer H. 2017 Heterochronic evolution explains novel body shape in a Triassic coelacanth from Switzerland. *Sci. Rep.* **7**, 13695. (doi:10.1038/s41598-017-13796-0)
46. Schultze H-P, Chorn J. 1997 The Permo-Carboniferous genus *Sagenodus* and the beginning of modern lungfish. *Contrib. Zool.* **67**, 9–70.
47. Schultze H-P. 2001 *Melanognathus*, a primitive dipnoan from the Lower Devonian of the Canadian arctic and the interrelationships of Devonian dipnoans. *J. Vertebr. Paleontol.* **21**, 781–794. (doi:10.1671/0272-4634(2001)021[0781:MAPDFT]2.0.CO;2)
48. Schultze H-P. 2004 Mesozoic sarcopterygians. In *Mesozoic Fishes 3 – Systematics, Paleoenvironments and Biodiversity* (eds G Arratia, A Tintori), pp. 463–492. München:

Verlag Dr. Friedrich Pfeil.

49. Criswell KE. 2015 The comparative osteology and phylogenetic relationships of African and South American lungfishes (Sarcopterygii: Dipnoi). *Zool. J. Linn. Soc.* **174**, 801–858. (doi:10.1111/zoj.12255)
50. Smithson TR, Richards KR, Clack JA. 2016 Lungfish diversity in Romer's Gap: reaction to the end-Devonian extinction. *Palaeontology* **59**, 29–44. (doi:10.1111/pala.12203)
51. Schultze H-P, Marshall CR. 1993 Contrasting the use of functional complexes and isolated characters in lungfish evolution. *Mem. Assoc. Australas. Palaeontol.* **15**, 211–224.
52. López-Arbarello A, Sferco E. 2018 Neopterygian phylogeny: the merger assay. *R. Soc. Open Sci.* **5**, 172337. (doi:10.1098/rsos.172337)
53. Bouckaert R, Heled J, Kühnert D, Vaughan T, Wu C-H, Xie D, Suchard MA, Rambaut A, Drummond AJ. 2014 BEAST 2: A Software Platform for Bayesian Evolutionary Analysis. *PLoS Comput. Biol.* **10**, e1003537. (doi:10.1371/journal.pcbi.1003537)
54. Bouckaert R *et al.* 2019 BEAST 2.5: An advanced software platform for Bayesian evolutionary analysis. *PLOS Comput. Biol.* **15**, e1006650. (doi:10.1371/journal.pcbi.1006650)
55. Stadler T. 2010 Sampling-through-time in birth–death trees. *J. Theor. Biol.* **267**, 396–404. (doi:10.1016/j.jtbi.2010.09.010)
56. Heath TA, Huelsenbeck JP, Stadler T. 2014 The fossilized birth-death process for coherent calibration of divergence-time estimates. *Proc. Natl. Acad. Sci.* **111**, E2957–E2966. (doi:10.1073/pnas.1319091111)
57. Arcila D, Pyron RA, Tyler JC, Ortí G, Betancur-R R. 2015 An evaluation of fossil tip-dating versus node-age calibrations in tetraodontiform fishes (Teleostei: Percomorphaceae). *Mol.*

Phylogenet. Evol. **82**, 131–145. (doi:10.1016/j.ympev.2014.10.011)

58. Grimm GW, Kapli P, Bomfleur B, McLoughlin S, Renner SS. 2015 Using More Than the Oldest Fossils: Dating Osmundaceae with Three Bayesian Clock Approaches. *Syst. Biol.* **64**, 396–405. (doi:10.1093/sysbio/syu108)
59. Zhang C, Stadler T, Klopfstein S, Heath TA, Ronquist F. 2016 Total-Evidence Dating under the Fossilized Birth–Death Process. *Syst. Biol.* **65**, 228–249. (doi:10.1093/sysbio/syv080)
60. Luo A, Duchêne DA, Zhang C, Zhu C-D, Ho SYW. 2019 A Simulation-Based Evaluation of Tip-Dating Under the Fossilized Birth–Death Process. *Syst. Biol.* **syz038**. (doi:10.1093/sysbio/syz038)
61. Lewis PO. 2001 A likelihood approach to estimating phylogeny from discrete morphological character data. *Syst. Biol.* **50**, 913–925. (doi:10.1080/106351501753462876)
62. Zhu M, Zhao W, Jia L, Lu J, Qiao T, Qu Q. 2009 The oldest articulated osteichthyan reveals mosaic gnathostome characters. *Nature* **458**, 469–474. (doi:10.1038/nature07855)
63. Matzke NJ, Wright A. 2016 Inferring node dates from tip dates in fossil Canidae: the importance of tree priors. *Biol. Lett.* **12**, 20160328. (doi:10.1098/rsbl.2016.0328)
64. Kemp A, Cavin L, Guinot G. 2017 Evolutionary history of lungfishes with a new phylogeny of post-Devonian genera. *Palaeogeogr. Palaeoclimatol. Palaeoecol.* **471**, 209–219. (doi:10.1016/j.palaeo.2016.12.051)
65. Longrich NR. 2017 A stem lepidosireniform lungfish (Sarcopterygia: Dipnoi) from the Upper Eocene of Libya, North Africa and implications for Cenozoic lungfish evolution. *Gondwana Res.* **42**, 140–150. (doi:10.1016/j.gr.2016.09.007)
66. Capobianco A, Friedman M. 2019 Vicariance and dispersal in southern hemisphere freshwater fish clades: a palaeontological perspective. *Biol. Rev.* **94**, 662–699.

(doi:10.1111/brv.12473)

67. Grande L. 2010 An Empirical and Synthetic Pattern Study of Gars (Lepisosteiformes) and Closely Related Species, Based Mostly on Skeletal Anatomy. The Resurrection of Holostei. *Copeia* **10**, 1–871.
68. Rambaut A, Drummond AJ, Xie D, Baele G, Suchard MA. 2018 Posterior Summarization in Bayesian Phylogenetics Using Tracer 1.7. *Syst. Biol.* **67**, 901–904. (doi:10.1093/sysbio/syy032)
69. Gradstein FM, Ogg JG, Schmitz MD, Ogg GM. 2012 *The Geologic Time Scale 2012*. 1st ed. Amsterdam; Boston: Elsevier.
70. Ogg JG, Ogg GM, Gradstein FM. 2016 *A Concise Geologic Time Scale 2016*. Amsterdam, Netherlands: Elsevier.
71. Gradstein FM, Ogg JG, Schmitz MD, Ogg GM. 2020 *The Geologic Time Scale 2020*. Amsterdam: Elsevier.
72. King B, Rücklin M. 2020 Tip dating with fossil sites and stratigraphic sequences. *PeerJ* **8**, e9368. (doi:10.7717/peerj.9368)
73. Revell LJ. 2012 phytools: an R package for phylogenetic comparative biology (and other things). *Methods Ecol. Evol.* **3**, 217–223. (doi:10.1111/j.2041-210X.2011.00169.x)
74. Paradis E, Claude J, Strimmer K. 2004 APE: Analyses of Phylogenetics and Evolution in R language. *Bioinformatics* **20**, 289–290. (doi:10.1093/bioinformatics/btg412)
75. Close RA, Johanson Z, Tyler JC, Harrington RC, Friedman M. 2016 Mosaicism in a new Eocene pufferfish highlights rapid morphological innovation near the origin of crown tetraodontiforms. *Palaeontology* **59**, 499–514. (doi:10.1111/pala.12245)
76. Jombart T *et al.* 2014 OutbreakTools: A new platform for disease outbreak analysis using the

R software. *Epidemics* **7**, 28–34. (doi:10.1016/j.epidem.2014.04.003)

77. R Core Team. 2013 R: A language and environment for statistical computing.
78. Wagner PJ. 2000 Exhaustion of morphologic character states among fossil taxa. *Evolution* **54**, 365–386. (doi:10.1111/j.0014-3820.2000.tb00040.x)
79. Wagner PJ, Ruta M, Coates MI. 2006 Evolutionary patterns in early tetrapods. II. Differing constraints on available character space among clades. *Proc. R. Soc. B Biol. Sci.* **273**, 2113–2118. (doi:10.1098/rspb.2006.3561)
80. Oyston JW, Hughes M, Wagner PJ, Gerber S, Wills MA. 2015 What limits the morphological disparity of clades? *Interface Focus* **5**, 20150042. (doi:10.1098/rsfs.2015.0042)
81. Brocklehurst N, Benson RJ. 2021 Multiple paths to morphological diversification during the origin of amniotes. *Nat. Ecol. Evol.* **5**, 1243–1249. (doi:10.1038/s41559-021-01516-x)
82. Brocklehurst N, Panciroli E, Benevento GL, Benson RBJ. 2021 Mammaliaform extinctions as a driver of the morphological radiation of Cenozoic mammals. *Curr. Biol.* **31**, 2955-2963.e4. (doi:10.1016/j.cub.2021.04.044)
83. Olsen AM, Westneat MW. 2015 StereoMorph: an R package for the collection of 3D landmarks and curves using a stereo camera set-up. *Methods Ecol. Evol.* **6**, 351–356. (doi:10.1111/2041-210X.12326)
84. Adams DC, Otárola-Castillo E. 2013 geomorph: an r package for the collection and analysis of geometric morphometric shape data. *Methods Ecol. Evol.* **4**, 393–399. (doi:10.1111/2041-210X.12035)
85. Baken EK, Collyer ML, Kaliontzopoulou A, Adams DC. 2021 geomorph v4.0 and gmShiny: Enhanced analytics and a new graphical interface for a comprehensive morphometric

experience. *Methods Ecol. Evol.* **12**, 2355–2363. (doi:10.1111/2041-210X.13723)

86. Clavel J, Escarguel G, Merceron G. 2015 mvMORPH: an R package for fitting multivariate evolutionary models to morphometric data. *Methods Ecol. Evol.* **6**, 1311–1319. (doi:10.1111/2041-210X.12420)
87. Hansen TF. 1997 Stabilizing selection and the comparative analysis of adaptation. *Evolution* **51**, 1341–1351. (doi:10.1111/j.1558-5646.1997.tb01457.x)
88. Ho LST, Ané C. 2014 Intrinsic inference difficulties for trait evolution with Ornstein-Uhlenbeck models. *Methods Ecol. Evol.* **5**, 1133–1146. (doi:10.1111/2041-210X.12285)
89. Blomberg SP, Garland Jr. T, Ives AR. 2003 Testing for phylogenetic signal in comparative data: behavioral traits are more labile. *Evolution* **57**, 717–745. (doi:10.1111/j.0014-3820.2003.tb00285.x)
90. Silvestro D, Kostikova A, Litsios G, Pearman PB, Salamin N. 2015 Measurement errors should always be incorporated in phylogenetic comparative analysis. *Methods Ecol. Evol.* **6**, 340–346. (doi:10.1111/2041-210X.12337)

Chapter 3 – A New ‘Phaneropleurid’-Grade Lungfish (Sarcopterygii, Dipnoi) From the Late Devonian (Frasnian) Fram Formation, Nunavut, Canada

3.1 Abstract

The Late Devonian was marked by significant anatomical shifts in vertebrates tied to the emergence of new freshwater environments. The fossils preserved at these localities, most famously the tetrapodomorphs and lungfishes, belonged to a fauna that was already rapidly developing into more modern forms. One group of lungfishes, the ‘phaneropleurids’, possess a collection of transitional traits, including the dorsal extent of the midline fins, an intermediate between the more primitive short-based second dorsal fin (e.g., porolepiform-like) and the more derived continuous median fin fringe (e.g., *Neoceratodus*-like). Here, I describe a rare, three-dimensionally preserved ‘phaneropleurid’-grade lungfish from the Late Devonian (Frasnian) Fram Formation in Canada, focusing primarily on cranial and articulated post-cranial material. I diagnose this new species of lungfish using the E bones scalloped laterally by the ‘M’ and ‘L’ bones, an elongated ‘B’ bone with a small anterior projection, expansive ornamentation on the skull roof that coarsens laterally, and a large body length of approximately one meter. I use additional material to enhance the description, including various skull roofs, a preserved braincase, incomplete lower jaw elements, opercula, shoulder girdle, and an articulated postcranial skeleton. The lungfish also possesses an elongated base of the second dorsal fin, a notable characteristic that places it among ‘phaneropleurids’ like the roughly contemporaneous *Scaumenacia curta* from Miguasha in Canada. Both lungfishes also share more general anatomy including the pattern of skull roof bones, toothplates, and shoulder girdle. The study of this and

other transitional lineages can provide much needed character data and contribute to a resolution of the persistent ambiguities in the patterns and interrelationships of the Devonian lungfish evolutionary tree.

3.2 Introduction

The Late Devonian is an important interval of anatomical and environmental change in vertebrates, with tetrapodomorphs representing the most celebrated example (Clack 2012). The first body fossils of digited tetrapods date to this interval and are often (Cressler et al. 2010; Daeschler and Cressler 2011), but not exclusively (Ahlberg 2018; Goedert et al. 2018), found in deposits representing new continental aquatic settings whose origins appear to reflect the early proliferation of terrestrial floras (Algeo et al. 2001; Davies and Gibling 2010; Morris et al. 2018). The Upper Devonian (Frasnian) Fram Formation of Ellesmere Island, Nunavut, Canada yields a significant vertebrate assemblage offering a glimpse of an early fluvial ecosystem (Daeschler et al. 2006; Downs et al. 2011, 2019). A series of expeditions (2000–2014) recovered numerous fishes similar to those known from other sites of similar age. Described examples include the antiarch placoderms *Asterolepis* (Downs et al. 2019) and *Bothriolepis* (Downs et al. 2016), the porolepiforms *Holoptychius* (Downs et al. 2013) and *Laccognathus* (Downs et al. 2011), the tetrapodomorph fish *Eusthenopteron* (Downs, et al. 2018), and—most famously—the elpistostegalians *Tiktaalik* (Daeschler et al. 2006) and *Qikiqtania* (Stewart et al. 2022). Lungfishes, the most species-rich group of Devonian sarcopterygians (Cloutier and Ahlberg 1996) and well-known from many roughly coeval sites representing similar continental-to-marginal marine ecosystems (Sallan and Coates 2010; Schultze 2010; Cloutier et al. 2011), are conspicuously absent from this roster of described vertebrates from the Fram Formation.

However, locality NV2K17 does yield abundant, well-preserved remains of a large (~1 meter total length) 'phaneropleurid' lungfish. These materials, representing the remains of several individuals in varying degrees of disarticulation and mentioned in accounts of other fishes from the Fram Formation (e.g., Downs et al. 2011), are the focus of this contribution.

'Phaneropleurids' represent an ill-defined and likely paraphyletic (Schultze and Marshall 1993) assortment of Middle-Late Devonian lungfishes, characterized principally by an elongated base of the second dorsal fin (Cloutier and Ahlberg 1996; Challands and den Blaauwen 2017). The namesake for this group—the Late Devonian (Famennian) *Phaneropleuron*—is relatively poorly known (Traquair 1871). Instead, 'phaneropleurids' have come to be defined using comparisons between various other genera, including the *Howidipterus* and *Barwickia* from Australia (Long 1992, 1993; Long and Clement 2009), Middle Devonian *Pentlandia* from Scotland (Jude et al. 2014; Challands and den Blaauwen 2017), and the Late Devonian *Scaumenacia* (Cloutier 1996, 1997; Boirot et al. 2022). The latter is perhaps the best-known of the 'phaneropleurid' group owing in part to their abundance within the Frasnian-age Miguasha Lagerstätte of Quebec, Canada, with nearly 1,500 individuals reported in a limited survey of major museum collections (Parent and Cloutier 1996).

'Phaneropleurids' collectively capture an intermediate morphology that straddles the transition between the plesiomorphic, short-based dorsal fins of most other Devonian lungfishes (i.e., a generalized sarcopterygian postcranial structure) and the long-based posterior dorsal fins common in post-Devonian forms (i.e., a modern lungfish-like postcranial structure) (Cloutier and Ahlberg 1996; Friedman 2010). As such, 'phaneropleurids' have featured prominently in models of evolutionary transformation within dipnoans beginning with Luis Dollo's (1895) iconic depiction of orthogenic change in lungfish postcranial anatomy. Nonetheless, the specifics of this

transformation remain elusive and, although different authors suggest contrasting views on the relative scope and composition of the group (Cloutier and Ahlberg 1996), characters in core 'phaneropleurids' like *Pentlandia* and *Scaumenacia* can be used to help document this change.

This comparative approach is typically used because the relationships of 'phaneropleurids' to one another and to other fossil lungfishes are highly unstable, reflecting broader issues of phylogenetic uncertainty among Devonian dipnoans (Miles 1977; Campbell and Barwick 1990; Schultze and Marshall 1993; Cloutier and Ahlberg 1996; Schultze 2001; Friedman 2007a; Qiao and Zhu 2009; Lloyd et al. 2011; Kemp et al. 2017). Two factors limit the information available for resolving the relationships of 'phaneropleurids'. First, many 'phaneropleurids' show substantially reduced ossification of the endoskeleton. This is most pronounced for anatomically complex structures like braincases that represent a significant source of phylogenetic characters for some lungfishes (Friedman 2007b) and other sarcopterygian lineages such as stem tetrapods (Coates and Friedman 2010; Friedman et al., in press). Boirot et al. (2022) report endocranial remains for both *Scaumenacia* and *Pentlandia* based on micro-CT scanning, but the available material is challenging and specific details are difficult to discern in the resulting models. Second, even in cases where 'phaneropleurids' are known from articulated individuals, these specimens are typically heavily flattened. Thus, individual bones cannot be easily examined in three dimensions, as is possible for some Devonian lungfishes (most notably those from the Late Devonian Gogo and Early Devonian Wee Jasper Lagerstätten in Australia) (Miles 1977; Campbell et al. 2009), further limiting available character data.

Significantly, remains from the Fram Formation address both of these gaps in our understanding. First, the new lungfish preserves the first well-preserved braincase material in a

‘phaneropleurid’ that can be examined *in situ* rather than indirectly through computed tomography. This consists of a somewhat compressed but otherwise intact occipital region directly comparable to that of other Devonian lungfishes represented by more complete neurocranial remains (e.g., Miles, 1977). Second, individual bones of the new lungfish from the Fram Formation are not fully flattened and instead provide substantial relief. Many individual bones are fully freed from the surrounding matrix, permitting detailed examination of all surfaces.

Here, I provide a detailed account of the anatomy in the lungfish from the Fram Formation, thereby filling important gaps in our present understanding of ‘phaneropleurid’ osteology. Comparisons are made to other early lungfishes, with a particular emphasis on identifying characters that might be useful additions to existing character lists used in phylogenetic analyses.

3.3 Materials and Methods

3.3.1 Mechanical Preparation

Specimens from the NV2K17 locality were mechanically prepared under a binocular microscope at the Academy of Natural Sciences of Drexel University, with most prepared by Fred Mullison.

3.3.2 Photography and Photogrammetry

Specimens were photographed at the Academy of Natural Sciences of Philadelphia at Drexel University and the University of Michigan Museum of Paleontology using a Nikon D810

SLR camera. For some specimens, I generated photogrammetric models following protocols for the University of Michigan Online Repository of Fossils (UMORF; https://umorf.ummp.lsa.umich.edu/wp/about/project-methods/). In brief, this entailed placing a specimen on a turntable in a light box, often on top of transparent plastic cubes and taking ~25 photographs at approximately equal rotational increments. These sets of images are taken with the camera set to three angular orientations with respect to the turntable: 60°, 45°, and 10°. Following this, the specimen is turned to the opposite face and the process repeated. For flatter fossils, they are turned upright and the process is repeated one final time. This series of photographs is then processed to generate a three-dimensional model in the software RealityCapture (Capturing Reality, Bratislava, Slovakia).

3.3.3 Computed Tomography

I produced two micro-computed tomography (μCT) scans of one specimen (NUFV 764) using a Nikon XT H 225ST (Xtek, Tring, UK) industrial scanner in the Computed Tomography in Earth and Environmental Science (CTEES) facility, Department of Earth and Environmental Sciences, University of Michigan. These scans were of (a) the entire skull roof and (b) a region-of-interest scan targeting neurocranial ossifications in the occipital region. Parameters for these scans are as follows: (a) 190 kV energy, 167 μA current, 1.43 s exposure, and a 1 mm copper filter (effective pixel size of 93.2485 μm and geometric magnification of 2.145) and (b) 180 kV energy, 185 μA current, 2.829 s exposure, and a 2 mm copper filter (effective pixel size of 46.1436 μm and geometric magnification of 4.334). Both scans took an optimized number of projections (3,142) and used the option to minimize ring artifacts. The resulting tomograms were

segmented using Materialise Mimics v19.0 (Materialise, Belgium), with surface meshes exported as PLY files.

3.3.4 3D Modeling and Image Rendering

Models derived from photogrammetry and μCT scanning were imported and rendered in Blender v4.0 (https://blender.org/). Custom shading, reflection, and ambient occlusion were added via a principled BSDF material node and the results were rendered using the cycles engine.

3.3.5 Anatomical Terminology

Here, I apply the standard alphabetic-numeric system of nomenclature for dermal bones of the lungfish skull roof and cheek following the convention first established by Foster-Cooper (1937). I recognize the homologies between several of these bones and those in more conventional sarcopterygians outlined by Ahlberg (1991). Terminology of other parts of cranial anatomy largely follows that of Miles (1977) and terminology for the components of the postcranial axial skeleton follow Ahlberg and Trewin (1994) (see Friedman 2010).

Institutional Abbreviations—**ANSP**, The Academy of Natural Sciences of Drexel University, Philadelphia, PA, U.S.A.; **NUFV**, Nunavut Fossil Vertebrate Collection, Canadian Museum of Nature, Ottawa, Canada.

3.4 Systematic Paleontology

OSTEICHTHYES Huxley, 1880

SARCOPTERYGII Romer, 1955

RHIPIDISTIA Cope, 1887 sensu Cloutier and Ahlberg, 1996

DIPNOMORPHA Ahlberg, 1991

DIPNOI Müller, 1845

'PHANEROPLEURIDAE' Huxley, 1861 sensu Cloutier and Ahlberg, 1996

SCAUMENACIA Traquair, 1893

SCAUMENACIA ORNATISSIMA, sp. nov.

Holotype—NUFV 793, an articulated postcranial axial skeleton (**Figure 3.1**) , including partial median fins and internal supports, scales, right clavicle and cleithrum, left clavicle, parasphenoid stalk, partial ceratohyal, left prearticular with toothplate, left entopterygoid toothplate, small accessory toothplate, and partial skull roof.

Etymology—From the Latin 'ornatus', ornate, in reference to the well-defined ornamentation covering most of the skull roof and which is well developed compared to other Devonian lungfishes in general and *Scaumenacia curta* in particular.

Referred Specimens— The following material found at the type locality with the holotype was used to complement the description: NUFV 737, left prearticular with tooth plate; NUFV 764, a partial skull roof, left pterygopalatine tooth plate, left prearticular tooth plate, right prearticular

tooth plate, partial right clavicle, partial parasphenoid, incomplete left cirumorbital series, operculum, and other unprepared or indeterminate elements, including a possible anocleithrum; NUFV 786, incomplete left prearticular with toothplate with pathological tooth rows; NUFV 792, radials; NUFV 793, articulated post cranial axial skeleton, scales, right clavicle and cleithrum, left clavicle, parasphenoid stalk, partial ceratohyal, left prearticular with toothplate, left entopterygoid toothplate, small accessory toothplate, partial skull roof, and additional debris; NUFV 1133, cleithrum and clavicle; NUFV 1160.3, partial parasphenoid, operculum, isolated skull roof bone, clavicle fragments, fragments of dermal shoulder girdle; NUFV 1160.7, partial skull roof; NUFV 1160.6, entopterygoid tooth plates, partial right prearticular tooth plate, fragments of infradentaries; NUFV 1160.8, right prearticular tooth plate; NUFV 1160.9, skull roof fragment; NUFV 1160.10, incomplete right circumorbital series; NUFV 1160.13, partial skull roof; NUFV 1227, left cleithrum and clavicle; NUFV 1222, partial left mandibular ramus with prearticular and infradentaries.

Diagnosis—Species of *Scaumenacia* characterized by both E bones scalloped laterally by the M and L2 bones, an elongated heptagonal B bone with a small anterior projection, well-developed and dense ornamentation on bones of the skull roof, and a large body size (~1 meter total length).

Type Locality, Horizon, and Age—NV2K17 locality (77°09′59.1″N, 86°16′9.42″W) of the Fram Formation near the eastern arm of Bird Fiord on southern Ellesmere Island, Nunavut Territory, Canada (Daeschler et al. 2006). Palynological data indicate an early to middle Frasnian age (*medius* and *maclarenii* zones; Chi and Hills 1976; Embry and Klovan 1976), with an approximate numerical age of 378.9–373 Ma (Chi and Hills 1976; Becker et al. 2020).


10 cm

Figure 3.1. *Scaumenacia ornatissima* holotype (NUFV 793), showing cranial and postcranial material in dorsal view.

3.5 Description

3.5.1 Skull

General Comments—Although several specimens preserve components of the skull, NUFV 764 (**Figure 3.2**) provides the most detailed information on the cranium and is the basis of much of the following description. Information from other specimens is noted where relevant. NUFV 764 includes an incomplete skull roof (**Figure 3.3**), partial palatal and lower jaw material including three tooth plates and a partial parasphenoid, the occipital region of the neurocranium and additional skeletal fragments.

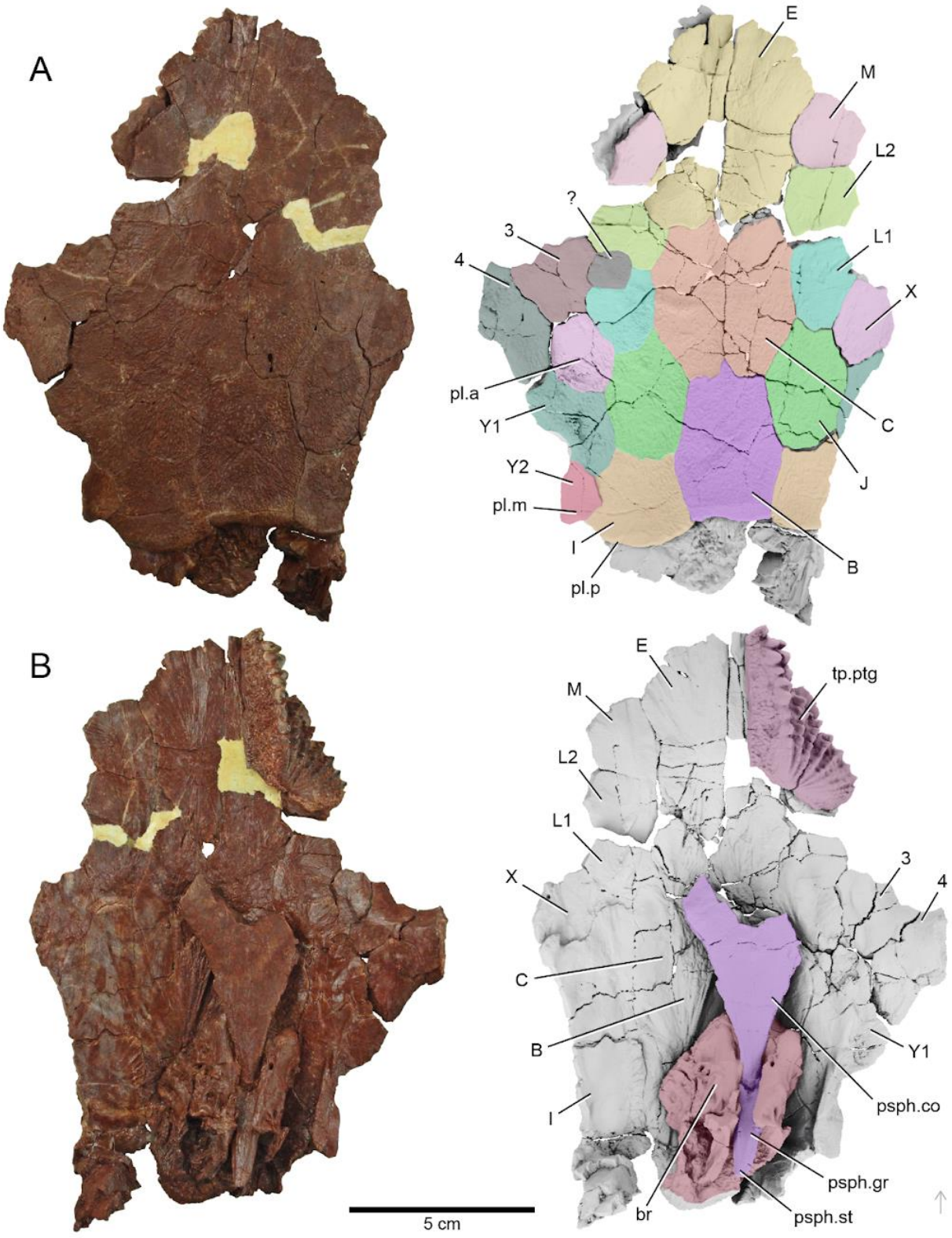

Figure 3.2. *Scaumenacia ornatissima*, skull roof, partial palate, and occipital ossification (NUFV 764). A, photograph and 3D render in dorsal view; B, photograph and 3D render in ventral view. Abbreviations: 3–4, circumorbital series of skull bones; B–E, median series of skull bones; br, braincase; I–M, lateral series of skull bones; pl.a, anterior pit line; pl.m, medial pit line; pl.p,

posterior pit line; psph.co, corpus of parasphenoid; psph.gr, groove of parasphenoid; psph.st, stalk of parasphenoid; tp.ptg, pterygoid tooth plate; X, X-bone from the lateral series of skull bones; Y1–Y2, Y-bones from the lateral series of skull bones; ?, unidentified bone from the lateral series of skull bones. Gray arrows point anteriorly.

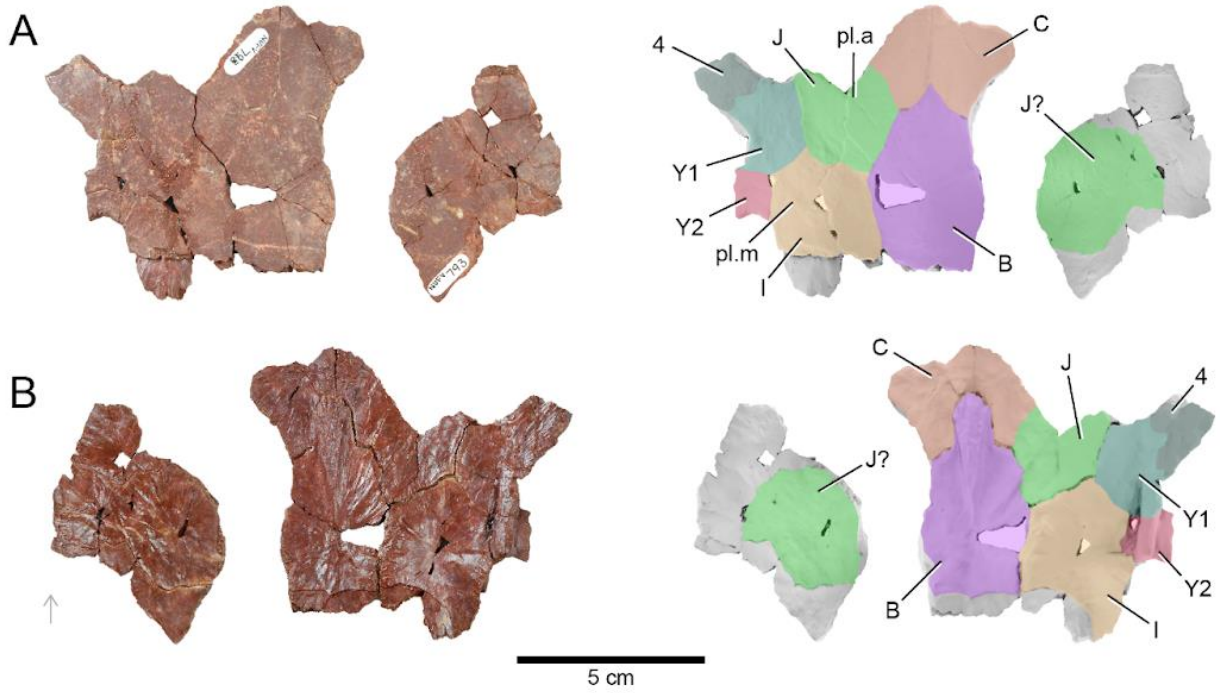

Figure 3.3. *Scaumenacia ornatissima*, fragmentary skull roof of holotype (NUFV 793). A, photograph and 3D render in dorsal view; B, photograph and 3D render in ventral view. Abbreviations: 4, bone 4 from the circumorbital series of skull bones; B–C, median series of skull bones; I–J, lateral series of skull bones; J?, unidentified bone from the lateral series of skull bones (likely J-bone); pl.a, anterior pit line; pl.m, medial pit line; Y1–Y2, Y-bones from the lateral series of skull bones. Gray arrows point anteriorly.

Snout—Although portions of the skull are preserved in multiple individuals, none preserves any components of the rostrum anterior to the E bones. The snout is therefore assumed to have been lost due to being fully unmineralized, poorly mineralized, or disarticulation.

Median Series of the Skull Roof—The median series of skull bones consists of, from posterior to anterior: a single B bone, paired C bones, and paired E bones. No specimen shows a D bone, and it is assumed to be absent (**Figure 3.2**–**Figure 3.5**).

The B bone is shaped like an anterodorsally elongated heptagon. It contributes to the rear margin of the skull roof posteriorly, contacts the I and J bones laterally, and the E bones anteriorly. Two pairs of well-developed grooves converge near the center of the B bone on its dorsal surface, defining an "X" shape (**Figure 3.6**). The anterior grooves are directed anterolaterally and align with, but do not join, corresponding grooves on the J bones. Collectively, these two segments borne by the B and J bones represent the anterior pit lines. The shorter, more posterior grooves, represent middle pit lines and are broadly separated from corresponding grooves on the I bone. The ornament on the dorsal surface of the B bone consists of closely packed, short, millimeter-scale ridges in the posterior half of the bone and more irregular ridges and protuberances in the anterior half. The posterior ridges are generally oriented toward the center of the bone. A triangular sheet of bone extends horizontally from the posterior margin of the B bone, at a level below that of the ornamented surface. This bears well-defined anteroposteriorly oriented grooves and lies in the same plane as prominent posterior extensions from the I bones. The visceral surface of the B bone is smooth, with the exception of a narrow, raised "V"-shaped feature on its anterior half. Similar structures in other Devonian lungfishes have been interpreted as an area of attachment for the median crista that suspends the neurocranium below the dermal skull roof (Miles 1977; Campbell and Barwick 1986; Friedman 2007a).

The paired C bones are longer than wide and contact each other along the midline apart from a narrow separation posteriorly by a triangular extension of the B bone. Due to the absence of the D bone, the C and E bones meet in a jagged suture anteriorly (Cloutier 1997). Each C bone contacts a J, K, and L bone laterally. The sutures between C and J and C and L are both oblique with respect to the long axis of the skull, while the suture between C and K is scalloped and

essentially oriented anteroposteriorly. Irregular protuberances and ridges ornament the dorsal surface of the posterior half of the C bones. The anterior half of the C bone is almost entirely smooth, with sparse ornamentation in a band extending parallel to the mesial margin where it contacts its antimere. The C bones bear no obvious evidence of sensory canals or pit lines, though the ventral surface of the C bone does bear a series of grooves on its anterior and posterior halves that converge at the center of ossification.

The paired E bones are longer than the C bones and are narrower posteriorly than they are anteriorly. Each E bone shows a distinctly scalloped suture along the lateral contact with the flanking M and L bones. The E bones bear no sign of sensory canals.

Lateral Series of the Skull Roof—Two series of bones flank each side of the median series of skull roof bones. The more mesial series contains only two bones, I and J. The more lateral series carries the otic and supraorbital canals and contains, from posterior to anterior: Y2, Y1, X, L1, L2, and M.

The I bone is the largest of the more mesial series. It contributes to the rear edge of the skull roof posteriorly, abuts the B bone mesially, and is scalloped laterally by the smaller, angular Y2 and the arrowhead-shaped Y1 bones. The dorsal surface of the I bone bears ornament similar to that of the adjacent B bone. A well-developed middle pit line extends laterally from near the center of the bone to its contact with bone Y2. A short posterolaterally directed groove located behind this transverse pit line represents the posterior pit line. A sheet of bone extends from the posterior margin of the I bone. Its dorsal surface lies in a plane ventral to the upper face of the skull roof, defining a distinct step. This shelf bears radiating grooves on its dorsal surface, and extends posteriorly as a prominent splint-like process. The posterior extension of the I bones

lies in the same plane as that of the B bone, defining a semicontinuous ledge tracing the rear margin of the skull roof.

The J bone resembles an anteroposteriorly elongated hexagon. It abuts the anterolateral edge of the B bone at a shallow angle and the posterolateral edge of the C bone obliquely with respect to the long axis of the skull. It is scalloped laterally by the X and anterolaterally by the L1 bones. The dorsal surface of the J bone bears ornament like that of adjacent bones. An anterolaterally directed groove located near the center of the bone represents a discontinuous extension of the anterior pit line on the B bone. The ventral surface of the J bone bears no major features.

The Y2 bone is small and scallops the I bone mesially at a pronounced triangular tip and obliquely abuts the Y1 bone anteriorly. It bears a short posterior spur that defines a distinct concavity in the posterior margin of the skull roof. A short segment of the middle pit line incises the dorsal surface of the Y2 bone, starting at the mesial suture with the I bone and terminating shortly thereafter. Sparse ornament ridges are present on the dorsal surface of the bone along with a few miniscule sensory canal pores. A thickened flange extends ventrally from the visceral surface of Y2 near its lateral margin. This prominently raised ridge extends on to Y1 and carries the otic sensory canal.

Bone Y1 bone is substantially larger than Y2, which it contacts posteriorly. The mesial margin of Y1 is gently convex and contacts the I and J bones. The anterior margin of Y1 is gently concave, and cradles bone X. The posterolateral margin of Y1, which would have accommodated the opercle in life, is convex anteriorly but strongly concave posteriorly, defining a shallow embayment in the lateral margin of the skull roof. The visceral surface of Y1 carries an

extension of the ventral flange from Y2, but the relief of this feature is substantially reduced, becoming a low swelling near the anterior margin of Y2.

The bone anterior to Y1 bears both a segment of the anterior pit line and the junction between the otic, infraorbital, and supraorbital sensory canals as gauged by the patterns of thickenings on its ventral surface. This unites the features present in separate X and K bones in *Dipterus*; consequently, such bones are sometimes termed KX (e.g., Westoll 1949; Miles 1977). However, we follow Cloutier's (1996) convention for *Scaumenacia* and term this bone X. Short ornament ridges are restricted to a band that traces the hexagonal border of the X bone on its dorsal surface. The central part of the bone bears tiny, round protuberances that are broadly separated from one another. Apart from low thickenings that reveal the course of sensory canals, the inner surface bears no major features.

The series bearing the supraorbital canal contains a variable number of bones anterior to the X bone both between and within individuals. Three bones appear to be the standard complement, identified here as L1, L2, and M following Cloutier's (1996) convention for *Scaumenacia curta*. The most posterior of these, L1, articulates with the anteromesial margin of X. It is longer than wide and bears modest ornamentation on its dorsal side, while the low thickening for the supraorbital canal extends anteromesially across its visceral surface. L2 and M lie anterior to L1, are subquadrate, and largely devoid of dorsal ornament. The thickening for the supraorbital canal defines a gentle curve on the ventral surface of these bones but is principally oriented anteroposteriorly. NUFV 764 and NUFV 794 bear a small, nearly circular bone that partially separates bones L1 and L2 but only on the anatomical left side.

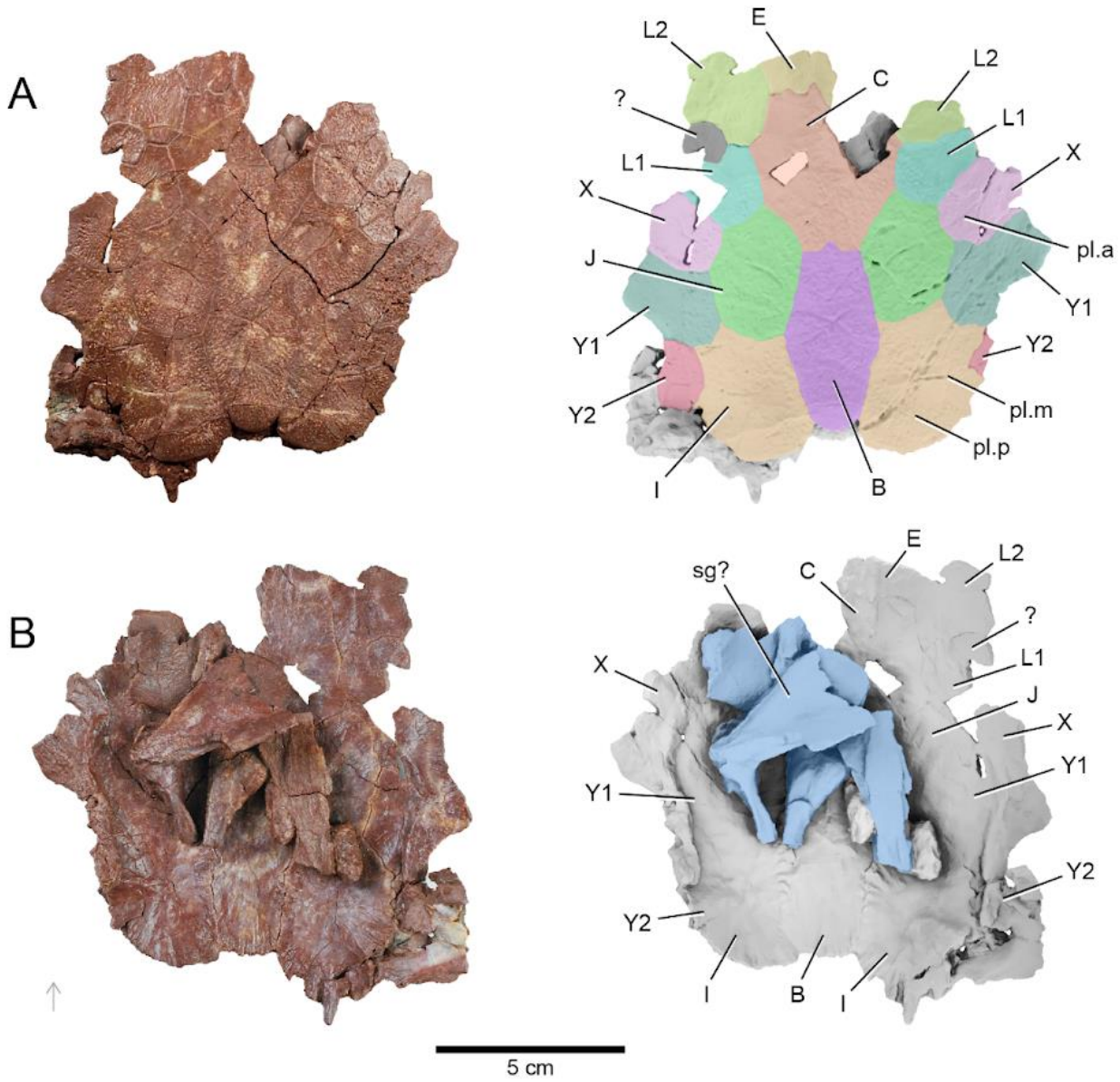

Figure 3.4. *Scaumenacia ornatissima*, partial skull roof and shoulder girdle (NUFV 794). A, photograph and 3D render in dorsal view; B, photograph and 3D render in ventral view. Abbreviations: B–E, median series of skull bones; I–L, lateral series of skull bones; pl.a, anterior pit line; pl.m, medial pit line; pl.p, posterior pit line; sg?, unidentified skeletal material (likely shoulder girdle); X, X-bone from the lateral series of skull bones; Y1–Y2, Y-bones from the lateral series of skull bones; ?, unidentified lateral series skull roof bone. Gray arrows point anteriorly.

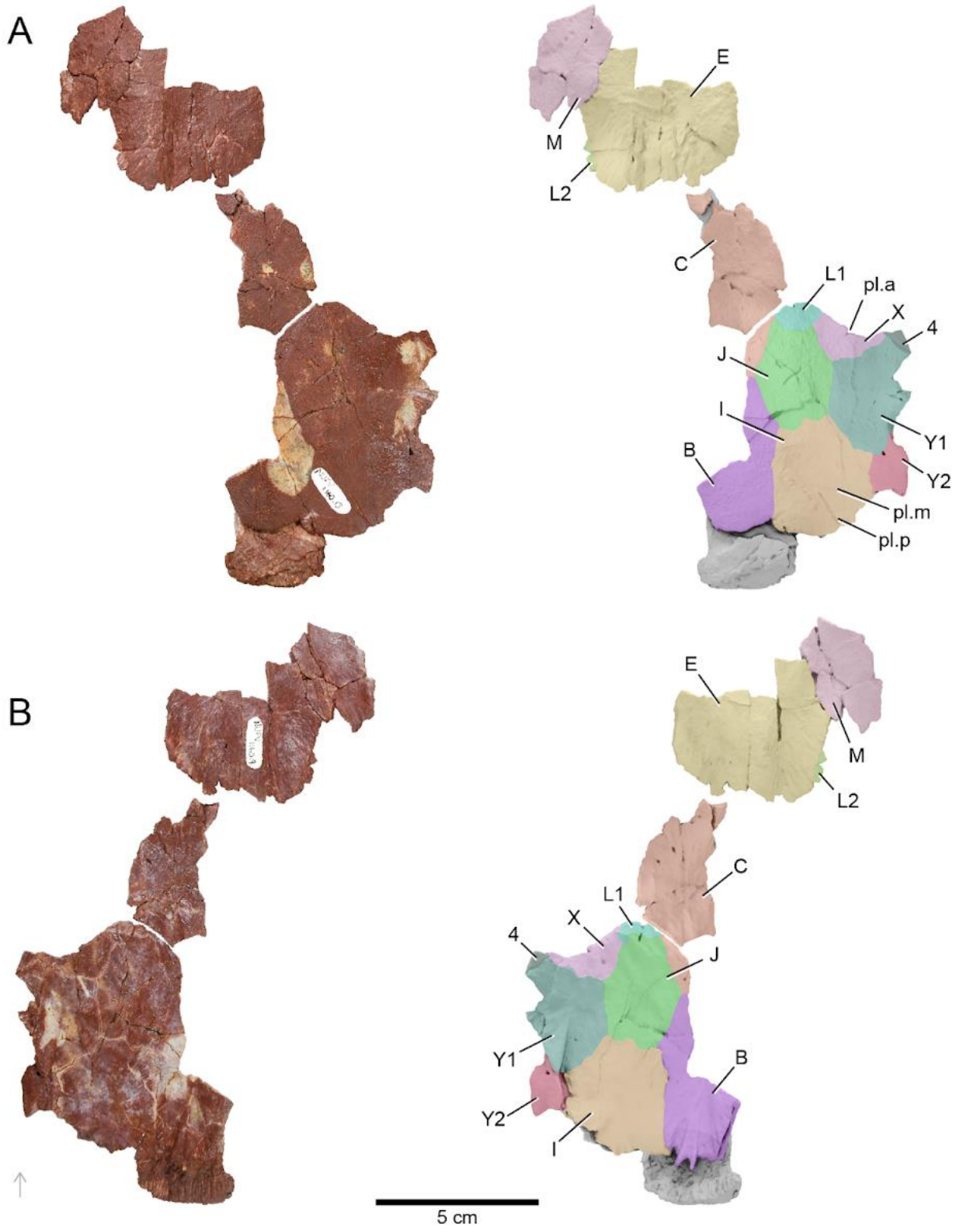

Figure 3.5. *Scaumenacia ornatissima*, skull roof (NUFV 1160.13, 1160.9). A, photograph and 3D render in dorsal view; B, photograph and 3D render in ventral view. Abbreviations: 4, bone 4 from the circumorbital series of skull bones; B–E, median

series of skull bones; I–M, lateral series of skull bones; pl.a, anterior pit line; pl.m, medial pit line; pl.p, posterior pit line; X, X-bone from the lateral series of skull bones; Y1–Y2, Y-bones from the lateral series of skull bones. Gray arrows point anteriorly.

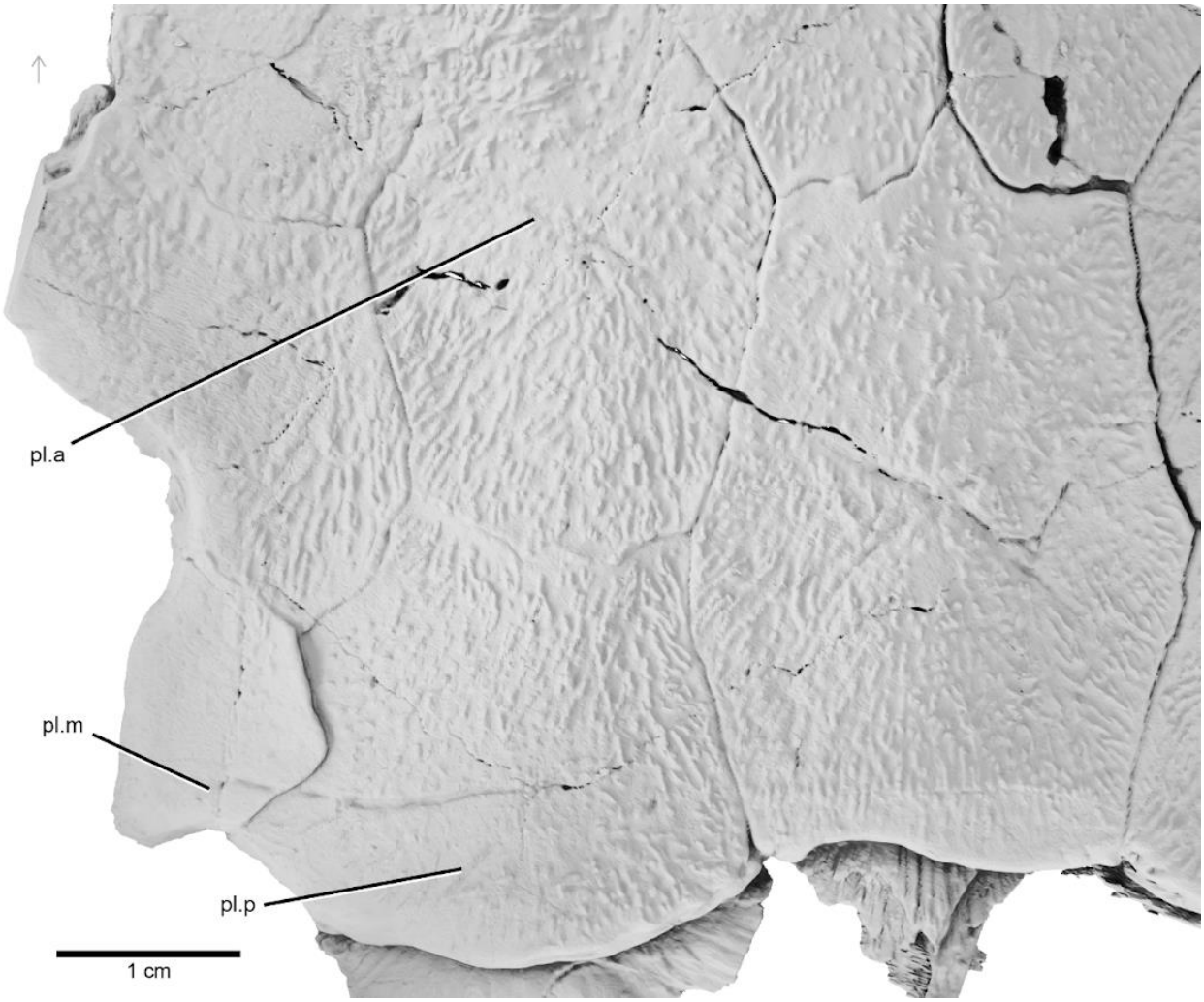

Figure 3.6. *Scaumenacia ornatissima*, skull roof close-up 3D render showing pit lines and extensive ornamentation (NUFV 764). Abbreviations: pl.a, anterior pit line; pl.m, medial pit line; pl.p, posterior pit line. Gray arrows point anteriorly.

Cheek and Circumorbital Region—No individual preserves an intact set of bones contributing to the cheek and surrounding the orbit. However, a near-complete complement is preserved between available specimens, with NUFV 764 preserving the dorsal-most parts of the series (bones 3 and 4) and NUFV 794 and 1160.10 preserving more posterior, ventral, and anterior segments (bones 5, 6, 7, 1b, and 2 and bones 5, 6, and 7, respectively). The description

provided here is a composite of these three individuals. Bone 3 is irregularly shaped, articulating with the bones X, L1, and L2 and contributing to the dorsal margin of the orbit. It bears a thickened ridge on its inner surface and a few small pores on its outer face suggesting it bears an accessory supraorbital branch of the infraorbital canal. Posteriorly, bone 3 articulates with the strap-shaped bone 4, which abuts Y1 and X mesially. A ventral articulation between bones 4 and 5 is assumed, but not preserved in any specimen. The posterior margin of bone 4 defines, along with bones Y1 and Y2, the dorsal portion of the embayment for the opercle, while its anterior margin makes a small contribution to the orbit posterior to that of bone 3. Bone 4 shows varied patterns of ornamentation on its external surface. Short ridges are present near its articulation with bones X and Y1, but the middle part of the bone is relatively smooth. The ventrolateral third of bone 4 bears coarse ornamentation, similar to that on the ventral and posterior circumorbitals. Bones 5, 6, and 7 are somewhat irregularly shaped bones that frame the posterior and ventral margins of the orbital opening. These show varying levels of surface sculpturing between individuals, ranging from densely pockmarked (NUFV 1160.10) to bearing prominent tubercular ornament (NUFV 794). As in many lungfishes, the exact shape of bones also differs between individuals. All three of these bones bear a broad thickening on their inner surface that marks the course of the infraorbital sensory canal. Rather than directly abutting, these bones overlap with the anterior part of each overlapped by the preceding ossification in the series. Bone 2 defines the anterodorsal margin of the orbit and is substantially longer than the more ventral circumorbitals. Like other bones immediately surrounding the eye, bone 2 bears a thickening on its inner surface, but it is unclear if it bore a sensory canal. A triangular bone, identified here as 1, articulates with the anterior margin of bones 2 and 7. It carries an extension of the infraorbital sensory canal from bone 2.

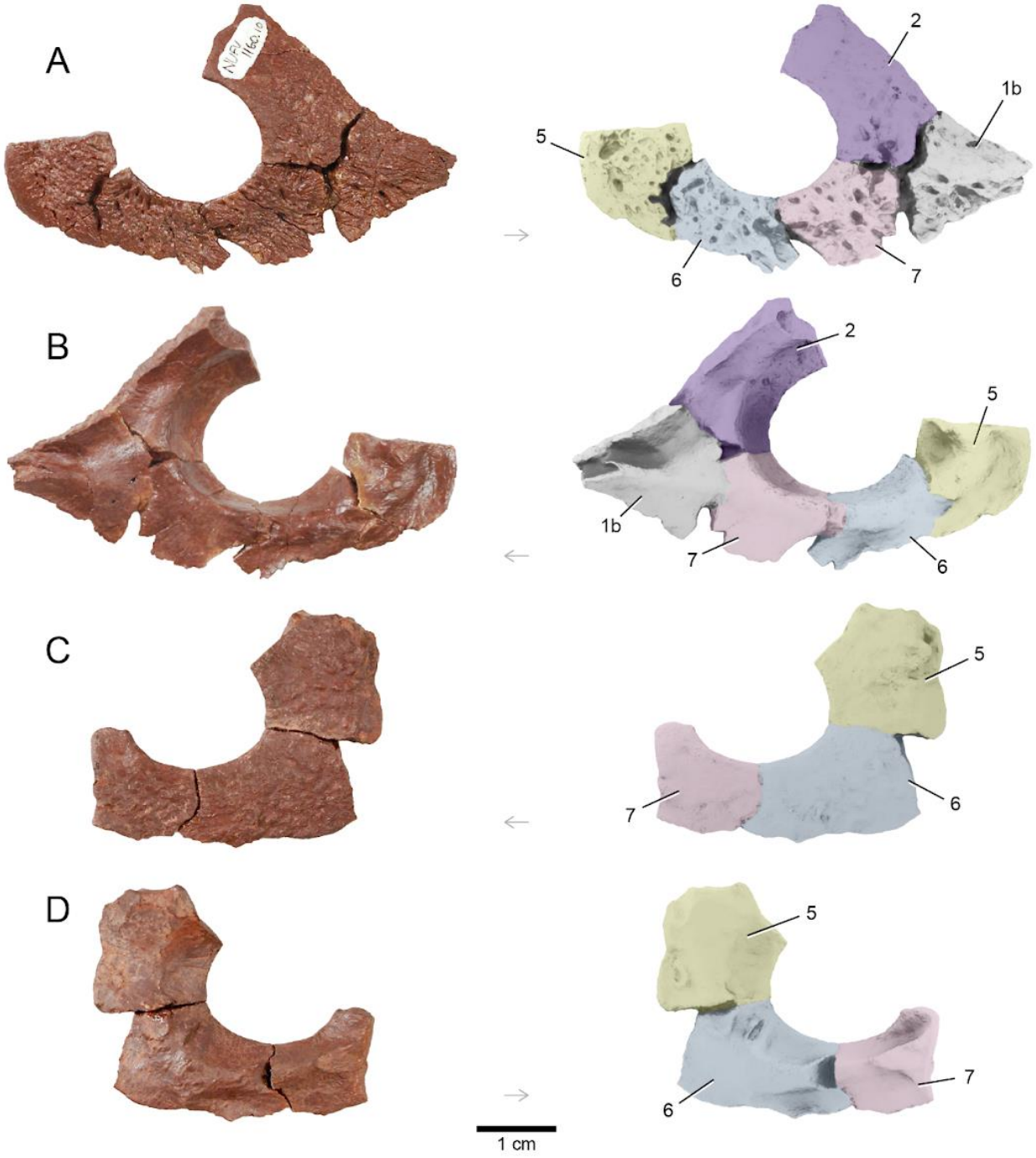

Figure 3.7. *Scaumenacia ornatissima*, circumorbital bones. A, photograph and 3D render in lateral view (NUFV 1160.10); B, photograph and 3D render in mesial view (NUFV 1160.10); C, photograph and 3D render in lateral view (NUFV 794); D, photograph and 3D render in mesial view (NUFV 794). Abbreviations: 1b, bone 1b from the circumorbital series of skull bones; 2, bone 2 from the circumorbital series of skull bones; 5–7, circumorbital series of skull bones. Gray arrows point anteriorly.

Operculogular Series— The opercle is the only component of the operculogular series identifiable in available material and is represented in specimens NUFV 764 and 794 (Fig. 8). Although the exact orientation of these specimens is hard to determine due to a lack of in situ preservation, the interpretations presented are inferred based on comparison with other Devonian lungfishes and personal observations from additional *Scaumenacia* fossils. In lateral view, the opercle is somewhat rounded, being approximately as long as it is deep. Its anterior margin is bilobed, with the more ventral of these lobes being the larger of the two and extending further anteriorly. The dorsal margin bears a pronounced hump at mid-length, possibly corresponding to the rounded embayment on the lateral margin of the skull roof contributed to by bones Y1 and Y2. The posterior margin of the opercle curves smoothly, while its ventral portion is generally straight. On the lateral surface it also has pustular ornamentation surrounding the center of the bone which, as it reaches the perimeter, transitions into short ornament ridges like those on the skull roof. This is especially noticeable along the anterior and posterior of the operculum. The inner surface of the opercle is generally smooth apart from a shallow depression offset anteriorly from the center of the bone and a slightly thickened ridge along the ventral lobe.

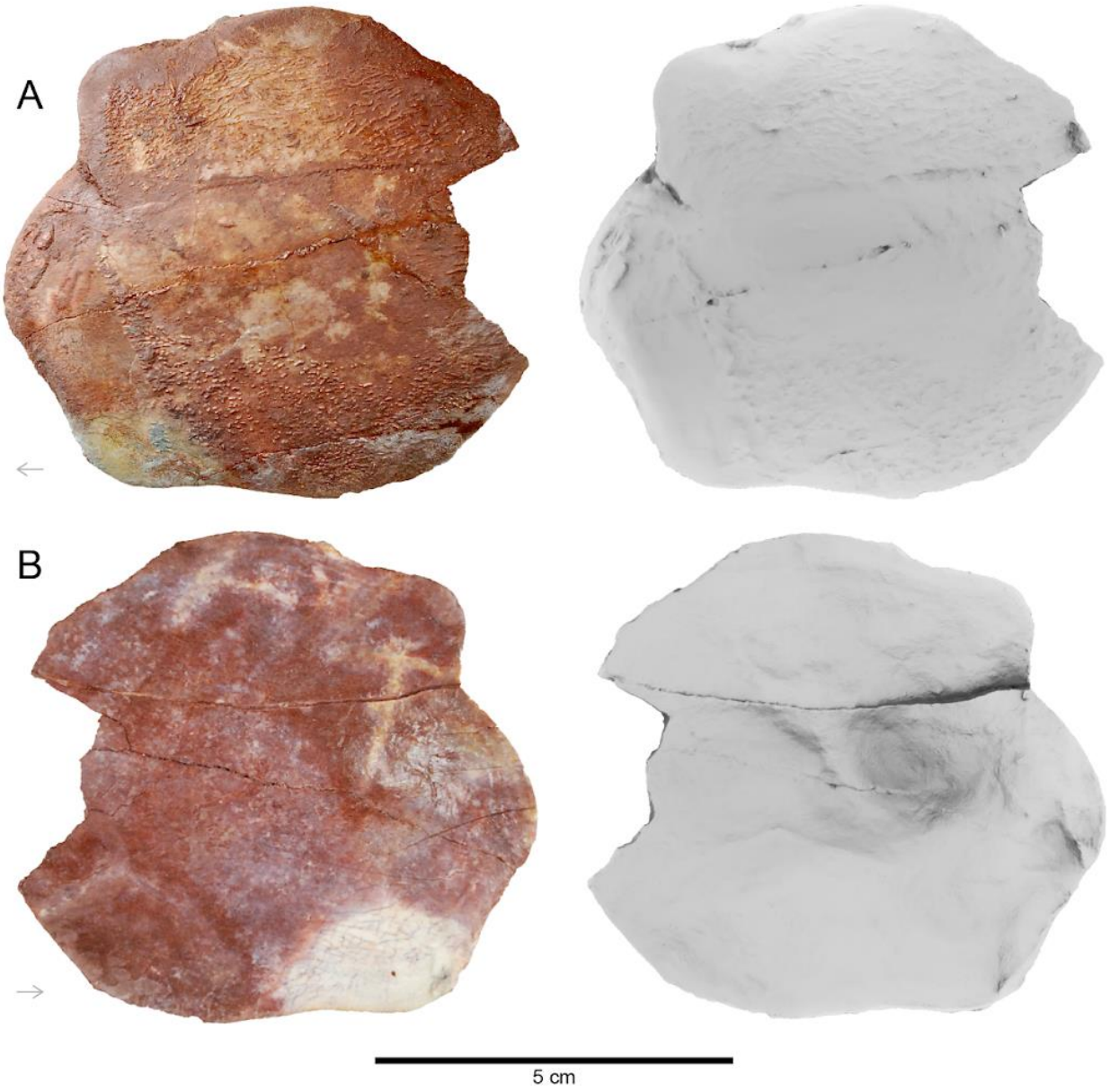

Figure 3.8. *Scaumenacia ornatissima*, opercle (NUFV 794). A, photograph and 3D render in lateral view; B, photograph and 3D render in mesial view. Gray arrows point anteriorly.

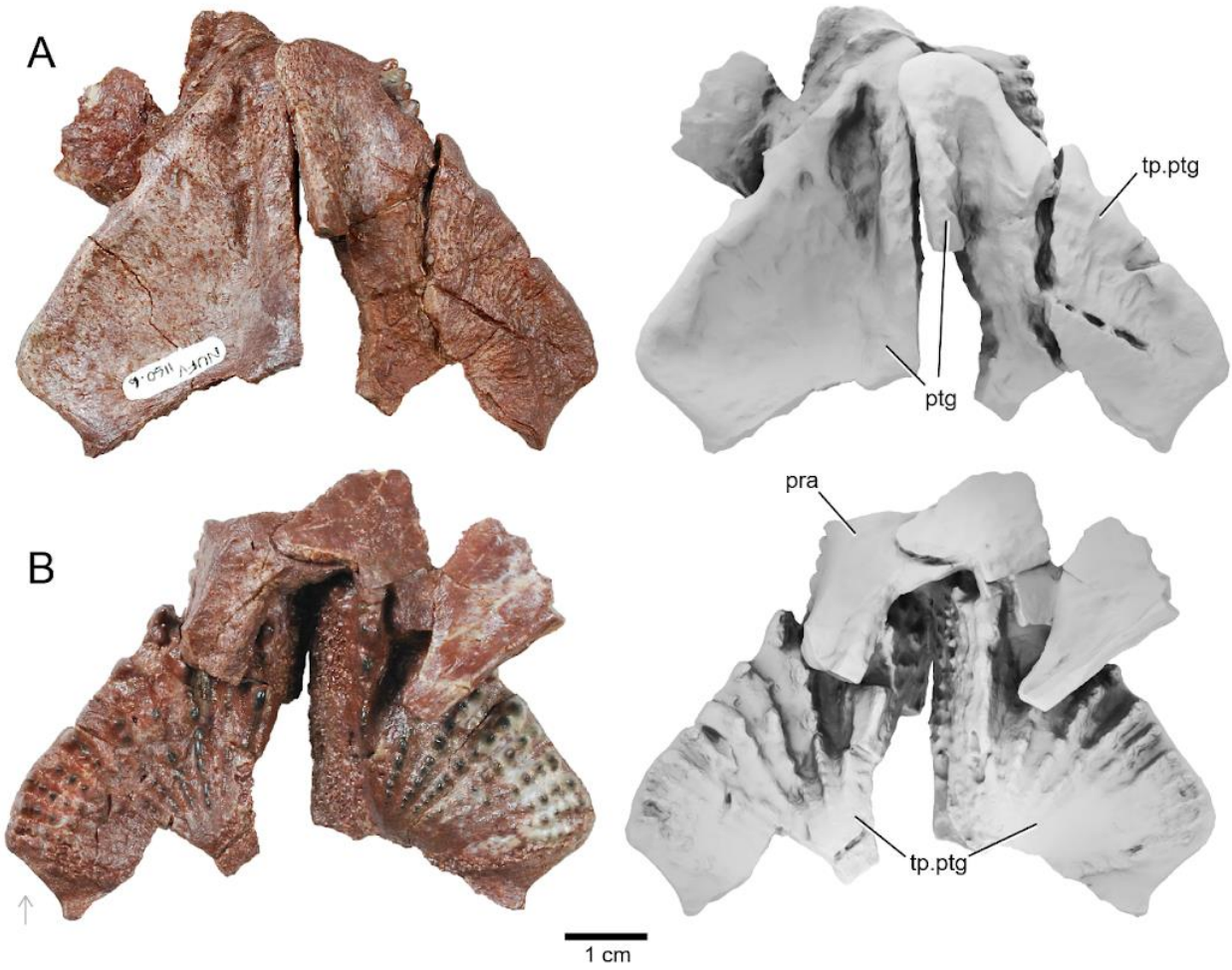

Figure 3.9. *Scaumenacia ornatissima*, articulated pterygoid toothplates and partial prearticular toothplates (NUFV 1160.6). A, photograph and 3D render in dorsal view; B, photograph and 3D render in ventral view. Abbreviations: pra, prearticular; ptg, pterygoid; tp.ptg, pterygoid toothplate. Gray arrows point anteriorly

Palate and Braincase—No single individual preserves a complete palate, so this description summarizes information from multiple specimens. Most of the palate, including the anteriormost portions are not preserved in the holotype specimen NUVF 793 (**Figure 3.2**). On the anatomical left side of the animal, an L-shaped pterygoid is fused to a single tooth plate bearing 8 clearly defined radiating rows of dentition. These rows consist of separate cusps with slightly rounded crowns, with individual ridges and cusps blending into one another in the heel of the tooth plate. The cusps are slightly compressed such that the long axis of each cusp is

aligned with its row, a characteristic that is particularly conspicuous in more mesial rows. The first row of teeth bears larger cusps, is longer than any of the others, and extends far anteriorly. The first and second tooth rows are also distinctive in that they are not single rows for their entire length; rather, each bears one (second row) or multiple (first row) loci near the front of the tooth plate bearing two cusps (lateral to one another). Denticles are present at the rear of the tooth plate and a broad denticle field extends the length of the tooth plate along its mesial border. Conical pits, matching the size and spacing of cusps, lie between the tooth rows, which may represent patterns of occlusion with the prearticular toothplate. The anatomical right tooth plate is detached from the palate but displays the same attributes as the left plate.

NUFV 1160.6 (**Figure 3.9**) preserves two nearly anatomically identical pterygoid tooth plates in articulation with one another. These tooth plates bear 11 rows of cusped teeth rather than the 8 in NUFV 764. When in articulation with each other, the tooth plates form a deep midline trough on the roof of the mouth lined with a dense field of irregularly arranged denticles. The dorsal surface of each pterygoid is smooth and relatively featureless with the exception of a thickened ridge that extends anteroposteriorly along the mesial margin of the bone and a shallow depression laterally, which lies between the ventral ridges denoting the first and second tooth rows.

No specimen preserves a complete parasphenoid. The most intact example is missing the anteriormost portion and can be seen in NUFV 764 (**Figure 3.10**). The parasphenoid consists of two regions: a diamond-shaped anterior corpus and posterior stalk. Only a small portion of the corpus is preserved anterior to the lateral angles, but the gap between the pterygoids suggests that the intact bone would have had a pointed apex. The ventral surface of the parasphenoid corpus is smooth, with no evidence of dentition. The parasphenoid stalk is long and narrow, tapering

tapers gradually toward its posterior end, where it terminates at a point rather than bifurcation. The ventral surface of the stalk is gently concave, forming a trough-shaped groove. The ventrolateral surface of the stalk defines elongated facets that extend the length of the projection on either side of the median trough. The posterior tip of the stalk extends beyond the posterior limit of ossification of the braincase.

Mineralization of the braincase is restricted to the occiput, and I interpret the anterior margin of ossification as likely corresponding to the position of the cranial fissure (**Figure 3.10**). The occiput has clearly been subjected to some taphonomic compression and appears sheared toward the anatomical left side of the specimen. Although the position of the parasphenoid relative to the ventral region of the occiput is exaggerated by compression, it seems that the occiput does bear a prominent midline depression to accommodate the parasphenoid stalk. The ventrolateral surface of the occipital ossification is covered with smooth perichondral bone, while vesicular, unfinished endoskeletal bone is exposed on its anterior and posterior faces. Multiple foramina pierce the occiput. The most prominent of these, located on the ventral surface of the occiput immediately adjacent to the parasphenoid stalk, represents the opening of a canal for the occipital artery. This foramen for the occipital artery is best preserved on the right side of the braincase, with a notch representing this feature mostly obscured by the parasphenoid stalk on the left side. Dorsal to the anatomical left foramen for the occipital artery are two smaller, closely spaced foramina that are likely for spino-occipital nerves based on comparisons with other early lungfishes (Miles 1977). Viewed posteriorly, the rear face of the occiput bears a pair of semicircular surfaces, one on each side. The right example is closely associated with a fragment interpreted as an incomplete cranial rib. A short spur extends from the proximal surface of this hatchet-shaped bone, adjacent to a flat surface representing the articular head. It also bears

a thin flange ventromesially that flattens halfway down its length and ends distally in a broken tip.

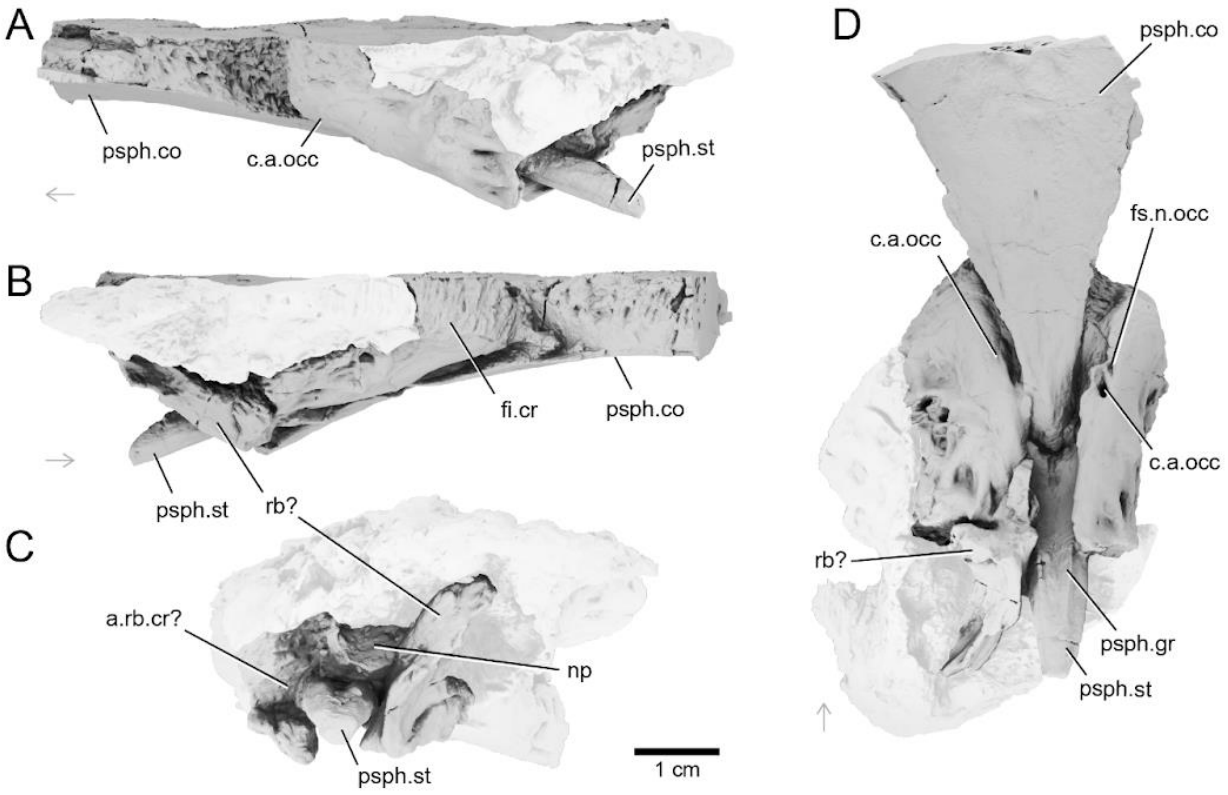

Figure 3.10. *Scaumenacia ornatissma*, 3D render of braincase and parasphenoid (NUFV 764). A, 3D render in right lateral view; B, 3D render in left lateral view; C, 3D render in posterior view; D, 3D render in ventral view. Abbreviations: a.rb.cr?, unidentified attachment (likely cranial rib attachment); c.a.occ, canal for the occipital artery; fi.cr, cranial fissure (combined term for the ventral otic fissure and lateral occipital fissure following Miles, 1977); fs.n.occ, fossa for the spinal occipital nerve(s); np, notochordal pit; psph.co, corpus of parasphenoid; psph.gr, groove of parasphenoid; psph.st, stalk of parasphenoid; rb?, unidentified rib (likely cranial rib). Light gray coloration represents the matrix. Gray arrows point anteriorly, excepting C, where anterior is into the page.

Lower Jaw—Specimen NUFV 764 preserves two prearticular tooth plates in position. Both are long, bearing 8 rows of cusped, slightly blunted teeth including a first row that bears larger cusps and extends much more anteriorly than the more lateral rows, matching the arrangement in the pterygoid tooth plates. The anatomical left tooth plate preserves only an incomplete prearticular, whereas the anatomical right tooth plate preservation is more complete.

In dorsal view, a broad trough separates the first dental row of each tooth plate, and extends parallel to it. This trough is floored by smooth bone and represents the symphyses between the right and left prearticulars, matching a similar gap between tooth plates of the palate. Posterior to the toothplate, the prearticular defines the mesial wall of a short opening to the adductor fossa (**Figure 3.11**). The prearticular bears a smooth ventral lamina in inner view that contributes to the lingual face of the mandible. The ventral margin of this lamina is elevated relative to the lower margin of the jaw but expands to meet the ventral margin of the infradentaries near the symphysis. The external dermal bones of the lower jaw appear limited to two infradentaries and there is no evidence of an ossified dentary in any of the material examined. The more posterior infradentary, conventionally interpreted as representing the fusion between the angular and surangular, covers most of the lateral surface of the mandible. It sutures obliquely with the much smaller, splint-like splenial.

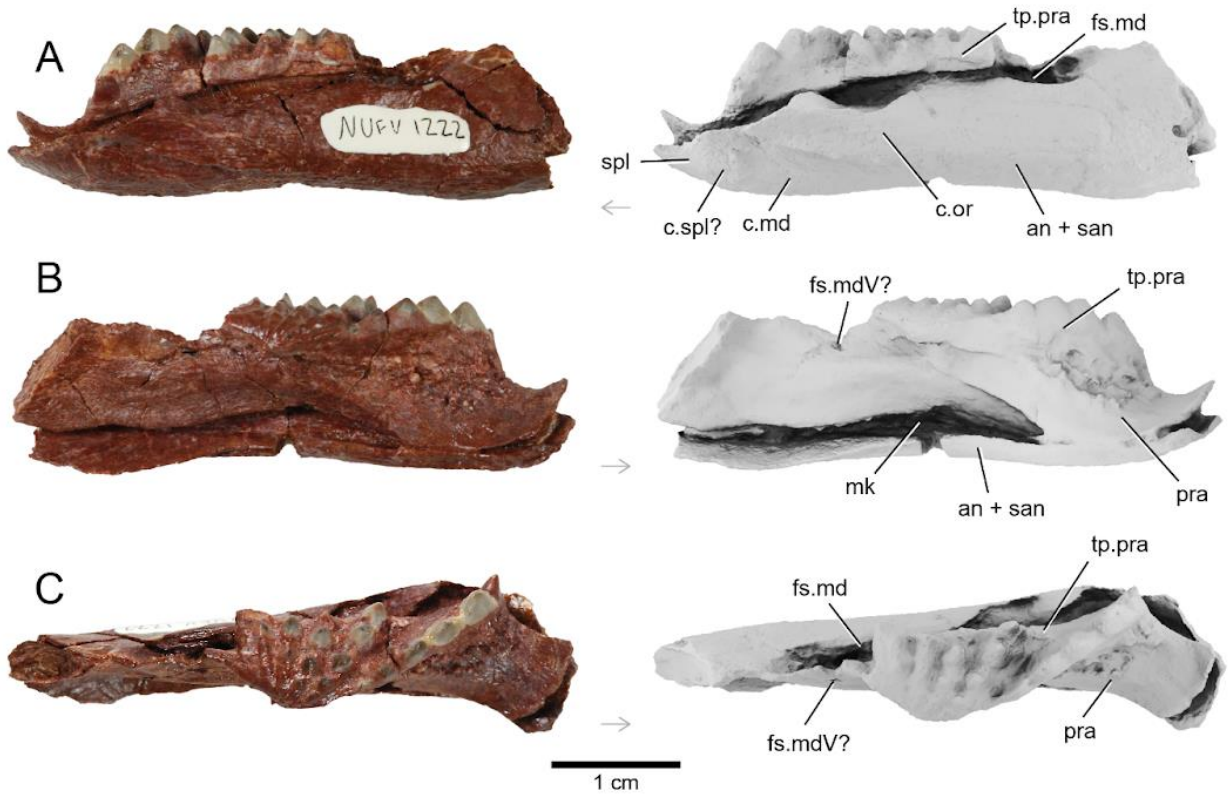

Figure 3.11. *Scaumenacia ornatissima*, left lower jaw (NUFV 1222). A, photograph and 3D render in lateral view; B, photograph and 3D render in mesial view; C, photograph and 3D render in dorsal view. Abbreviations: an, angular; c.md, mandibular lateral line canal; c.or, oral lateral line canal; c.spl?, unidentified canal (likely splenial lateral line canal); fs.md, mandibular fossa; fs.mdV?, unidentified fossa (likely fossa for mandibular nerve V); mk, Meckel's cartilage; pra, prearticular; san, surangular; tp.pra, prearticular toothplate. Gray arrows point anteriorly.

3.5.2 Hyoid Arch

Hyoid Apparatus—Only portions of the ventral hyoid arch are preserved, represented in NUFV 764 and NUFV 1323 (**Figure 3.12**). Because these bones are not preserved in place, their handedness and orientation is inferred based on comparison with other early lungfishes. The hourglass-shaped ceratohyal is flat mesially and bears a thick, anteroposteriorly oriented crest on its lateral face. The anterior has a triangular, blunted arrowhead shape from which the crest originates. The middle of the specimen is strongly constricted, with the ventral margin having a pronounced concavity with an area for the attachment of the interhyoideus muscle and the dorsal

margin having a less severe concavity. The uneven posterior surface exposes endoskeletal bone, indicating that a substantial cartilaginous extension of the ceratohyal may have been present. The hypohyal is represented only by a trapezoidal fragment preserved in articulation with the anterior of the ceratohyal in NUFV 1323. The thick crest on the lateral surface of the ceratohyal is continuous with a similar crest on the hypohyal that thins dorsally and is inferred to be the attachment point of the levator hyoideus muscle.

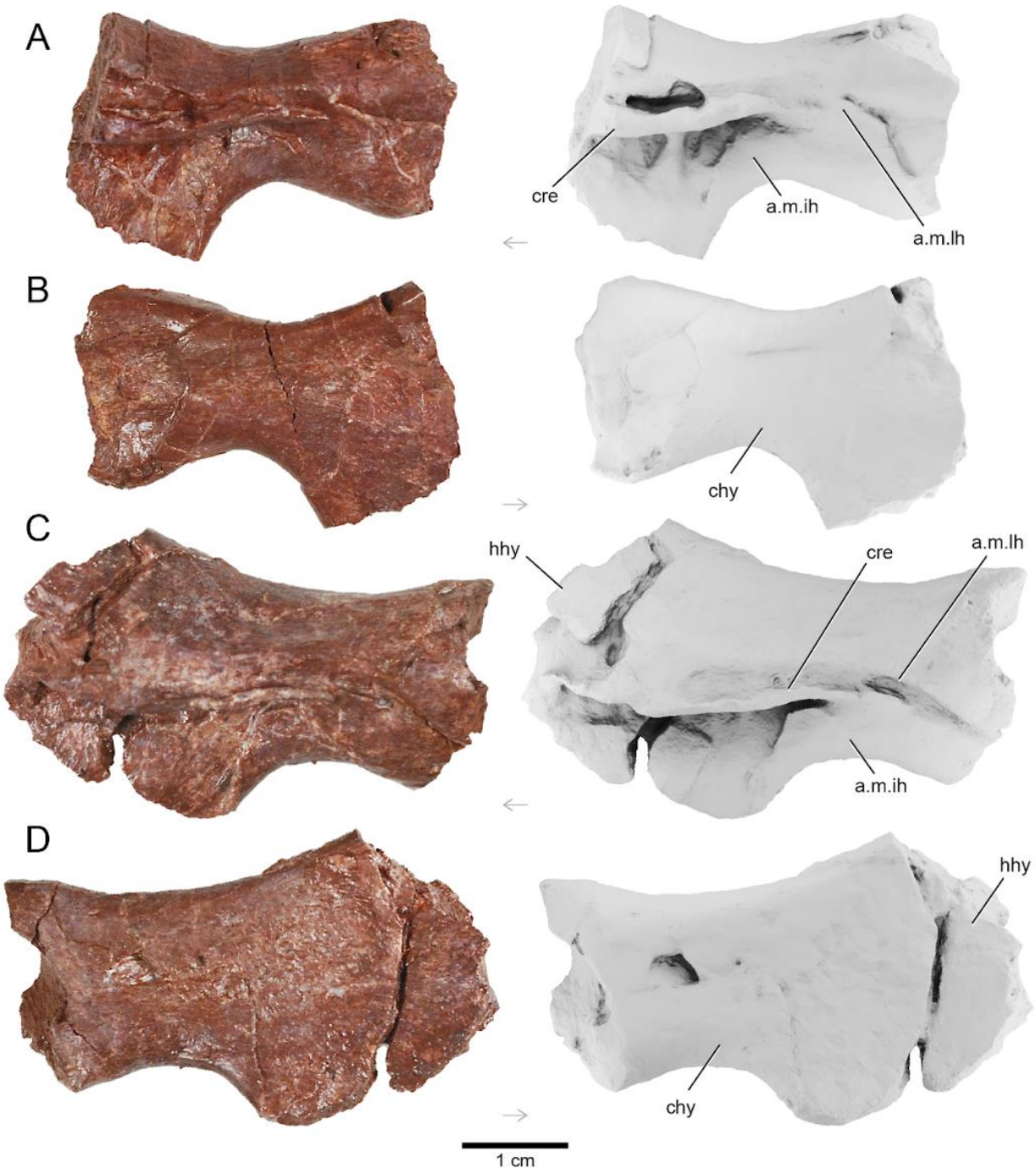

Figure 3.12. *Scaumenacia ornatissima*, two anatomically right ceratohyal photographs and 3D renders in lateral and mesial views. A, NUFV 764 photograph and 3D render in lateral view; B, photograph and 3D render in mesial view of the same; C, NUFV 1323 photograph and 3D render in lateral view; D, photograph and 3D render in mesial view of the same. Abbreviations: a.m.ih, groove for the attachment of the interhyoideus muscle; a.m.lh, area of attachment for the levator hyoideus muscle; chy, ceratohyal; cre, crest; hhy, hypohyal. Gray arrows point anteriorly.

3.5.3 Postcranium Including Appendicular Skeleton

Shoulder Girdle—NUFV 1227 (**Figure 3.13**) and NUFV 793 (**Figure 3.14**–**Figure 3.15**) preserve associated cleithrum and clavicles, and NUFV 793 additionally preserves a possible fragment of the anocleithrum (**Figure 3.14**–**Figure 3.15**). In lateral view, the cleithrum is generally trapezoidal in shape, with a curved ridge extending across the long axis of its lateral face. This separates the bone into distinct laminae: the more anterior branchial lamina and the more posterior lateral lamina. The branchial lamina is generally smooth with the exception of some radiating ridges. The posterior edge of the outturned ridge is associated with a coarse, vesicular surface texture that appears patchily on the lateral lamina. This sculpture is most pronounced ventrally, and its development and form vary between individuals. The postbranchial lamina is uniformly thin, with the lateral lamina being generally thicker. This is particularly pronounced at the ventral end of the cleithrum where it articulates with the clavicle. The inner surface of the cleithrum is concave and smooth, with the exception of fine radiating grooves on the branchial lamina. The clavicle consists of two major parts. The first is a crescent-shaped body representing a continuation of the lateral lamina of the cleithrum, whose outer surface bears mottled ornamentation similar to the lateral lamina of the cleithrum. The second is a gently curved, spade-shaped section which attaches perpendicular to the end of the lateral lamina. There is a small postbranchial lamina that defines a concave triangular region between the main body of the cleithrum and the thickened section that articulates with the clavicle. A presumed anocleithrum can only be seen in NUFV 793 articulating with the dorsal region of the cleithrum. It has a smooth texture.

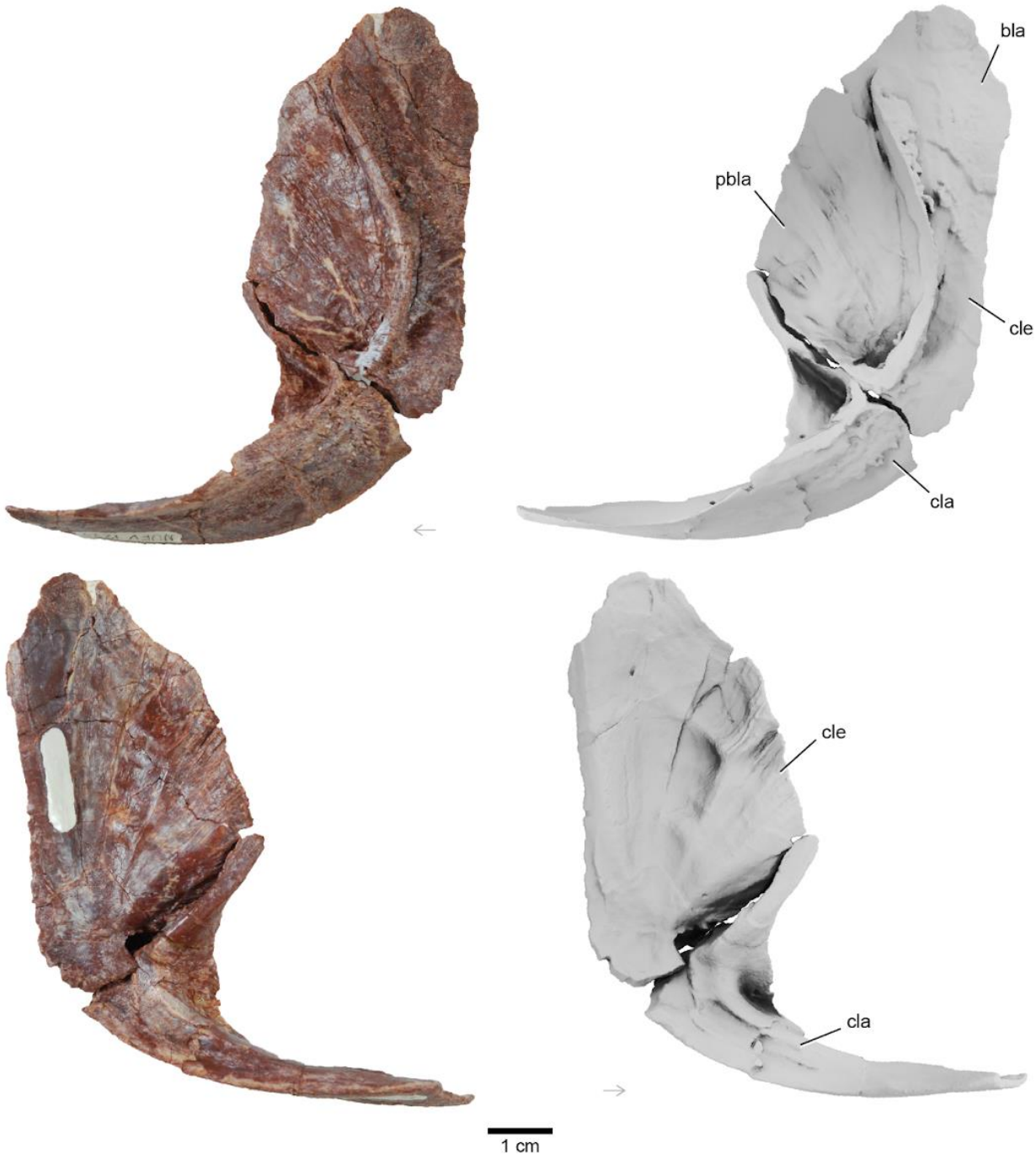

Figure 3.13. *Scaumenacia ornatissima*, cleithrum and clavicle photographs and 3D renders in lateral and mesial views (NUFV 1227). A, photograph and 3D render in lateral view; B, photograph and 3D render in mesial view. Abbreviations: bla, branchial lamina; cla, clavicle; cle, cleithrum; pbla, post-branchial lamina. Gray arrows point anteriorly.

General Comments on the Postcranial Skeleton—Specimen NUFV 793 represents a dorsoventrally flattened postcranial skeleton that is split into two blocks, one anterior and one

posterior (**Figure 3.14**). The more anterior of these two blocks is the largest and includes the posterior stalk of the parasphenoid, portions of the right dermal shoulder girdle (cleithrum, clavicle, and partial anocleithrum), the left clavicle, much of the abdominal axial column, and a small portion of the caudal axial skeleton (**Figure 3.15**). The details of the skeleton are preserved on both the dorsal and ventral sides but are most fully exposed in dorsal view. Squamation is also preserved in this primary block (**Figure 3.17**). A second block belonging to NUFV 793 preserves components of a long-based dorsal fin, including lepidotrichia and the underlying endoskeletal supports (**Figure 3.16**). This post-cranial material, taken together with the relatively complete NUFV 794 cranium, suggests a total length of approximately 1 meter.

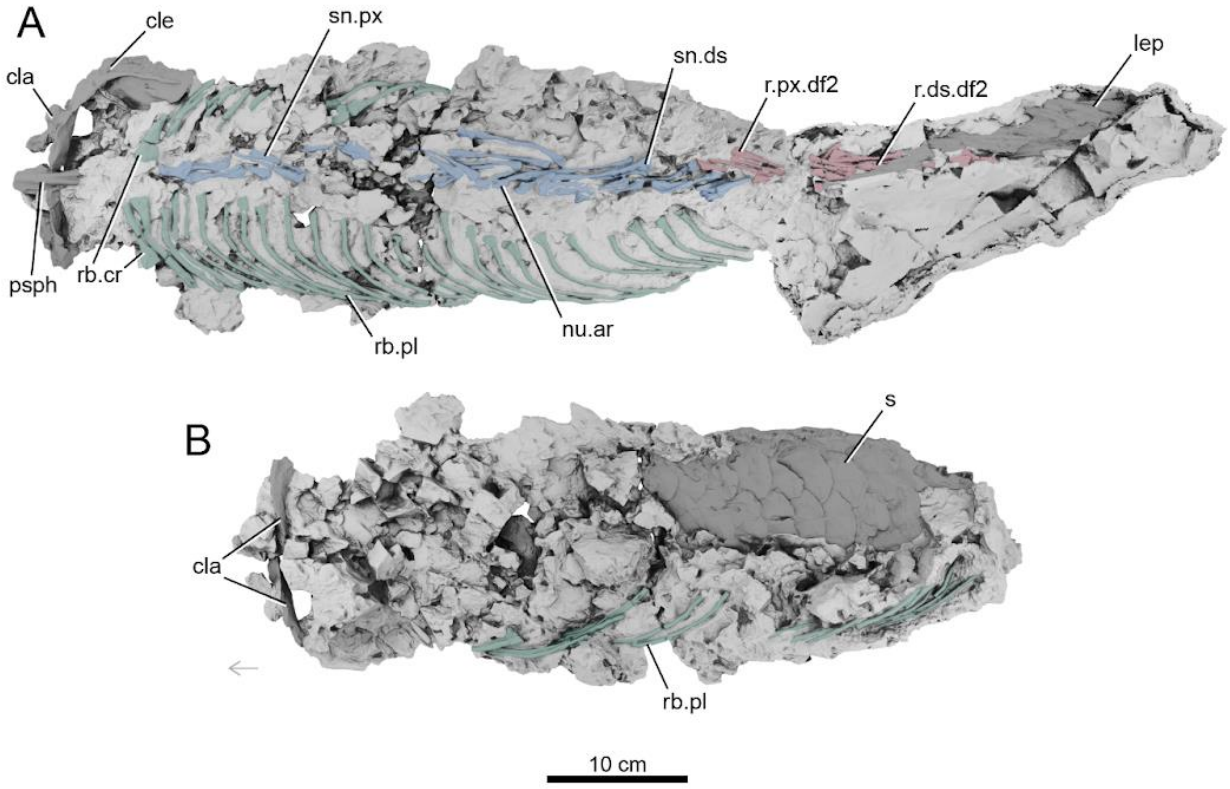

Figure 3.14. *Scaumenacia ornatissima*, 3D renders of the holotype (NUFV 793) in A, dorsal view, including the posterior caudal block; and B, ventral view, with posterior caudal block omitted (no bone is exposed on this surface). Abbreviations: cla, clavicle; cle, cleithrum; lep.df2, lepidotrichia of the second dorsal fin; nu.ar, neural arch; psph, parasphenoid; rb.cr, cranial ribs; rb.pl, pleural ribs; r.px.df2, proximal radials of the second dorsal fin; sn.ds, distal supraneurals; sn.px, proximal supraneurals. Black shading denotes dermally derived skeletal elements. Gray arrows point anteriorly.

Ribs—The ribs are best preserved on the left, dorsal side of the specimen (**Figure 3.14**). The two most anterior ribs are thickened relative to the rest of the ribs and expand distally (**Figure 3.15**). Although robust examples like these are generally interpreted as cranial ribs, comparison with NUFV 764, which does show a rib in articulation with the braincase, suggests that these exposed examples might lie behind the posterior limit of the occiput. On the anatomical left side of the fossil in dorsal view, a full set of 26 curved ribs trail behind the thickened anterior ribs in dorsal view, becoming thinner and more gracile towards the posterior of the animal. The distal ends of most ribs are either buried or broken. On the anatomical right side in dorsal view, only nine curved ribs are visible behind the robust anterior ribs in dorsal view, with sediment concealing an area expected to contain around one or two additional ribs between the fourth and next exposed rib. One of the ribs on the right side of the animal appears to show localized swelling on the midlength of the shaft, which may indicate a healed fracture in life. On the anatomical right side in ventral view (**Figure 3.14**), a partial set of 17 curved ribs are visible through the specimen.

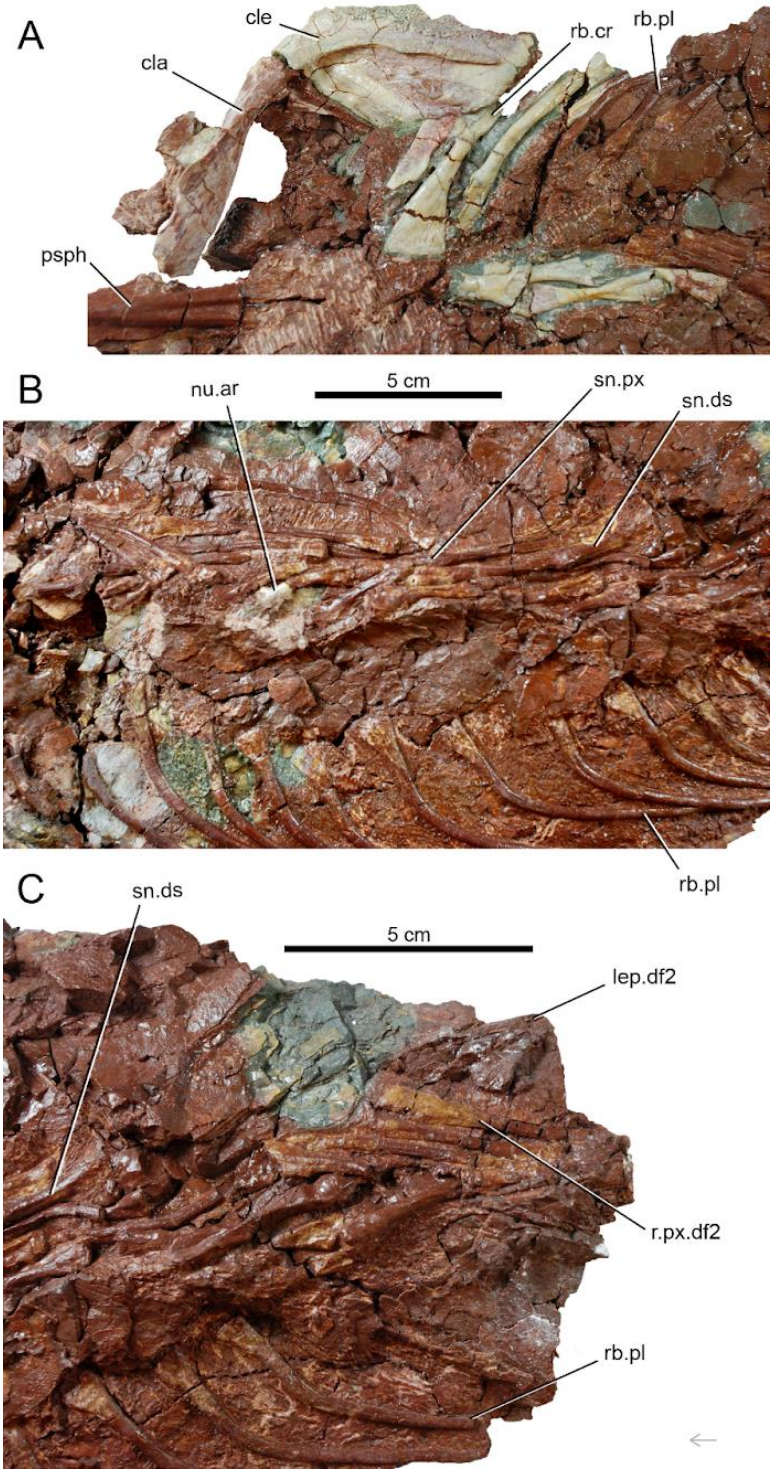

Figure 3.15. *Scaumenacia ornatissima*, close-up photographs of the holotype (NUFV 793) postcranial block in dorsal view. A, photograph of the anteriormost anatomical right in dorsal view; B, photograph of the center of the block in dorsal view; C, photograph of the posteriormost extent of the block in dorsal view. Abbreviations: cla, clavicle; cle, cleithrum; lep.df2, lepidotrichia of the second dorsal fin; nu.ar, neural arch; psph, parasphenoid; r.px.df2, proximal radials of the second dorsal fin; rb.cr, cranial ribs; rb.pl, pleural ribs; sn.ds, distal supraneurals; sn.px, proximal supraneurals. Gray arrows point anteriorly

Vertebral Column and Median Fins—Supraneurals, radials, and haemal spines are preserved overlying one another along the midline of the specimen between the two series of ribs (**Figure 3.15**). Assignments of individual rod-like bones to a specific series is difficult due to their preservation and taphonomic displacement. At least seven endoskeletal rods with constricted midregions are preserved immediately posterior to the skull. The first of these is overlapped by a stout, hourglass-shaped bone of uncertain identity. They appear to be relatively straight and flare distally and proximally. Their cross section is circular at midlength and more elliptic distally and proximally. The principal block is damaged along the middle, creating a region where details are more difficult to discern. In contrast to the median endoskeletal structures in the anterior part of the specimen, which appear to comprise a single series, immediately posterior to the break, the endoskeletal rods appear as two series: one dorsal and one ventral. The proximal bones are slender and smaller than the anterior series, with the proximal end of each bone showing anterior and posterior facets that appear to contact the previous and next bones in the series—similar to zygapophyses. The distal tip of each of these bones articulates with a long, slender bone over twice as long as itself and nearly twice as long as each individual bone in the anterior series. This series includes 10 of these articulating bones before the first bone identified as a radial based on its probable contribution to the dorsal fin. The posteriormost portion of the block preserves four radials that articulate with, and are superficial to, the previous series. The first one is incomplete distally; however, extending its hypothetical trajectory intersects with the first set of lepidotrichia. From the second bone onward in this first block, there is a direct articulation with lepidotrichia and no additional series of distal radials. The axial skeleton extends onto a second block (**Figure 3.16**) that has broken from the larger, anterior block. This second block continues the middle and anterior portion of the second dorsal

fin. It contains four bones directly articulating with lepidotrichia that lie parallel to the vertebral axis. Additional disarticulated lepidotrichia overlie these, offset by approximately 45 degrees from the midline.

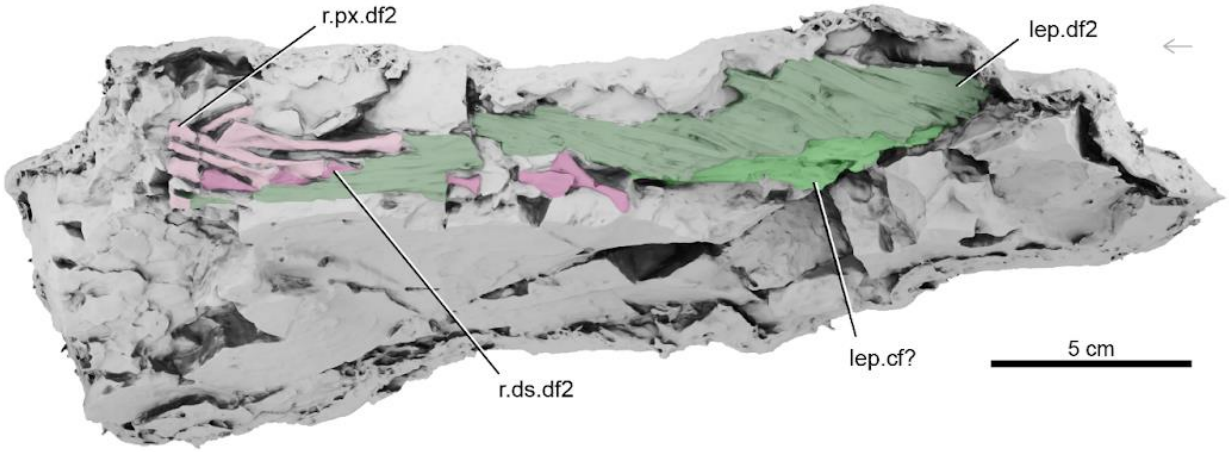

Figure 3.16. *Scaumenacia ornatissima*, close-up 3D render of the holotype (NUFV 793) caudal block in oblique dorsal view. Abbreviations: lep.cf?, unidentified lepidotrichia (likely lepidotrichia from the caudal fin); lep.df2, lepidotrichia from the second dorsal fin; r.ds.df2, distal radials from the second dorsal fin; r.px.df2, proximal radials from the second dorsal fin. Gray arrows point anteriorly.

Scales—The posterior half of the ventral side of the first block has 15 slightly elliptical scales (**Figure 3.17**). These scales are located on the anatomical left side of the fossil and are split into two series: one medial series with seven scales and one lateral series with eight scales. The longest axis of each scale is just over half the size of the longest axis of the cleithrum. Five of the anteriormost scales bear fine, anteroposterior vermiform ornamentation on their free fields, and the posteriormost scale on the medial series shows some pustular ornamentation. This ornamentation extends less than half of the free field of the scale beginning from the posterior margin. There are two other visible but partially obscured sets of scales of similar size on the dorsal side of the primary block. The first lies underneath ribs 11–12 when counting from the first thickened rib anteriorly on the anatomical left side. The second is 10 cm from the center

break on the anatomical right side. The anteriormost part of the second block contains a set of at least 10 partially overlapping scales. The long axis of these is significantly shorter compared to the measurements from the sales on the ventral side of the primary block—only around one quarter the size of the cleithrum. However, these scales continue to show vermiform ornamentation that now extends approximately half the length of the free field.

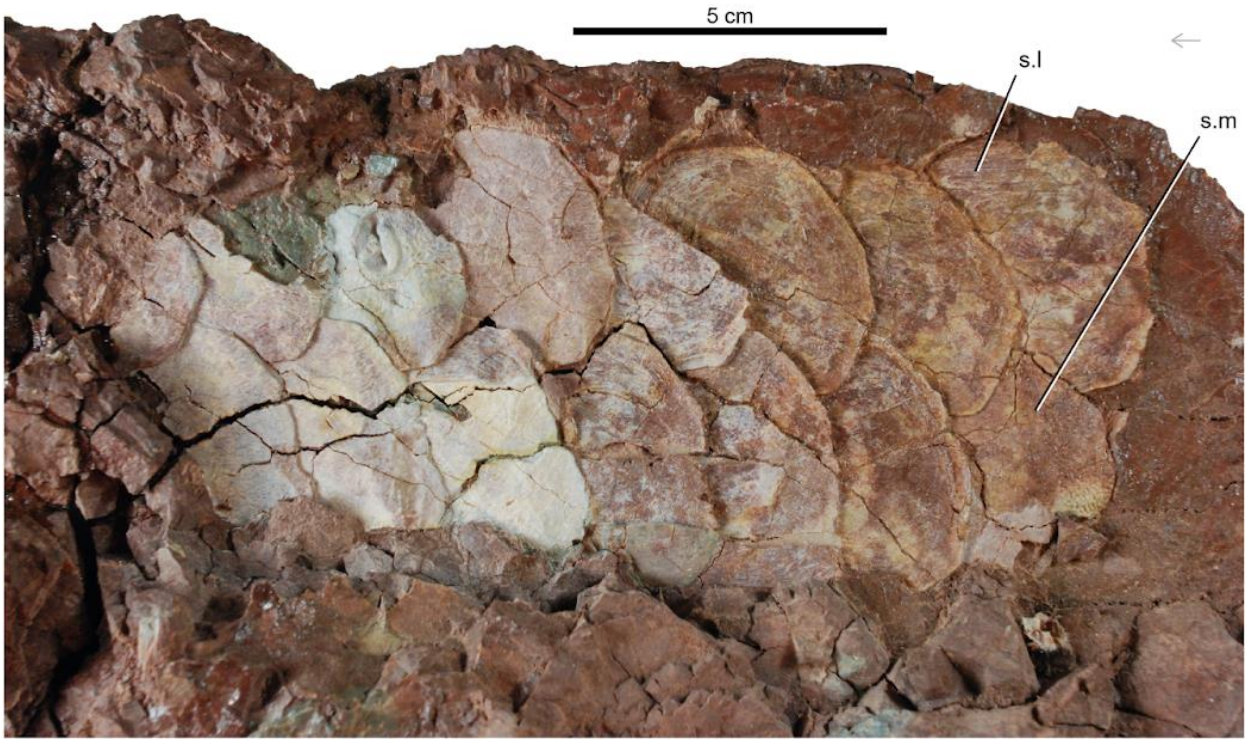

Figure 3.17. *Scaumenacia ornatissima*, close-up photograph of the holotype (NUFV 793) postcranial block in ventral view. Abbreviations: s.l, lateral series of scales; s.m, medial series of scales. Gray arrow points anteriorly.

3.6 Discussion

3.6.1 The Fram Formation Lungfish as a 'Phaneropleurid'

Scaumenacia ornatissima differs in at least one key characteristic from the majority of other Late Devonian lungfishes. Instead of the stouter and robust lower jaws observed in

chirodipterids such as *Chirodipterus* and *Pillararhynchus*, *S. ornatissima* has a thinner and longer lower jaw. Unlike denticled rhynchodipterids such as *Rhynchodipterus* and *Griphognathus*, *S. ornatissima* has large tooth plates. *S. ornatissima* also lacks the elongation of skull roof bones to create long snouts present in the aforementioned rhynchodipterids as well as in the 'fleurantiids' (e.g., *Fleurantia* and *Barwickia*). Finally, *S. ornatissima* differs markedly from genera that have a short posterior dorsal fin, such as *Dipterus*, though it does share the presence of cranial ribs with *Dipterus* and other more derived freshwater forms. These comparisons leave 'phaneropleurids' such as *Phaneropleuron* and *Pentlandia*, which possess several derived characters, including large B, C, and E bones; a generally absent D bone; a lack of cosmine; thin, rounded scales; and a discrete second dorsal fin equal to more than a quarter of the total length of the animal (Cloutier 1996; Cloutier and Ahlberg 1996). Although ambiguities surrounding the coherence of 'phaneropleurids' are well-documented (Huxley 1861; Günther 1880; Hoernes 1884; Woodward 1891; Berg 1940; Schultze and Marshall 1993; Cloutier 1996, 1997; Cloutier and Ahlberg 1996; Challands and den Blaauwen 2017), cladistic analyses generally recover taxa historically aligned with 'phaneropleurids' as closely related to one another but potentially intermixing with other assemblages (e.g., 'fleurantiids') (Schultze and Marshall 1993; Challands and den Blaauwen 2017).

However, the most conspicuous characteristic necessary to examine the affinities of *S. ornatissima* to other 'phaneropleurids' is the elongated second dorsal fin, the geometry of which varies considerably and is often summarized using example conditions in other Devonian lungfishes (Friedman 2010). The first condition is borne by *Barwickia* (Long 1992; Long and Clement 2009), *Howidipterus* (Long 1992; Long and Clement 2009), and *Pentlandia* (Jude et al. 2014; Challands and den Blaauwen 2017), which have a short-based first dorsal fin supported by

a well-developed basal plate and a long-based second dorsal fin supported by a basal plate that bears radials, trailed by additional radials not borne by the basal plate. The second condition in *Fleurantia*, which is sometimes aligned with 'phaneropleurids,' shows a short-based first dorsal fin with a basal plate and a long-based second dorsal fin supported only by radials with no basal plate. A third condition is shown in *Scaumenacia*, which has a low, long-based first dorsal fin consisting of a shallow fringe of fin rays unsupported by any mineralized radials, trailed by a long-based second dorsal fin supported only by radials with no basal plate. A final condition is found in *Phaneropleuron* (Huxley 1861; Traquair 1871), where the first dorsal fin is lacking and the second dorsal fin forms a continuous dorsal fringe (Friedman 2010; Challands and den Blaauwen 2017). The Fram Formation lungfish lacks any radials or basal plate supporting a first dorsal fin, and its second dorsal fin is supported exclusively by radials with no basal plate. This is more in line with *Scaumenacia* and perhaps *Phaneropleuron* than to *Fleurantia*, *Barwickia*, and *Howidipterus*.

3.6.2 Comparisons to Scaumenacia

The roughly contemporary *Scaumenacia curta* from Miguasha, Quebec, shares additional aspects with the Fram Formation lungfish that other lungfishes covered previously do not. First, the pattern of skull roof bones is essentially identical, except for the lack of A, D, or 8–9 bones. Most of these discrepancies may be taphonomic; however, the lack of a D bone is plausible given the variability observed in *Scaumenacia*. Second, the tooth plates have an elongated medial row bearing larger cusps, with that row along with the second one each bearing loci anteriorly with two cusps lateral to one another. Third, the overall size, proportions, and lamina

of the cleithrum and clavicle are the same, including the surface where both articulate. The anocleithrum is not preserved well enough to make an adequate comparison.

The most conspicuous differences between the Fram Formation 'phaneropleurid' and *Scaumenacia curta* relate to overall body size, ornamentation of the cranial bones, and minor differences in the shapes of contacts between bones of the skull roof. In terms of body size, the total length of *S. ornatissima* is estimated at around one meter, which is more than five times the size of most adult *S. curta*. In terms of bone patterns, we were unable to find any skulls of *S. curta* published or shown as reconstructions in the literature that displayed: (1) both E bones scalloped laterally by the M and L2 bones or (2) an elongated heptagonal B bone with a small anterior projection. The first refers to the curving mesially of the lateral perimeter of the E bones to create a concave (i.e., "scalloped") appearance along the suture point with the M and L2 bones (see **Figure 3.2**). In *S. curta,* both those suture points are straight and unaffected by any of the bones in the lateral series (Cloutier 1996, 1997). The second refers to the overall shape (subrectangular heptagon) and anterior projection (from modest to elongated) of the B bone in *S. curta*. Conversely, in *S. ornatissima,* all B bones examined were noticeably elongated in a similar way to the C and E bones. In some (e.g., NUVF 794, see **Figure 3.4**), this elongation was more pronounced than in others—on the order of more than two times as long as they were wide. Further, regardless of the rectangular extent of the B bone, the anterior projection was never elongated in any of the skull roofs examined herein. Finally, when present in *S. curta*, ornament is generally pustular and sparsely occupies the perimeter of the skull roof and lateral series, never covering the medial series. This can be most readily observed in the literature in both interpretive drawings (Cloutier 1996: Fig. 2, 1997: Figs. 5, 8) as well as photographic plates (Cloutier 1996:

Fig. 4, 1997: Fig. 6). In contrast, *S. ornatissima* has relatively coarse ornamentation consisting of short ridges on most of the skull roof bones and deep pitting on the circumorbital bones.

3.6.3 Functional Implications of the Anatomy

Although contentious phylogenetically due to the proposal by Campbell & Barwick (1990) being contradicted by recent studies (Qiao & Zhu 2015, Challands et al. 2019, Luo et al 2021), lungfish tooth plate morphology can still be used independently to assess ecology. Pterygoid tooth plates with rows of blunted teeth and an elongated medial tooth row and denticle field are found in *S. ornatissima* and other Devonian lungfishes such as *Rhinodipterus* and *Scaumenacia*. Narrower prearticular tooth plates (more similar to *Pentlandia macroptera* than to *Dipterus* or *Pinnalongus*) are moved via musculature attached to a short adductor fossa. This combination of characters is incompatible with those inferred to be used for suction feeding in rhynchodipterids like *Griphognathus* (e.g., elongated snout, oblique insertion of a small adductor muscle, denticulated field in place of tooth plates, etc.). The characters observed in *S. ornatissima* are more likely to be associated with active prey capture and crushing, though I cannot infer if it would have been a ram feeder.

However, it is likely that *S. ornatissima* may have used buccal pumping to aid in prey capture and in air gulping due to the presence of cranial ribs buttressing the shoulder girdle along with the support from the elongated posterior stalk of the parasphenoid. There is wide support for both of these being associated with air breathing from their first appearance in Devonian lungfishes (*Dipterus* for the cranial ribs and *Rhinodipterus* for the long parasphenoid stalk) to those in the modern day. *S. ornatissima* appears to straddle this transition too, halfway between a rigid shoulder girdle and small buccal cavity in marine lungfishes of the Devonian and a mobile

pectoral girdle and a large pectoral girdle for modern lungfishes. This arrangement may have allowed *S. ornatissima* to create some negative pressure in the buccal cavity to aid in prey capture and respiration

3.7 Conclusion

The lungfish material collected at the Upper Devonian Fram Formation of Ellesmere Island, Nunavut, Canada has been found to be a rare, exceptionally preserved new species of *Scaumenacia*: *Scaumenacia ornatissima*. Most of the skeletal material is similar to the abundantly examined material from *S. curta* from nearby Lagerstätten (Cloutier 1996, 1997; Boirot et al. 2022). It also possesses characteristics traditionally ascribed to transitional lungfishes from the Middle Devonian onwards that could be examined in future cladistic analyses, such as cranial ribs and a parasphenoid with a long stalk (Long 1993; Cloutier and Ahlberg 1996), tooth plates, and the elongation of the base of the second dorsal fin (Dollo 1895; Cloutier and Ahlberg 1996; Friedman 2010; Challands and den Blaauwen 2017). However, the skull roof differs in the lateral scalloping of the E bones by the M and L bones, an elongated B bone with a small anterior projection, and the extensive ornamentation covering much of the skull roof and becoming more prominent laterally. Additionally, the estimated size of the specimen is at least five times larger (~1m) than the estimated average size of other *Scaumenacia*. These anatomical differences, along with the lack of *S. curta* otherwise found at Ellesmere Island, may indicate the presence of a new species of buccal pumping lungfish, crushing food along the banks of an ancient freshwater ecosystem. Cumulatively, the mosaic of characters that make up this fossil should contribute to future cladistic work on ‘phaneropleurids’ and the backbone of the transition of lungfishes into their modern forms.

3.8 References

Ahlberg, P.E., 2018. Follow the footprints and mind the gaps: a new look at the origin of tetrapods. Earth Environ. Sci. Trans. R. Soc. Edinb. 109, 115–137. https://doi.org/10.1017/S1755691018000695

Ahlberg, P.E., 1991. A re-examination of sarcopterygian interrelationships, with special reference to the Porolepiformes. Zool. J. Linn. Soc. 103, 241–287. https://doi.org/10.1111/j.1096-3642.1991.tb00905.x

Ahlberg, P.E., Trewin, N.H., 1994. The postcranial skeleton of the Middle Devonian lungfish *Dipterus valenciennesi*. Trans. R. Soc. Edinb. Earth Sci. 85, 159–175. https://doi.org/10.1017/S0263593300003588

Algeo, T.J., Scheckler, S.E., Maynard, J.B., 2001. 12. Effects of the Middle to Late Devonian Spread of Vascular Land Plants on Weathering Regimes, Marine Biotas, and Global Climate, in: Gensel, P.G., Edwards, D. (Eds.), Plants Invade the Land. Columbia University Press, pp. 213–236. https://doi.org/10.7312/gens11160-013

Becker, R.T., Marshall, J.E.A., Da Silva, A.-C., Agterberg, F.P., Gradstein, F.M., Ogg, J.G., 2020. The Devonian Period, in: Geologic Time Scale 2020. Elsevier, pp. 733–810. https://doi.org/10.1016/B978-0-12-824360-2.00022-X

Berg, L.S., 1940. Classification of fishes both recent and fossil. Tr. Zool. Instituta 5, 85–517.

Boirot, M., Challands, T., Cloutier, R., 2022. Paedomorphosis and neurocranial ossification in two Devonian lungfishes. Acta Palaeontol. Pol. 67. https://doi.org/10.4202/app.00841.2020

Campbell, K.S.W., Barwick, R.E., 1990. Paleozoic Dipnoan Phylogeny: Functional Complexes and Evolution Without Parsimony. Paleobiology 16, 143–169.

Campbell, K.S.W., Barwick, R.E., 1986. Paleozoic lungfishes—a review. J. Morphol. 190, 93–131. https://doi.org/10.1002/jmor.1051900409

Campbell, K.S.W., Barwick, R.E., Senden, T.J., 2009. Evolution of dipnoans (lungfish) in the Early Devonian of southeastern Australia. Alcheringa Australas. J. Palaeontol. 33, 59–78. https://doi.org/10.1080/03115510802618300

Challands, T., den Blaauwen, J., 2017. A redescription of the Middle Devonian dipnoan *Pentlandia macroptera* Traquair, 1889, and an assessment of the Phaneropleuridae. Zool. J. Linn. Soc. 180, 414–460. https://doi.org/10.1111/zoj.12491

Chi, B.I., Hills, L.V., 1976. Biostratigraphy and Taxonomy of Devonian Megaspores, Arctic Canada. Bull. Can. Pet. Geol. 24, 640–818. https://doi.org/10.35767/gscpgbull.24.4.640

Clack, J.A., 2012. Gaining Ground: The Origin and Evolution of Tetrapods. Indiana University Press, Bloomington & Indianapolis.

Cloutier, R., 1997. Morphologie et variations du toit crânien du Dipneuste Scaumenacia curta (Whiteaves) (Sarcopterygii), du Dévonien supérieur du Québec. Geodiversitas 19, 61–105.

Cloutier, R., 1996. Dipnoi (Akinetia: Sarcopterygii), in: Schultze, H.-P., Cloutier, R. (Eds.), Devonian Fishes and Plants of Miguasha, Quebec, Canada. Verlag Dr. Friedrich Pfeil, München, pp. 198–226.

Cloutier, R., Ahlberg, P.E., 1996. Morphology, characters, and the interrelationships of basal sarcopterygians, in: Stiassny, M.L.J., Parenti, L.R., Johnson, G.D. (Eds.), Interrelationships of Fishes. Academic Press, Inc., New York, pp. 445–479. https://doi.org/10.1016/B978-012670950-6/50018-7

Cloutier, R., Proust, J.-N., Tessier, B., 2011. The Miguasha Fossil-Fish-Lagerstätte: a consequence of the Devonian land–sea interactions. Palaeobiodiversity Palaeoenvironments 91, 293–323. https://doi.org/10.1007/s12549-011-0058-0

Coates, M.I., Friedman, M., 2010. *Litoptychus bryanti* and characteristics of stem tetrapod neurocrania, in: Elliott, D.K., Maisey, J.G., Yu, X., Miao, D. (Eds.), Morphology, Phylogeny and Paleobiogeography of Fossil Fishes: Honoring Meemann Chang. Verlag Dr. Friedrich Pfeil, München, Germany, pp. 389–416.

Cope, E. D., 1887. Geology and palaeontology. Am. Nat. 1887, 1014–1019.

Cressler, W.L., Daeschler, E.B., Slingerland, R., Peterson, D.A., 2010. Terrestrialization in the Late Devonian: a palaeoecological overview of the Red Hill site, Pennsylvania, USA. Geol. Soc. Lond. Spec. Publ. 339, 111–128. https://doi.org/10.1144/SP339.10

Daeschler, E.B., Cressler, W.L., 2011. Late Devonian paleontology and paleoenvironments at Red Hill and other fossil sites in the Catskill Formation of north-central Pennsylvania, in: From the Shield to the Sea: Geological Field Trips from the 2011 Joint Meeting of the GSA Northeastern and North-Central Sections. Geological Society of America, pp. 1–16. https://doi.org/10.1130/2011.0020(01)

Daeschler, E.B., Shubin, N.H., Jenkins Jr, F.A., 2006. A Devonian tetrapod-like fish and the evolution of the tetrapod body plan. Nature 440, 757–763. https://doi.org/10.1038/nature04639

Davies, N.S., Gibling, M.R., 2010. Paleozoic vegetation and the Siluro-Devonian rise of fluvial lateral accretion sets. Geology 38, 51–54. https://doi.org/10.1130/G30443.1

Dollo, L., 1895. Sur la phylogénie des Dipneustes. Bull. Société Belge Géologie Paléontol. Hydrol. 9, 79–128.

Downs, J.P., Daeschler, E.B., Garcia, V.E., Shubin, N.H., 2016. A new large-bodied species of *Bothriolepis* (Antiarchi) from the Upper Devonian of Ellesmere Island, Nunavut, Canada. J. Vertebr. Paleontol. 36, e1221833. https://doi.org/10.1080/02724634.2016.1221833

Downs, J.P., Daeschler, E.B., Jenkins, F.A., Shubin, N.H., 2013. *Holoptychius bergmanni* sp. nov. (Sarcopterygii, Porolepiformes) from the Upper Devonian of Nunavut, Canada, and a Review of *Holoptychius* Taxonomy. Proc. Acad. Nat. Sci. Phila. 162, 47–59. https://doi.org/10.1635/053.162.0104

Downs, J.P., Daeschler, E.B., Jenkins, F.A., Shubin, N.H., 2011. A new species of Laccognathus (Sarcopterygii, Porolepiformes) from the Late Devonian of Ellesmere Island, Nunavut, Canada. J. Vertebr. Paleontol. 31, 981–996. https://doi.org/10.1080/02724634.2011.599462

Downs, J.P., Daeschler, E.B., Lo, N., Carey, E.N., Shubin, N.H., 2019. *Asterolepis alticristata* n. sp. (Antiarchi) from the Upper Devonian (Frasnian) of Nunavut, Canada, and a report on the antiarch diversity of the Fram Formation. Geodiversitas 41, 679. https://doi.org/10.5252/geodiversitas2019v41a19

Downs, J.P., Daeschler, E.B., Long, A.M., Shubin, N.H., 2018. *Eusthenopteron jenkinsi* sp. nov. (Sarcopterygii, Tristichopteridae) from the Upper Devonian of Nunavut, Canada, and a Review of *Eusthenopteron* Taxonomy. Breviora 562, 1–24. https://doi.org/10.3099/MCZ44.1

Embry, A.F., Klovan, J.E., 1976. The Middle-Upper Devonian Clastic Wedge of the Franklinian Geosyncline. Bull. Can. Pet. Geol. 24, 485–639. https://doi.org/10.35767/gscpgbull.24.4.485

Friedman, M., 2010. Postcranial evolution in early lungfishes (Dipnoi: Sarcopterygii): new insights from *Soederberghia groenlandica*, in: Elliott, D.K., Maisey, J.G., Yu, X., Miao, D. (Eds.), Morphology, Phylogeny and Paleobiogeography of Fossil Fishes: Honoring Meemann Chang. Verlag Dr. Friedrich Pfeil, München, Germany, pp. 299–324.

Friedman, M., 2007a. The interrelationships of Devonian lungfishes (Sarcopterygii: Dipnoi) as inferred from neurocranial evidence and new data from the genus *Soederberghia* Lehman, 1959. Zool. J. Linn. Soc. 151, 115–171. https://doi.org/10.1111/j.1096-3642.2007.00320.x

Friedman, M., 2007b. Styloichthys as the oldest coelacanth: Implications for early osteichthyan interrelationships. J. Syst. Palaeontol. 5, 289–343. https://doi.org/10.1017/S1477201907002052

Goedert, J., Lécuyer, C., Amiot, R., Arnaud-Godet, F., Wang, X., Cui, L., Cuny, G., Douay, G., Fourel, F., Panczer, G., Simon, L., Steyer, J.-S., Zhu, M., 2018. Euryhaline ecology of early tetrapods revealed by stable isotopes. Nature 558, 68–72. https://doi.org/10.1038/s41586-018-0159-2

Günther, A.C.L.G., 1880. An Introduction to the Study of Fishes. Adam and Charles Black, Edinburgh.

Hoernes, R., 1884. Elemente der Palaeontologie (Palaeozoologie). Von Veit & Co., Leipzig.

Huxley, T.H., 1880. On the application of the laws of evolution to the arrangement of the Vertebrata and more particularly of the Mammalia. Proc. Zool. Soc. Lond. 1880, 649–662.

Huxley, T.H., 1861. Preliminary essay upon the systematic arrangement of the fishes of the Devonian epoch. Mem. Geol. Surv. U. K. Fig. Descr. Br. Org. Remains 10, 1–40.

Jude, E., Johanson, Z., Kearsley, A., Friedman, M., 2014. Early evolution of the lungfish pectoral-fin endoskeleton: evidence from the Middle Devonian (Givetian) *Pentlandia macroptera*. Front. Earth Sci. 2. https://doi.org/10.3389/feart.2014.00018

Kemp, A., Cavin, L., Guinot, G., 2017. Evolutionary history of lungfishes with a new phylogeny of post-Devonian genera. Palaeogeogr. Palaeoclimatol. Palaeoecol. 471, 209–219. https://doi.org/10.1016/j.palaeo.2016.12.051

Lloyd, G.T., Wang, S.C., Brusatte, S.L., 2011. Identifying heterogeneity in rates of morphological evolution: discrete character change in the evolution of lungfish (Sarcopterygii; Dipnoi). Evolution 66, 330–348. https://doi.org/10.1111/j.1558-5646.2011.01460.x

Long, J.A., 1993. Cranial ribs in Devonian lungfishes and the origin of air-breathing. Mem. Assoc. Australas. Palaeontol. 15, 199–209.

Long, J.A., 1992. Cranial anatomy of two new Late Devonian lungfishes (Pisces: Dipnoi) from Mount Howitt, Victoria. Rec. Aust. Mus. 44, 299–318. https://doi.org/10.3853/j.0067-1975.44.1992.37

Long, J.A., Clement, A.M., 2009. The postcranial anatomy of two Middle Devonian lungfishes (Osteichthyes, Dipnoi) from Mt. Howitt, Victoria, Australia. Mem. Mus. Vic. 66, 189–202.

Miles, R.S., 1977. Dipnoan (lungfish) skulls and the relationships of the group: a study based on new species from the Devonian of Australia. Zool. J. Linn. Soc. 61, 1–328. https://doi.org/10.1111/j.1096-3642.1977.tb01031.x

Morris, J.L., Puttick, M.N., Clark, J.W., Edwards, D., Kenrick, P., Pressel, S., Wellman, C.H., Yang, Z., Schneider, H., Donoghue, P.C.J., 2018. The timescale of early land plant evolution. Proc. Natl. Acad. Sci. 115. https://doi.org/10.1073/pnas.1719588115

Müller, J.P., 1845. Uber den Bau und die Grenzen der Ganoiden und über das natüliche System der Fische. Abh. Akad. Wiss. Zu Berl. 1844, 117–216.

Parent, N., Cloutier, R., 1996. Distribution and preservation of fossils in the Escuminac Formation, in: Cloutier, R., Schultze, H.-P. (Eds.), Devonian Fishes and Plants of Miguasha, Quebec, Canada. Verlag Dr. Friedrich Pfeil, München, pp. 54–78.

Qiao, T., Zhu, M., 2009. A new tooth-plated lungfish from the Middle Devonian of Yunnan, China, and its phylogenetic relationships. Acta Zool. 90, 236–252. https://doi.org/10.1111/j.1463-6395.2008.00381.x

Romer, A.S., 1955. Herpetichthyes, Amphibioidei, Choanichthyes or Sarcopterygii? Nature 176, 126–126. https://doi.org/10.1038/176126a0

Sallan, L.C., Coates, M.I., 2010. End-Devonian extinction and a bottleneck in the early evolution of modern jawed vertebrates. Proc. Natl. Acad. Sci. 107, 10131–10135. https://doi.org/10.1073/pnas.0914000107

Schultze, H.-P., 2010. The late Middle Devonian fauna of Red Hill I, Nevada, and its paleobiogeographic implications. Foss. Rec. 13, 285–295. https://doi.org/10.1002/mmng.201000001

Schultze, H.-P., 2001. *Melanognathus*, a primitive dipnoan from the Lower Devonian of the Canadian arctic and the interrelationships of Devonian dipnoans. J. Vertebr. Paleontol. 21, 781–794. https://doi.org/10.1671/0272-4634(2001)021[0781:MAPDFT]2.0.CO;2

Schultze, H.-P., Marshall, C.R., 1993. Contrasting the use of functional complexes and isolated characters in lungfish evolution. Mem. Assoc. Australas. Palaeontol. 15, 211–224.

Stewart, T.A., Lemberg, J.B., Daly, A., Daeschler, E.B., Shubin, N.H., 2022. A new elpistostegalian from the Late Devonian of the Canadian Arctic. Nature 608, 563–568. https://doi.org/10.1038/s41586-022-04990-w

Traquair, R.H., 1893. VI.—Notes on the Devonian Fishes of Campbelltown and Scaumenac Bay in Canada,—No. 3: Fishes From the Upper Devonian of Dalhousie, Scaumenac Bay. Geol. Mag. 10, 262–267. https://doi.org/10.1017/S0016756800170517

Traquair, R.H., 1871. I.—Notes on the Genus *Phaneropleuron* (Huxley), with a Description of a New Species from the Carboniferous Formation. Geol. Mag. 8, 529–535. https://doi.org/10.1017/S0016756800193306

Westoll, T.S., 1949. On the evolution of the Dipnoi, in: Jepsen, G.L., Mayr, E., Simpson, G.G. (Eds.), Genetics, Paleontology and Evolution. Princeton University Press, Princeton, NJ, pp. 121–184.

Woodward, A.S., 1891. Catalogue of the Fossil Fishes in the British Museum (Natural History). Part II. Taylor & Francis, London.

Chapter 4 – Diversification of Jaw Geometry During the Initial Radiation of Lobe-Finned Fishes (Osteichthyes: Sarcopterygii) Was Shaped by Variability Between Major Lineages

4.1 Abstract

The origin of sarcopterygian fishes around 420 million years ago is associated with the rapid appearance of several specialized lineages. Some of the most striking differences between these groups relate to morphology of the feeding apparatus and suggest ecology may have been a major axis of diversification among early lobe-finned fishes. Key examples include consolidated dental plates, reduction of marginal jaw bones and their associated dentitions, and elaboration of fangs, with these features associated with substantial variation in overall mandibular geometry. Such putative ecological divergence, alongside evidence that individual sarcopterygian lineages show high rates of evolutionary change early in their history, marks this event as a possible episode of adaptive radiation. Significantly, this would represent one of the earliest examples of this phenomenon in jawed fishes. Here, I explicitly test the hypothesis of adaptive radiation in early sarcopterygians by focusing on mandibles as a taphonomically robust, taxonomically diagnostic, and functionally well-understood anatomical component. I assembled a dataset of 58 three-dimensionally preserved jaws of total-group Sarcopterygii obtained by CT scanning or photogrammetry. Most are dipnoans or tetrapodomorphs (i.e., members of the lungfish or tetrapod total group), plus a smaller sample of coelacanth, stem sarcopterygians, and taxa of less certain phylogenetic placement. I developed a landmarking scheme of 6 fixed landmarks and 5 curves with sliding semilandmarks capturing overall jaw shape and orientation, including aspects of the glenoid and adductor fossa. I paired these data with a composite phylogenetic tree with

branch durations informed by the ages of fossil tips. I examined the fit of three models of trait evolution to these shape data in a multivariate framework: Brownian motion (BM; diffusive evolution at a constant rate), Accelerating/Decelerating Rates (ACDC; diffusive evolution with a rising or declining rate over time, the latter of which corresponds to an Early Burst and theoretical predictions for adaptive radiation), and Ornstein-Uhlenbeck (OU; constant rates of change with a central tendency limiting the accumulation of variation over time). My results indicate that EB is the best-supported model for jaw shape evolution for the clade. However, there is little evidence that individual sarcopterygian sub-groups correspond to this early burst pattern, with most best fit by a diffusive, constant-rates model. This implies that the initial appearance of the well-defined sarcopterygian lineages (dipnoans, porolepiforms, tetrapodomorphs, actinistians) was characterized by rapid divergence between these groups, with lower rates of change within those lineages.

4.2 Introduction

Gnathostomes—jawed animals with backbones—are the most diverse group of vertebrates in today's aquatic and terrestrial ecosystems. Although the earliest jawed fishes date to the early Silurian (Andreev et al. 2022a, 2022b; Friedman 2022; Zhu et al. 2022), it is only in the Devonian so-called "Age of Fishes" the gnathostomes become the most taxonomically diverse vertebrates in most fossil faunas (Janvier 1996; Anderson et al. 2011; Friedman and Sallan 2012). In contrast to modern aquatic vertebrate ecosystems, which are dominated by actinopterygians (ray-finned fishes) (Friedman and Sallan 2012; Friedman 2022), the most diverse jawed fishes in Devonian faunas were placoderms (Young 2010), an extinct assemblage of armored stem gnathostomes, and sarcopterygians (lobe-finned fishes) (Clement 2019), the

group from which all terrestrial vertebrates would emerge. The variety of Devonian lobe-finned fishes is particularly striking given that today's sarcopterygians show limited anatomical and taxonomic diversity, often presented as slowly evolving "living fossils." Conversely, their Devonian progenitors are known from a variety of depositional environments ranging from rivers to lakes to coral reefs (Trewin 1986; Long and Trinajstic 2010; Daeschler and Cressler 2011) and display early innovations in feeding ecology (Zhu and Yu 2004; Cui et al. 2022) and body form (Friedman and Coates 2006).

This bolsters several lines of circumstantial evidence hinting at the early history of sarcopterygians being an interval of rapid phenotypic change. First, multiple anatomically distinct lineages first appear during a short interval in the latest Silurian and Early Devonian, with the oldest records of tetrapodomorphs (total group tetrapods), dipnoans (crown group lungfishes), porolepiforms (non-dipnoan dipnomorphs), actinistians (total group coelacanths), and onychodonts known from this span (Chang 1995; Johanson et al. 2006; Clément and Ahlberg 2010; Lu and Zhu 2010; Lu et al. 2012). Second, surveys of discrete characters and functional measurements gathered from two-dimensional images of mandibles point to rapid accumulation of disparity in sarcopterygian lower jaws around the same time (Anderson et al. 2011). Third, historical difficulties in resolving the relationships among extant lungfishes, coelacanths, and tetrapods with molecular data (reviewed in Brinkmann et al. 2004; Rokas and Carroll 2006) point to relatively rapid splits near the base of the sarcopterygian crown group. This pattern may superficially bear the hallmarks of an adaptive radiation (Schluter 2000).

Originally recorded by Osborn (1902), later redefined by Simpson (1953), and finally recontextualized by Schluter (2000), the term adaptive radiation has been the subject of extensive debate for over half a century (Simões et al. 2016). Much like "living fossil," what began as a

simple descriptor for lineages diverging from one adaptive type into different, diverging adaptive zones (Simpson 1953) has expanded to encompass essentially any diversification event. Only within the past couple of decades has the scale of the problem been explored and, out of the ensuing discussions, a multifaceted and nuanced understanding of adaptive radiations has emerged (Gavrilets and Losos 2009; Harmon et al. 2010; Givnish 2015, 2015; Soulebeau et al. 2015; Simões et al. 2016; Stroud and Losos 2016). Under this framework, adaptive radiations are defined as rapid diversification most frequently caused by biotic factors that can occur sympatrically and include ecomorphological divergence (see Simões et al. 2016).

Past efforts to quantify macroevolutionary patterns in early sarcopterygians have been focused on overviews of disparity through time across the group as a whole (Anderson et al. 2011) or estimated rates of change in sarcopterygian subclades by combining phenotypic data with phylogenetic hypotheses in a comparative framework (Lloyd et al. 2011; Anderson et al. 2013; Cui et al. 2022; Chapter 2 of this Dissertation). However, testing the hypothesis of adaptive radiation in early sarcopterygians requires a broader quantitative phenotypic dataset that can be leveraged alongside the relatively mature phylogenies available for most major lineages of lobe-finned fishes (Schultze 2000; Zhu et al. 2017; Luo et al. 2021; Toriño et al. 2021). Although whole bodies represent a major source of phenotypic data for comparative analyses of fossil (Friedman 2010) and extant (Claverie and Wainwright 2014) groups, most early sarcopterygians are not known from articulated individuals. Luckily, many sarcopterygians have left a record of well-preserved lower jaws, which can be identified to the generic or species level and are intimately tied to their environment through the acquisition and processing of food (Wainwright et al. 2000)

Jaws are a well-studied system in vertebrate function and ecomorphology (Wainwright et al. 2000; Westneat 2003, 2004), with the mandibles of early sarcopterygians preserving key features present in extant fishes (e.g., the glenoid defining the fulcrum of the jaw modeled as a simple lever) (Westneat 2004) as well as additional information generally not available from skeletal data in living species (e.g., cross-sectional area of adductor musculature, delimited by the bony perimeter of the adductor fossa) (Westneat 2003). They can also be used as proxies to estimate ecomorphological adaptations through time (Anderson et al. 2011, 2013). Jaws therefore represent a powerful system for addressing questions relating to evolutionary radiations through phenotypic evolution in fossil fishes (Bellwood 2003; Anderson 2008; Cawley et al. 2021; Deakin et al. 2022) and gnathostomes more broadly (Ahlberg and Clack 1998; Wainwright et al. 2000; Westneat 2003, 2004; Botella et al. 2007; Anderson et al. 2011, 2013; Brazeau and Friedman 2014; Hill et al. 2018).

Here, I assess whether sarcopterygians experienced an episode of adaptive radiation early in their clade history using jaws as a corollary. Noting the circumstantial evidence and past efforts discussed above, I hypothesize that the evolution of the morphology of their mandible from the late Silurian to the Late Devonian should be best fit by a model of phenotypic evolution with high rates in the past when they initially diversified that decelerate to the recent—an Early Burst.

4.3 Methods

4.3.1 Dataset

I collected 70 jaws from 23 institutions representing sarcopterygians across the late Silurian and Devonian, including actinistians (n = 3), porolepiforms (n = 14), dipnoans (n = 21),

and tetrapodomorphs (n = 28), along with early diverging, stem sarcopterygians (n = 4). Of those, eight were repeats that were averaged down to 3 unique taxa in the geometric morphometrics stage and seven specimens were removed from the dataset due to the lack of one or more regions where landmarks were to be placed. The final 58 jaw dataset comprises nearly every available lobe-finned species with complete, three-dimensionally preserved jaws.

4.3.2 3D Data Generation and Standardization

I sourced the jaw data via photogrammetry, newly generated CT scans or those provided by collaborators, and datasets available through supplementary materials or hosted on archives like MorphoSource (https://morphosource.org). The photogrammetric methods involved placing a fossil in a light box with a turntable inside, rotating, and taking ~25 photographs of its opposing faces at three different angles with respect to the turntable (60°, 45°, and 10°). For an in-depth explanation, refer to the protocols for the University of Michigan Online Repository of Fossils (UMORF; https://umorf.ummp.lsa.umich.edu/wp/about/project-methods/). I then imported the photographs into the software RealityCapture (Capturing Reality, Bratislava, Slovakia) and processed them to generate a 3D model. The computed tomography (μCT) scans used a Nikon XT H 225ST (Xtek, Tring, UK) industrial scanner in the Computed Tomography in Earth and Environmental Science (CTEES) facility, Department of Earth and Environmental Sciences, University of Michigan. All scanning parameters, including voltage, current, exposure, resolution, and filter, are available via the Deep Blue repository for all fossils in our dataset. The tomograms were segmented using Materialise Mimics v19.0 (Materialise, Belgium) and surface meshes were exported as PLY files.

The subsequent shapefile standardization process for the models involved five phases: cleaning, mirroring, rescaling, retrodeforming, and decimating. First, the files were cleaned of any digitally unattached polygons. Second, (a) all jaws belonging to the anatomical left side of an animal were mirrored to be right and (b) whole jaws where the left side was higher quality than the right were also mirrored. Third, I rescaled all models in MeshLab (Cignoni et al. 2008) to millimeters from their original scale (mostly microns for CT scanned models). Fourth, *Cryptolepis grossi* was retrodeformed to unbend the posterior third of the jaw using an armature with 6 joints in Blender v4.0 (https://blender.org/) and following DeVries et al. (2022). Last, any shapefiles with over two million faces were decimated using MeshLab's 'Simplification: Quadratic Edge Collapse Decimation' effect (Garland and Heckbert 2023) and data from the original vertices were transferred to the decimated model using 'Sampling: Vertex Attribute Transfer' (Cignoni et al. 1999). Due to my sampling focusing on capturing the whole jaw, any shapefiles that were missing regions where landmarks would be placed were removed from the dataset. Licensing information for all final models is also available via Deep Blue.

4.3.3 Landmarking

I landmarked all shapefiles in 3D Slicer (Fedorov et al. 2012) following the scheme in **Figure 4.1**. I placed a total of six fixed landmarks: (1) anteriormost margin of the symphysis, (2) ventralmost margin of the symphysis, (3) posterolateralmost edge of the glenoid fossa, (4) anterolateralmost edge of the glenoid fossa, (5) posterolateralmost edge of the glenoid fossa, and (6) anterior (triple juncture) of the adductor fossa. Additionally, I placed five curves with 120 sliding semilandmarks: (1) anterior margin of the symphysis (10 semilandmarks between landmarks 1 and 2), (2) ventral outline of the jaw (30 semilandmarks between landmarks 2 and

3), (3) interior margin of the glenoid fossa (30 semilandmarks between landmarks 3 and 4), (4) interior margin of the adductor fossa (20 semilandmarks between landmarks 5 and 6), and (5) dorsal outline of the jaw (30 semilandmarks between landmarks 3 and 1). Where there were holes in the mesh or some other obstruction, the curve would be drawn following the estimated original location of the missing or infilled anatomy. This landmark scheme allowed us to extract information about mechanically important components of the jaws as a system; namely, the entire lateral outline of the jaw, the surface that articulates with the skull, and the insertion point of the muscle used to open and close the jaw. In doing so, I hoped to capture fine-grained patterns of disparity that could be tied to hypotheses of feeding ecology posited in the literature (e.g., Clement 2012).

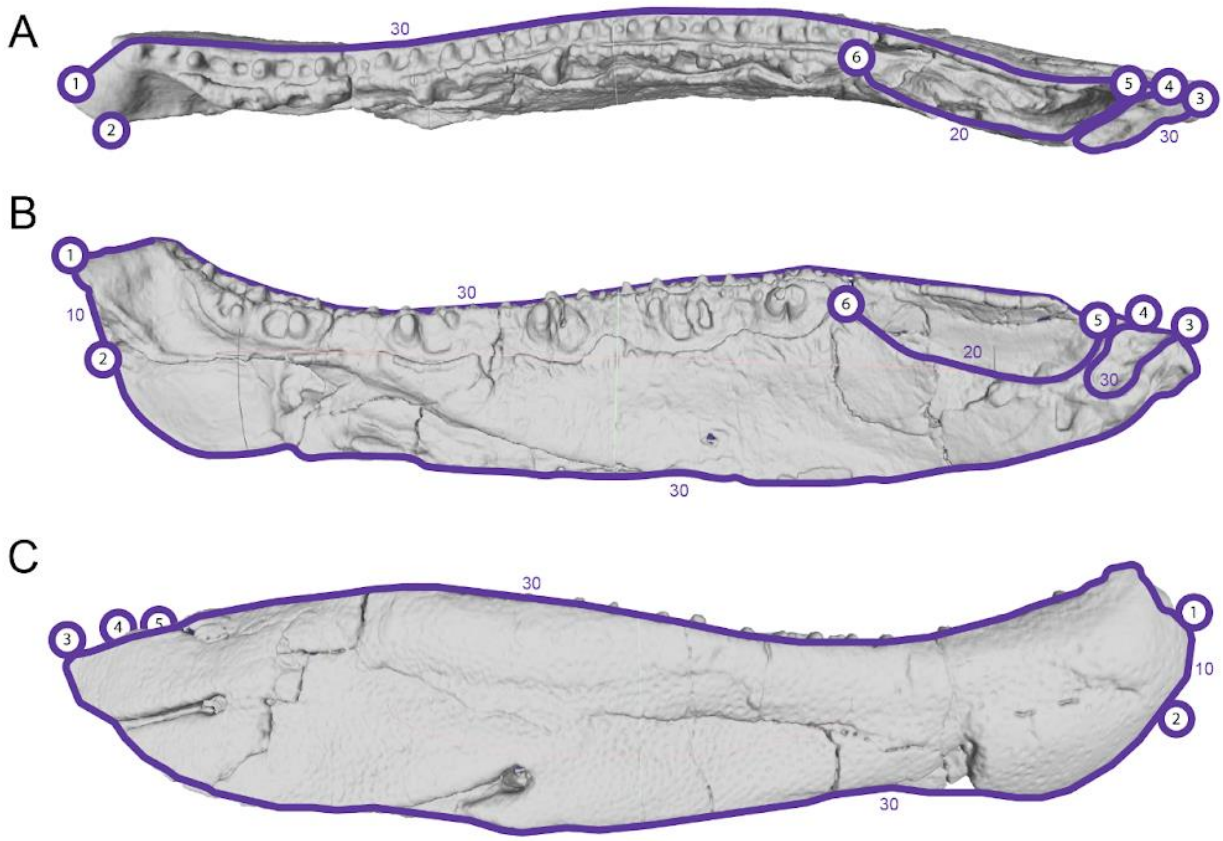

Figure 4.1. Jaw landmarking scheme overlaid on the stem sarcopterygian *Psarolepis romeri* in (a) dorsal, (b) mesial, and (c) lateral views. Single landmarks are in circles, while semilandmarks are not encircled and represent numerical totals for each adjacent curve. Landmarks 1, 2, and curve 1 capture the shape of the symphysis. Landmarks 3 and 4 are placed along the lateral most extent of the glenoid fossa, while curve 3 outlines the shape of the fossa. Landmarks 5 and 6 mark the length of the adductor fossa, while curve 4 follows the mesial shape of the fossa. Along with landmarks 1, 2, and 3, curves 1, 2, and 5 together trace the entire lateral outline of the jaw.

4.3.4 Geometric Morphometrics

The unaligned landmark and semi-landmark coordinate data were read into R (R Core Team 2013) using the 'read.markups' function in *SlicerMorphR* (v0.0.1.0) (Zhang 2024). I cleaned, organized, and transformed the data into a 3D array with the 'arrayspecs' function in the *geomorph* package (v4.0.7) (Adams and Otárola-Castillo 2013; Baken et al. 2021). I then used 'define.sliders' to create a matrix which allowed the semilandmarks to slide to minimize Procrustes distances between datasets (Gunz et al. 2005); Procrustes transformed the data using

'gpagen' to eliminate differences in position, size, and orientation (Rohlf and Slice 1990); and performed a Principal Components Analysis (PCA; via 'gm.prcomp'). I generated morphospace plots with convex hulls ('shapeHulls') encapsulating the principal clades (**Figure 4.2**) and also the principal clades across time (**Figure 4.3**). I also performed a Procrustes Analysis of Variance (ANOVA) using the 'procD.lm' function to test 'coords ~ clade' and 'coords ~ age' for a total of 1000 iterations. The 'RRPP' flag was set to TRUE because my dataset included more than three groups in the analysis. A summary of the statistics from both ANOVAs are reported in **Table 4.1**.

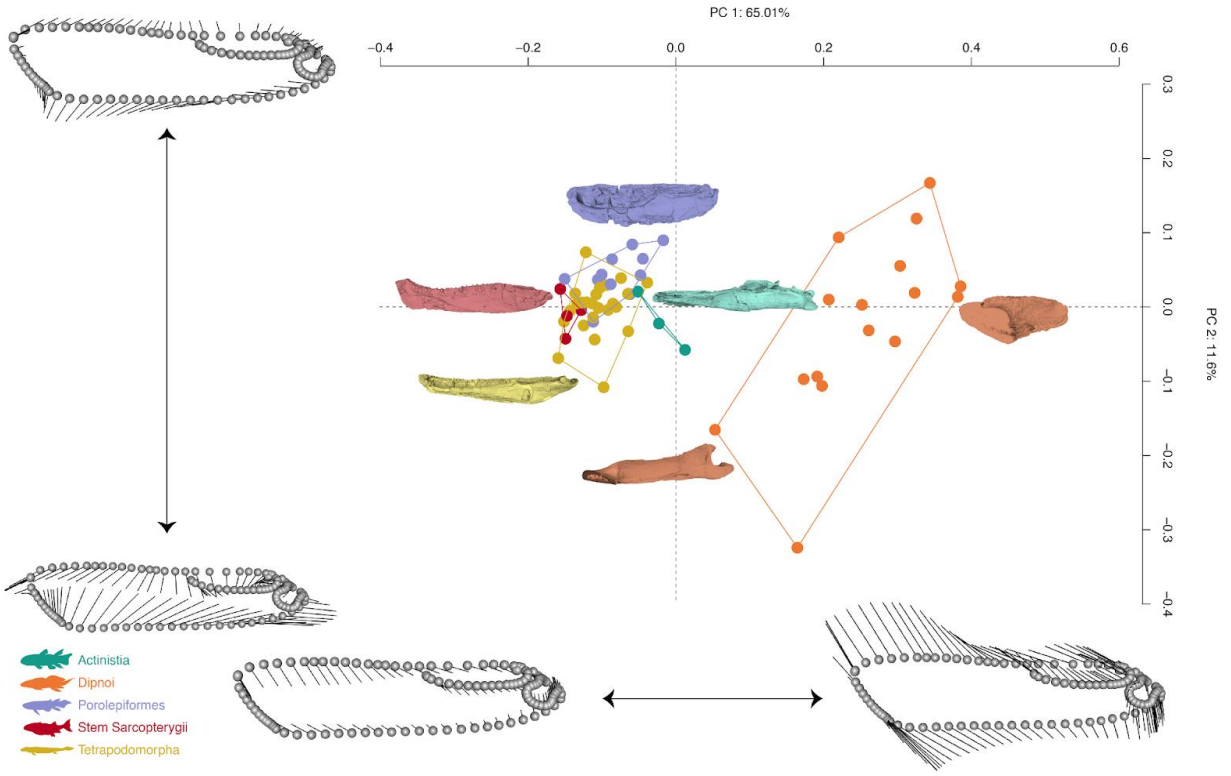

Figure 4.2. Morphospace for lower jaws of late Silurian to Late Devonian sarcopterygian fishes using landmark-based geometric morphometrics. PC 1 explains 65.01% of the variation in jaw shape, with the right half being occupied by the more derived lungfish condition and the left half being occupied by everything that is closer to the average sarcopterygian jaw. This average jaw is represented by the 3D models along the periphery and show the vectors required to move the average value for all landmarks and semilandmarks to the minimum and maximum values along each axis. PC 2 explains 11.6% variation in jaw shape and is related to the compression of the lateral margin of the jaw. Model jaws from each dataset and convex hulls around five principal assemblages: stem sarcopterygians, actinistians, porolepiforms, dipnoans, and tetrapodomorphs. Silhouettes from PhyloPic, *Tiktaalik* silhouette by *Nobu Tamura* (CC BY-SA 3.0)

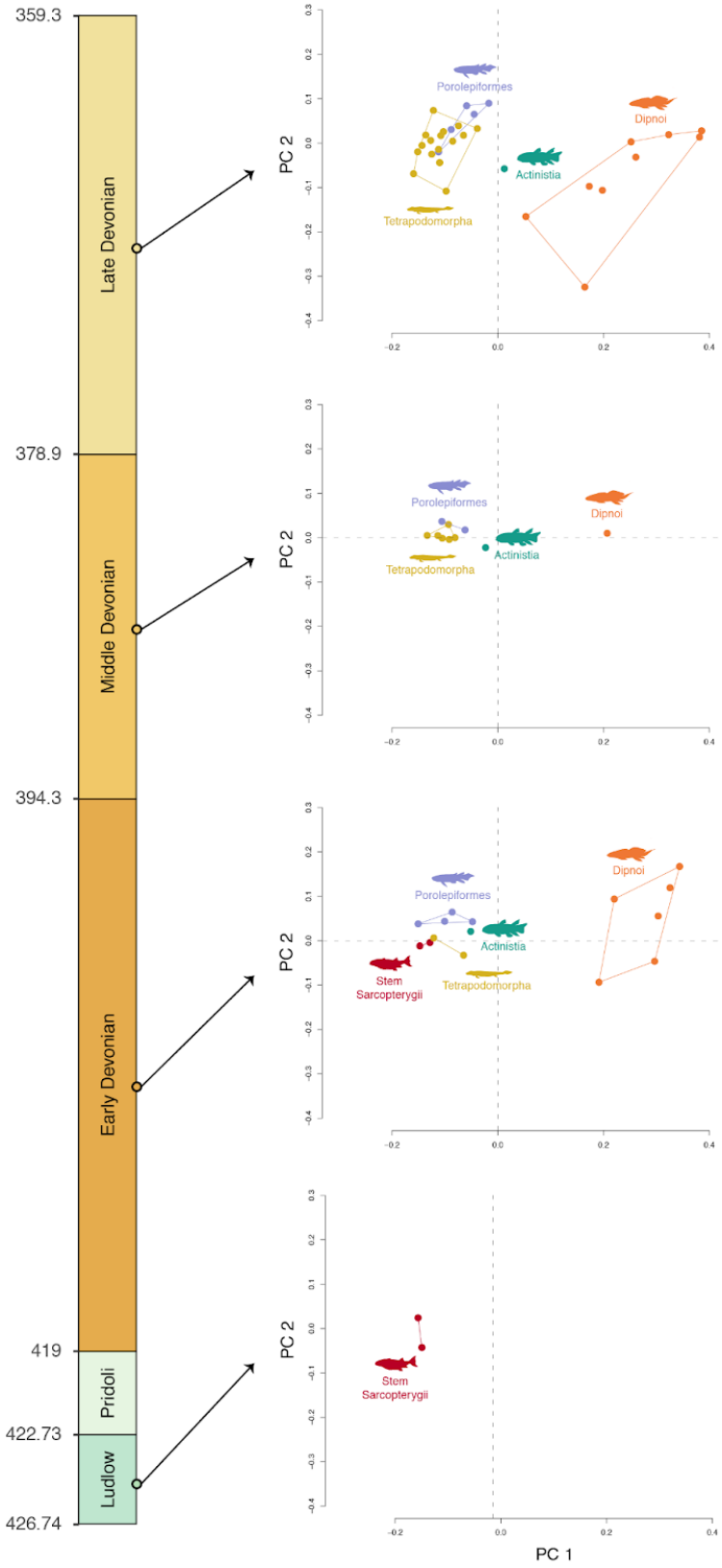
359.3
Late Devonian
378.9
Middle Devonian
394.3
Early Devonian
419
Pridoli
422.73
Ludlow
426.74
PC 2
PC 1
Porolepiformes
Dipnoi
Actinistia
Tetrapodomorpha
Stem Sarcopterygii

Figure 4.3. Morphospace through time for lower jaws of late Silurian to Late Devonian sarcopterygian fishes. This morphospace shows the same two axes as **Figure 4.2**, except only displaying the taxa that lived during each labeled time slice. All groups except the dipnoans remain more or less in the same morphospace throughout. By the end of the Devonian, the largest morphospace occupation was by tetrapodomorphs and dipnoans. Convex hulls around five principal assemblages: stem sarcopterygians, actinistians, porolepiforms, dipnoans, and tetrapodomorphs. Silhouettes from PhyloPic, *Tiktaalik* silhouette by *Nobu Tamura* (CC BY-SA 3.0).

4.3.5 Phylogenetic Tree Construction

I constructed a composite phylogenetic tree using the most recently published trees for coelacanths, porolepiforms, lungfishes, and tetrapodomorphs from Toriño et al (2021), Schultze (2000), Lloyd et al (2011), and Zhu et al (2017), respectively. In cases where taxa present in my shape data were missing from the previously published trees, they were added to each tree manually using TreeGraph2 (Stöver and Müller 2010) and using the most well-established relationships from the literature. In the singular case where a tree was in conflict with a key, well-supported relationship in the literature (i.e., *Styloichthys changae* and *Miguashaia grossi* as successive sister-lineages to the rest of the coelacanths), it was also manually adjusted using TreeGraph2. I confirmed the ages for each taxon using the primary literature and additional reference material where needed (e.g., Gradstein et al. 2020). The tree was grafted in R and then *post-hoc* time calibrated using 'timePaleoPhy' from the *paleotree* package (v3.4.5) (Bapst 2012). The root age was set to 426 Ma, polytomies were arbitrarily resolved via setting 'randres' to TRUE and 100 trees were randomly generated this way using 'ntrees', 'add.term' allowed the branches to terminate at the last appearance datum (LAD) of each group (Lloyd et al. 2011), and tips not in my jaw shape dataset were automatically dropped (Bapst 2012). I set 'type' to 'equal' as it uses a neutral method to apportion time when scaling a tree by extending lineages back using sister taxa as a reference (Ruta et al. 2006; Brusatte 2011; Lloyd et al. 2011), . The

timescaled tree was then plotted with colors denoting the principal clades and ages standardized to conform to Gradstein et al. (2020) (**Figure 4.3**).

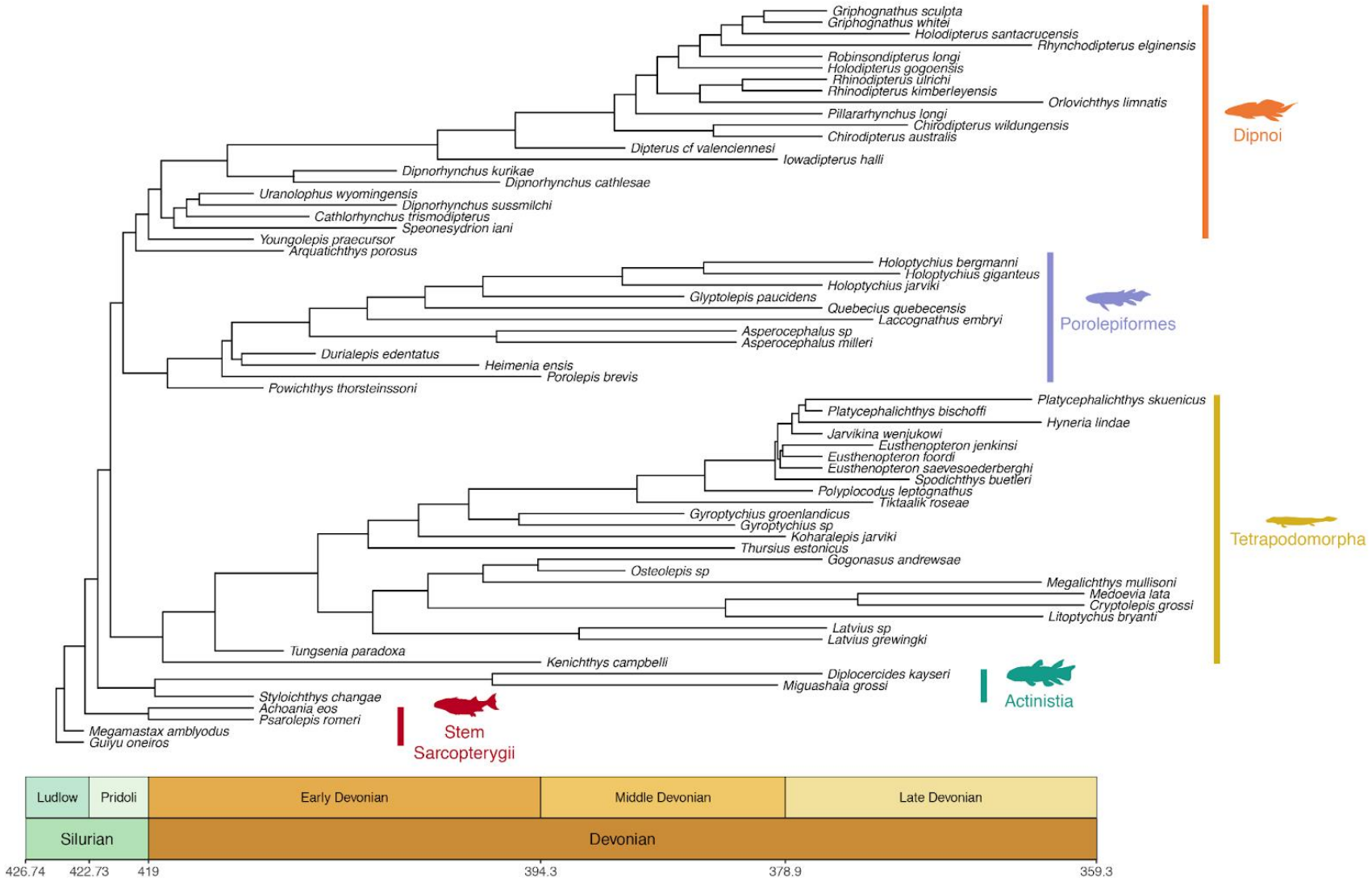
Griphognathus sculpta
Griphognathus whitei
Holodipterus santacrucensis
Rhynchodipterus elginensis
Robinsondipterus longi
Holodipterus gogoensis
Rhinodipterus ulrichi
Rhinodipterus kimberleyensis
Orlovichthys limnatis
Pillararhynchus longi
Chirodipterus wildungensis
Chirodipterus australis
Dipterus cf valenciennesi
Iowadipterus halli
Dipnorhynchus kurikae
Dipnorhynchus cathlesae
Uranolophus wyomingensis
Dipnorhynchus sussmilchi
Cathlorhynchus trismodipterus
Speonesydrion iani
Youngolepis praecursor
Arquatichthys porosus
Dipnoi
Holoptychius bergmanni
Holoptychius giganteus
Holoptychius jarviki
Glyptolepis paucidens
Quebecius quebecensis
Laccognathus embryi
Asperocephalus sp
Asperocephalus milleri
Durialepis edentatus
Heimenia ensis
Porolepis brevis
Powichthys thorsteinssoni
Porolepiformes
Platycephalichthys skuenicus
Platycephalichthys bischoffi
Hyneria lindae
Jarvikina wenjukowi
Eusthenopteron jenkinsi
Eusthenopteron foordi
Eusthenopteron saevesoederberghi
Spodichthys buetleri
Polyplocodus leptognathus
Tiktaalik roseae
Gyroptychius groenlandicus
Gyroptychius sp
Koharalepis jarviki
Thursius estonicus
Gogonasus andrewsae
Osteolepis sp
Megalichthys mullisoni
Medoevia lata
Cryptolepis grossi
Litoptychus bryanti
Latvius sp
Latvius grewingki
Tungsenia paradoxa
Kenichthys campbelli
Tetrapodomorpha
Diplocercides kayseri
Miguashaia grossi
Actinistia
Styloichthys changae
Achoania eos
Psarolepis romeri
Megamastax amblyodus
Guiyu oneiros
Stem
Sarcopterygii
Ludlow
Pridoli
Early Devonian
Middle Devonian
Late Devonian
Silurian
Devonian
426.74
422.73
419
394.3
378.9
359.3

Figure 4.4. Timescaled tree of Sarcopterygii with five principal assemblages highlighted: stem sarcopterygians, actinistians, porolepiforms, lungfishes, and tetrapodomorphs. The tree is a composite of multiple published hypotheses, each focusing on different parts of sarcopterygian phylogeny. Polytomies have been randomly resolved and this is the first tree generated out of 100. Silhouettes from PhyloPic, *Tiktaalik* silhouette by *Nobu Tamura* (CC BY-SA 3.0).

4.3.6 Evolutionary Model Fitting

I fit three competing models of trait evolution: two constant rates models (Brownian Motion [BM] and Ornstein-Uhlenbeck [OU]) and one accelerating-decelerating rates model (ACDC, of which Early Burst [EB] is a special case). All three models are variants of a random walk, but BM is likened to diffusive evolution where disparity accumulates constantly through time; OU has an additional parameter that constrains its random walk about a central tendency that is often interpreted biologically as, for example, an adaptive peak or zone; and ACDC also has an additional parameter that either makes the rate of diffusion decline or increase over time. In the special EB case with a negative decay parameter, disparity expands explosively in the past and much more slowly in the present, which corresponds to theoretical predictions for an adaptive radiation (Schluter 2000; Alfaro et al. 2009; Gavrilets and Losos 2009; Harmon et al. 2010; Lloyd et al. 2011; Stroud and Losos 2016).

The model fitting was unable to run properly on datasets that contained few taxa, so the data were subsetted per clade to (1) porolepiforms (n = 11), (2) dipnoans (n = 16), and (3) tetrapodomorphs (n = 24), alongside the full dataset of all sarcopterygians (n = 58). To quantitatively assess uncertainty, I fit the three models to each dataset using all of the timescaled, randomly resolved trees from ‘timePaleoPhy’ (‘ntrees’ = 100). The trees, along with the PC axes that accounted for 95% of the variation in each group (see scree plots in **Figure C9**), were then used as inputs to fit the three models using penalized likelihood (Clavel et al. 2019) via ‘mvgls’ in *mvMORPH* (v1.1.9) (Clavel et al., 2015) with the following flags: ‘scale.height’ = FALSE,

‘egmod’ = "PL-LOOCV", ‘penalty’ = "RidgeArch", ‘target’ = "unitVariance", and ‘error’ = TRUE. The latter is recommended for empirical datasets as it helps automatically account for variation via an additional nuisance parameter (Silvestro et al. 2015; Clavel et al. 2019). The upper bound for the OU model fitting was manually set to 10 due to a recommendation from the ‘mvgls’ output to increase the search space. I calculated Generalized Information Criterion (GIC) scores (Konishi and Kitagawa, Genshiro 1996; Konishi and Kitagawa 2008; Clavel et al. 2019) and weights (GICw) for all model fitting analyses and reported the variation of the distribution of the scores as well as the parameter estimates (**Figure 4.7**–**Figure 4.10**, **Figure C10**).

4.4 Results

4.4.1 Morphospace

PC 1 accounted for 65.01% of the disparity and is interpreted as being principally due to changes to the symphysis, adductor fossa, and thicker jaws associated with derived lungfishes. PC 2 accounted for 11.6% of the variation and is interpreted as being the compression of the lateral margin of the jaw into a spade shape and the enlarging of the glenoid (**Figure 4.2**). PC 3 accounted for 6.8% of the disparity and is interpreted as being related to the coelacanth jaw shape, including a smaller symphysis, a larger adductor fossa occupying most of the lingual side of the mandible, and the jaw becoming thin and gracile (**Figure 4.5**).

Stem sarcopterygians are all clustered together in the center on the left half of the morphospace, likely indicating an average-sized symphysis with a slightly below average sized adductor fossa. Both porolepiforms and tetrapodomorphs essentially occupy the same shape space, except some taxa from the former are further from the middle and the latter’s morphospace is slightly larger but spread near evenly in the center of the space. Cumulatively,

these three groups are the closest to the average sarcopterygian jaw. Coelacanths appear to occupy their own morphospace on PC 3 and lungfishes occupy the largest shape space, with substantial disparity both *among* lungfishes as well as *between* lungfishes and all other sarcopterygians. They can have large or small symphyses, large or small fossa, long or short mandibles as a whole, or a host of other combinations. Further axes beyond PC 5 are much less informative due to the clustering of the data about the center of the morphospace (**Figure 4.6**). When plotting PC 1 vs PC 2 over time from the late Silurian to the Late Devonian, all clades except for lungfishes occupy similar areas of the morphospace over the interval surveyed. The area occupied by lungfishes expands and contracts over time (**Figure 4.3**), but this is likely driven by sampling bias due to the presence of exceptionally rich lungfish assemblages in the Early and Late Devonian, and a lack of three-dimensionally preserved mandibles for most Middle Devonian lungfishes. An ANOVA using the Procrustes shape variables found no major variation among sarcopterygians relating to stratigraphic age (i.e., late Silurian, Early–Late Devonian) ($p = 0.142$) (**Table 4.1**). However, there is a highly significant difference ($p = 0.001$) as a function of clade membership (i.e., stem sarcopterygians, actinistians, porolepiforms, dipnoans, and tetrapodomorphs).

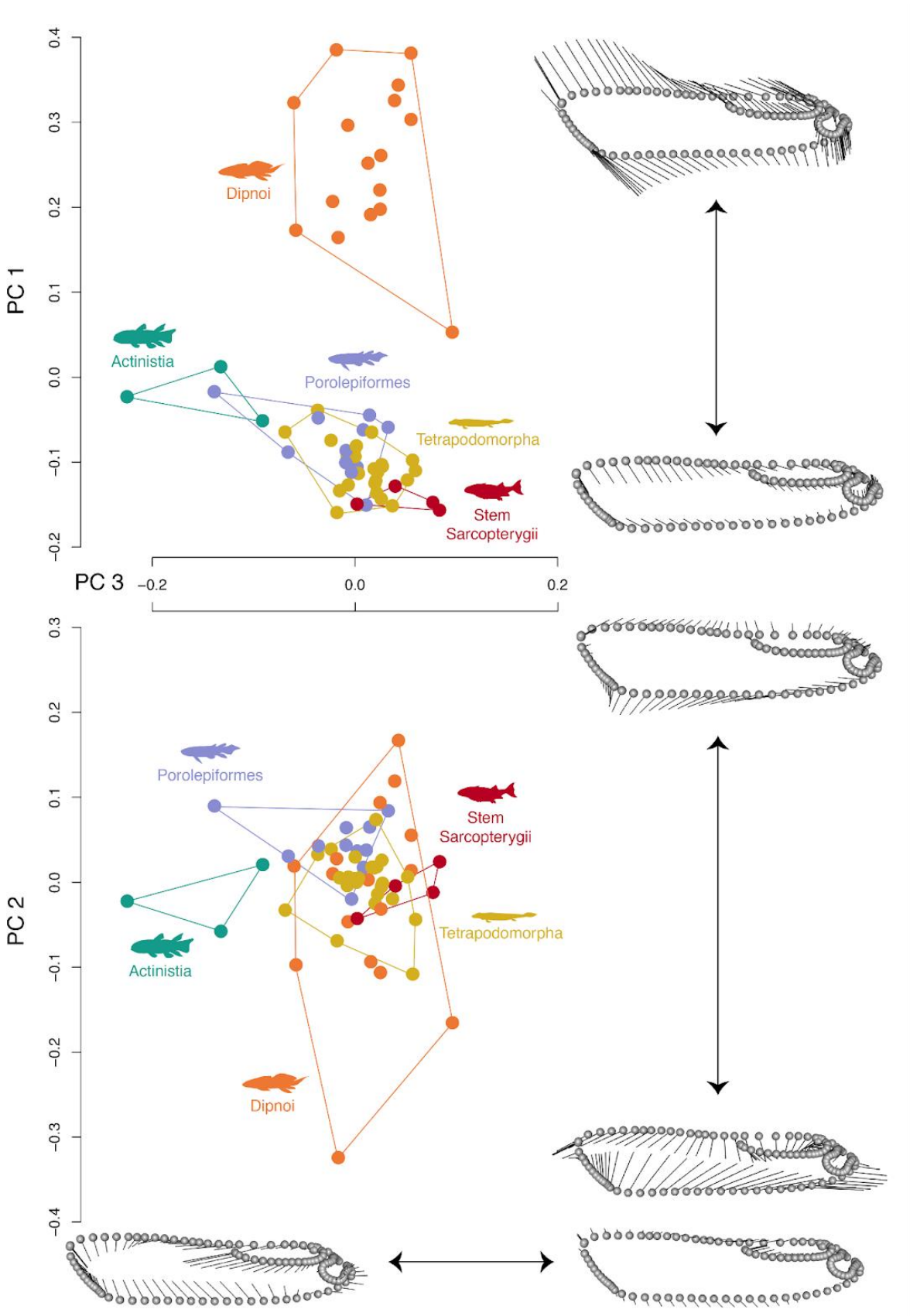
PC 1
PC 2
PC 3
Dipnoi
Actinistia
Porolepiformes
Tetrapodomorpha
Stem
Sarcopterygii
0.4
0.3
0.2
0.1
0.0
−0.1
−0.2
−0.3
−0.4
−0.2
0.0
0.2

Figure 4.5. Morphospace for lower jaws of late Silurian to Late Devonian sarcopterygian fishes using landmark-based geometric morphometrics. PC 1 summarizes 65.01% and PC 2 summarizes 11.6% of the variation in jaw shape, both of which were discussed in **Figure 4.2**. PC 3 summarizes 6.8% of the variation, with the left half being occupied by the more derived coelacanth condition, including a smaller symphysis, the enlargement of the anterior extent of the adductor fossa, and the thinning of the lateral outline of the jaw. The average jaw is represented by the 3D models along the periphery and show the vectors required to move the average value for all landmarks and semilandmarks to the minimum and maximum values along each axis. Convex hulls around five principal assemblages: stem sarcopterygians, actinistians, porolepiforms, dipnoans, and tetrapodomorphs. Silhouettes from PhyloPic, *Tiktaalik* silhouette by *Nobu Tamura* (CC BY-SA 3.0).

Table 4.1. Summary of the procrustes ANOVA on the source of shape variation in the sarcopterygian lower jaws dataset as a function of clades and ages. Rsq row represents the contribution to the overall variation and significant *p*-values are in bold with an asterisk. Clades are statistically tied to shape variation, whereas the time bins to which the taxa are assigned are not.

Statistic	clade	age
Rsq	0.64305	0.07781
F	23.87	1.5188
Z	6.0642	1.1449
p	**0.001***	0.142

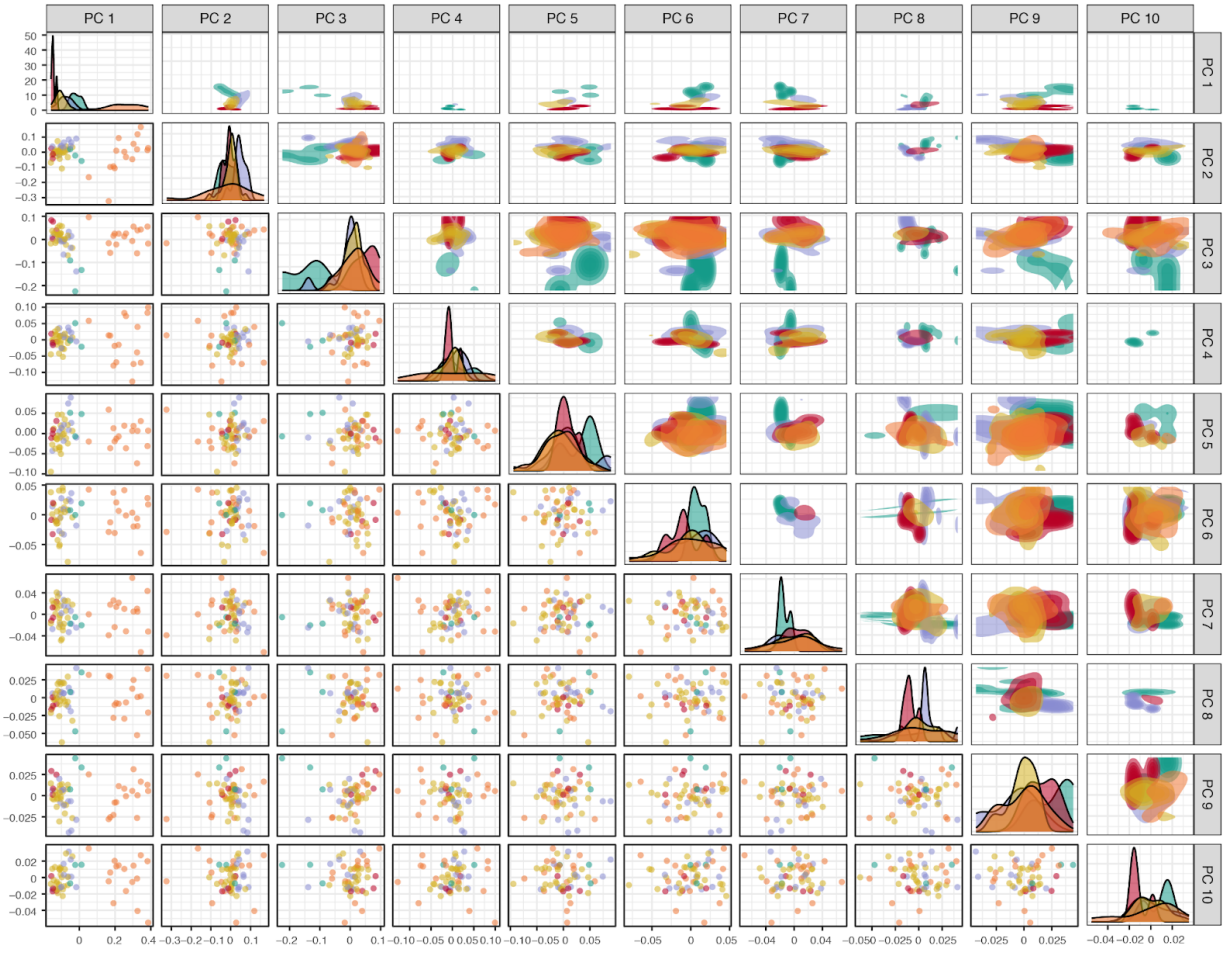

Figure 4.6. Morphospace (below diagonal) and paired density plots (above diagonal) of lower jaws in late Silurian to Late Devonian sarcopterygian fishes for PC axes summarizing 95% of the variability (10 total). The first 3 PCs were discussed in **Figure 4.2**, **Figure 4.3**, and **Figure 4.5**. Although dipnoans occupy the largest morphospace across all PCs, the density plots clearly show coelacanths occupy their own region on multiple axes as well. Density plots help visualize the degradation of informativeness as all taxa begin to overlap by PC 5. Colors match the ones labeling the five principal assemblages in all other figures: stem sarcopterygians (red), actinistians (teal), porolepiforms (light purple), dipnoans (orange), and tetrapodomorphs (yellow).

4.4.2 Model Fitting

The best fit evolutionary model for sarcopterygians was ACDC with declining rates, corresponding to the Early Burst variant of the model (GICw ~ 0.67) (**Figure 4.7**). The exponential change in evolutionary rate (*b*) for sarcopterygians was negative (*b* ~ -0.0226; 95% CI: -0.046, 0.011; **Figure C10**), implying rates two times lower at the tips than those at the root.

Of the subclade-specific datasets, both the dipnoans (GICw ~ 0.58) (**Figure 4.8**) and porolepiforms (GICw ~ 0.65) (**Figure 4.9**) are best fit by a BM model of diffusive evolution. The dipnoans had an average dispersion (mean of the sigma covariance matrix diagonal) of 5.67 x 10^{-5} and a spread (square root of the determinant of the sigma covariance matrix) of 5.21 x 10^{-20} (95% CI on dispersion: 5.05 x 10^{-5}, 6.34 x 10^{-5}; 95% CI on spread: 2.87 x 10^{-20}, 8.16 x 10^{-20}; **Figure C10**). The porolepiforms had an average dispersion of 7.04 x 10^{-12} and a spread of 3.49 x 10^{-34} (95% CI on dispersion: 1.11 x 10^{-17}, 1.28 x 10^{-11}; 95% CI on spread: 1.38 x 10^{-51}, 2.10 x 10^{-33}; **Figure C10**). This equates to dipnoans having higher average variability and low overall dispersion, while the porolepiforms had lower average variability and coupled with much lower dispersion. Conversely, tetrapods are best fit by an ACDC model with declining rates of evolution (GICw ~ 44.9%) (**Figure 4.10**). However, the confidence intervals of BM (GICw ~ 32.8%) fully overlapped with the distribution of GICw for EB, implying a failure to reject the null model of diffusive evolution. Although the average rate decay parameter for tetrapodomorphs is more negative (-0.068; 95% CI: -0.264, 0) than for sarcopterygians as a whole (-0.0226), the confidence intervals overlap 0. This translates into rates that are more likely to be 0 on any random tree that was fitted rather than be negative, as the decay parameter on an Early Burst should be.

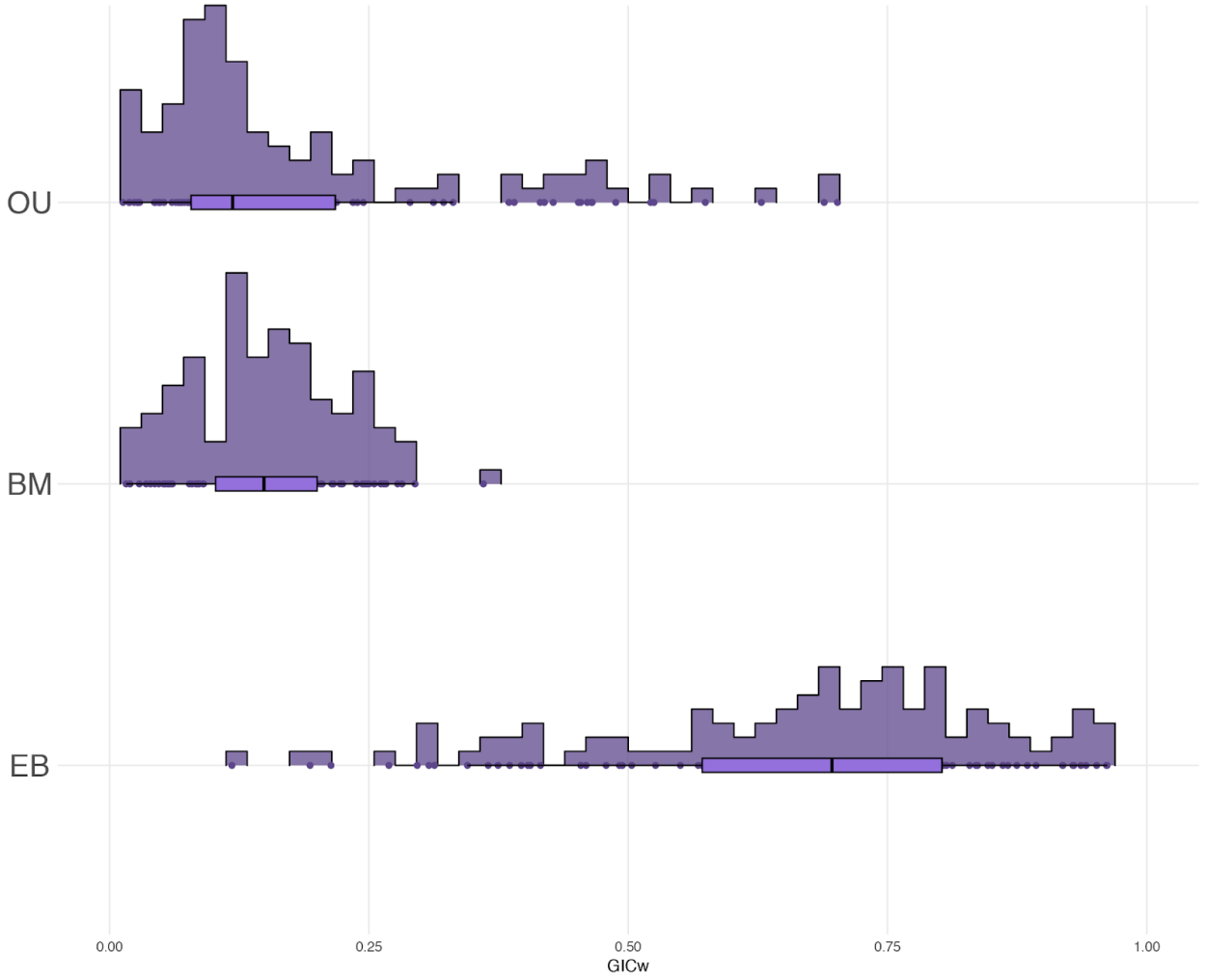

Figure 4.7. Distribution of GICw for evolutionary model fitting on 100 trees using 95% of the PCs from the full sarcopterygian dataset. Vertical bars represent relative frequencies and horizontal axes have box plots of the same relative frequencies. EB is the best fit model, with GICw ~ 67%.

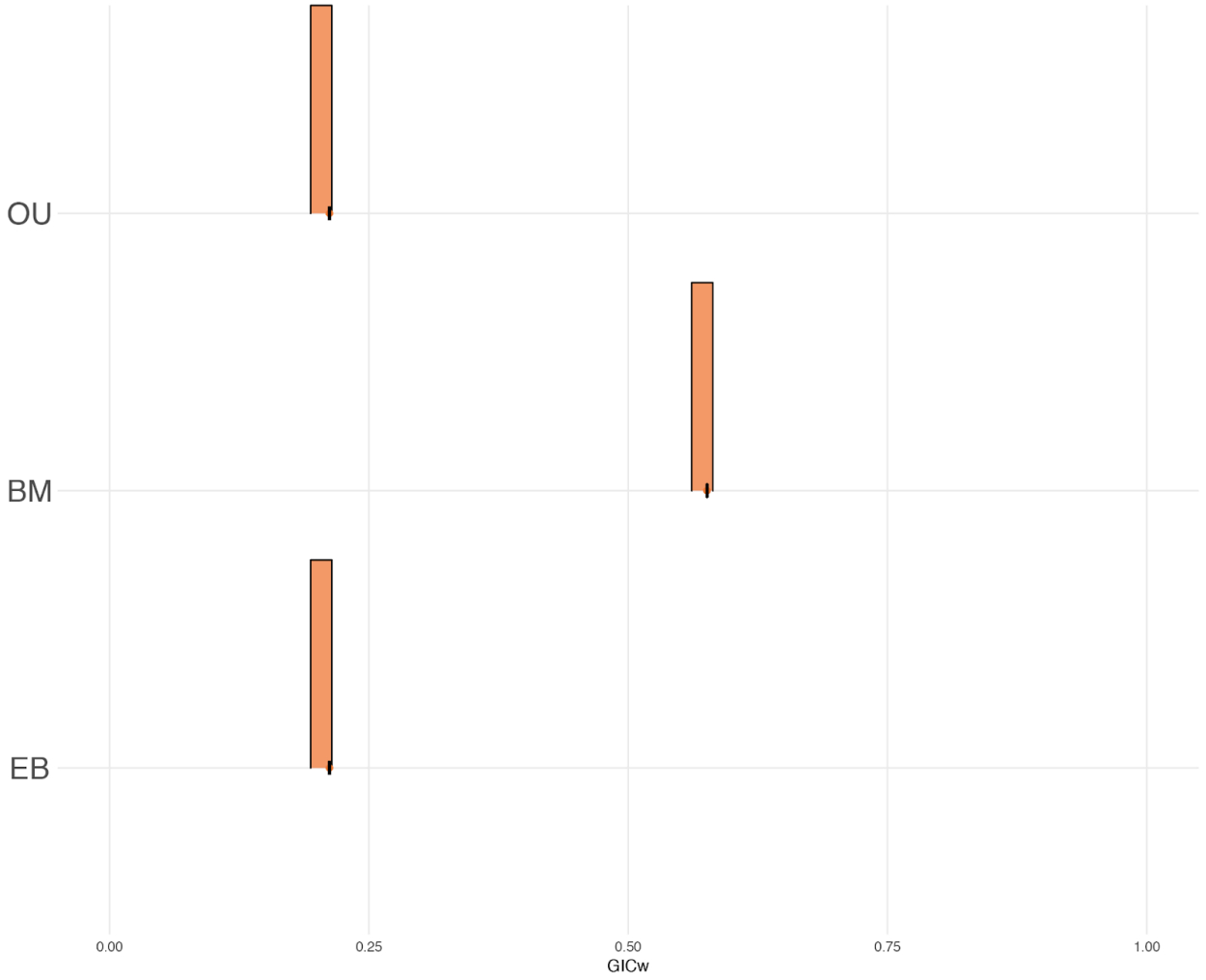

Figure 4.8. Distribution of GICw for evolutionary model fitting on 100 trees using 95% of the PCs from the subsetted dipnoan dataset. BM is the best fit model, with GICw ~ 58%.Vertical bars represent relative frequencies and horizontal axes have box plots of the same relative frequencies. This distribution is the most constrained in variability of all per-clade model fit tests due to there being fewer unresolved polytomies on the lungfish source tree.

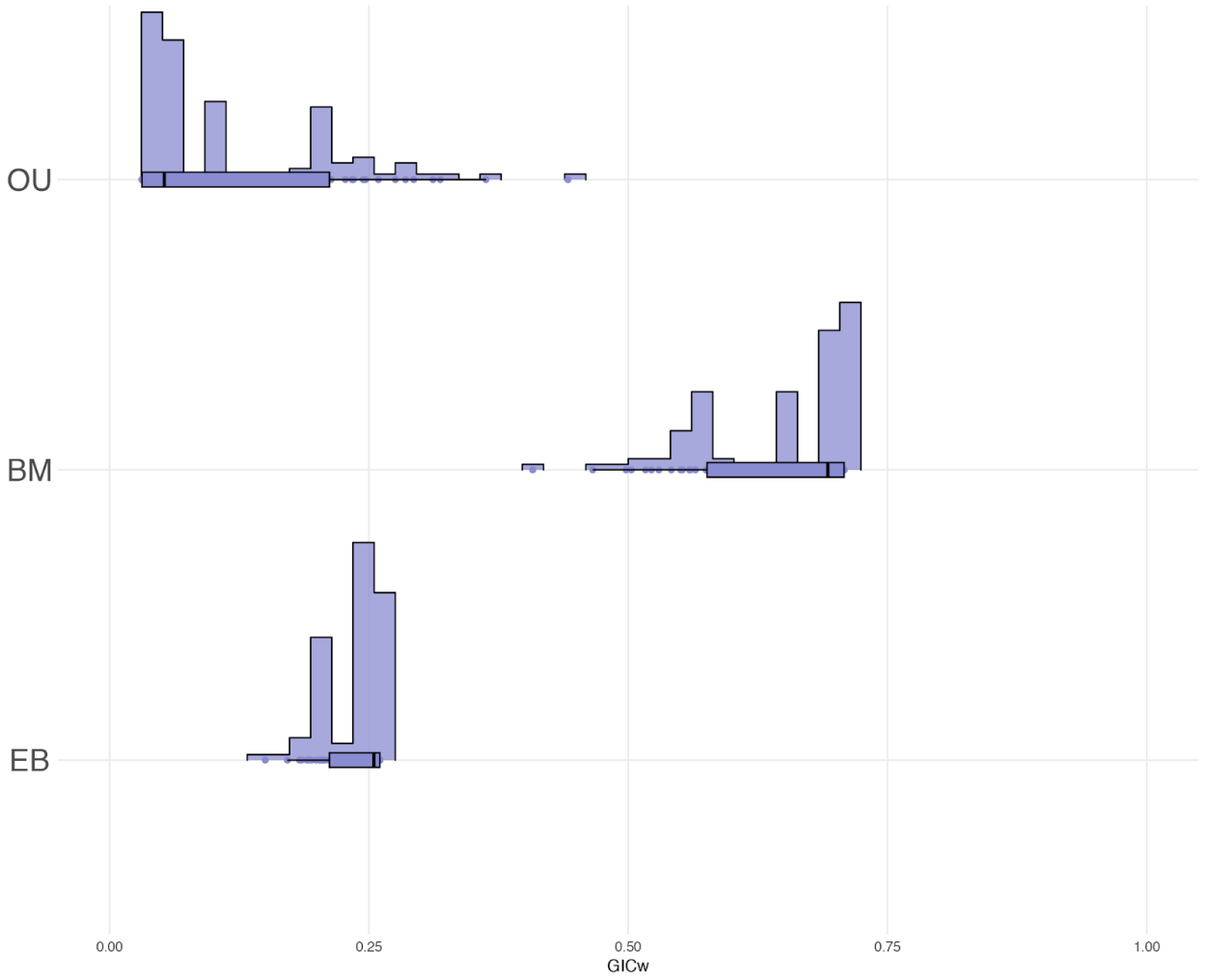

Figure 4.9. Distribution of GICw for evolutionary model fitting on 100 trees using 95% of the PCs from the subsetted porolepiform dataset. BM is the best fit model, with GICw ~ 65%. Vertical bars represent relative frequencies and horizontal axes have box plots of the same relative frequencies.

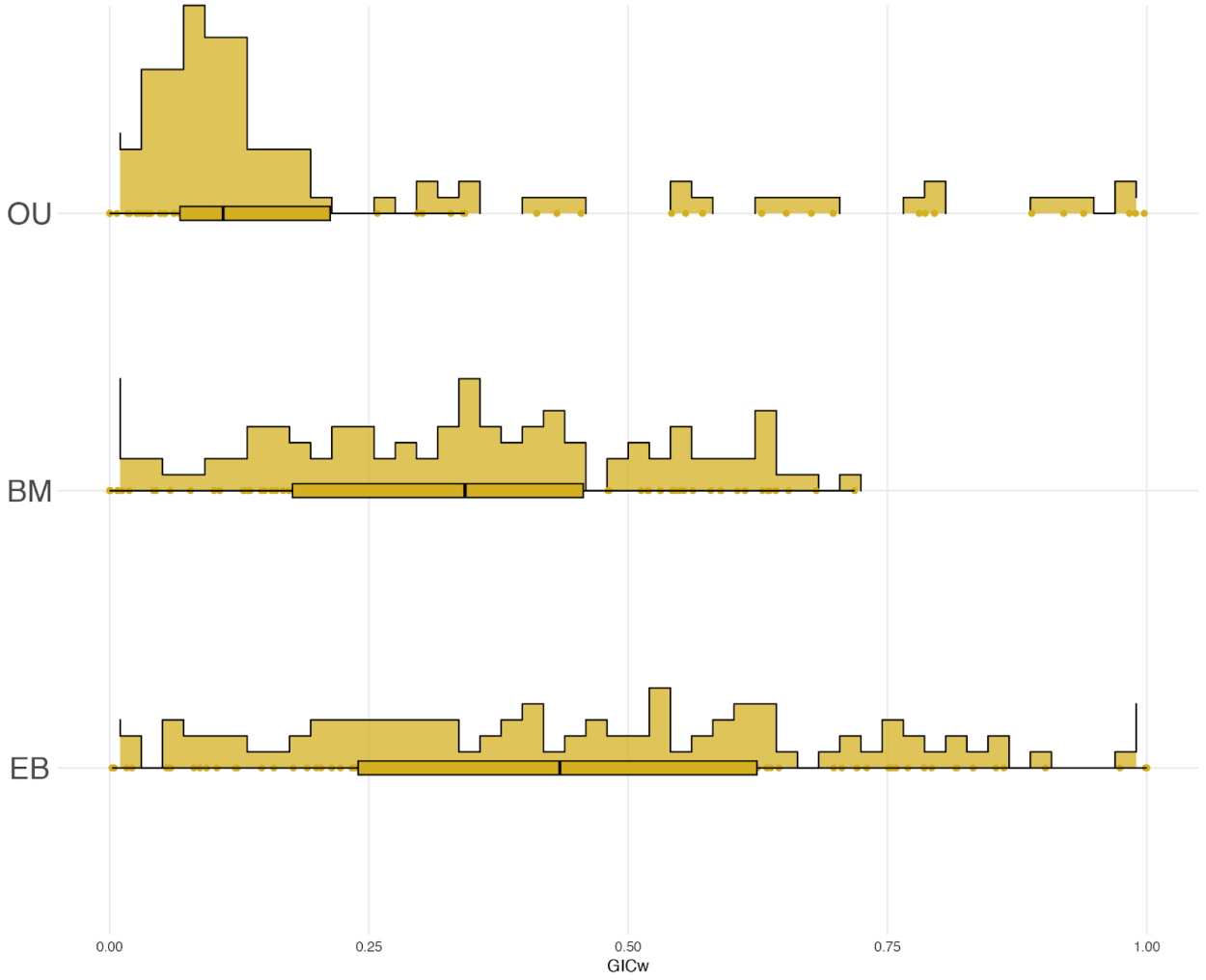

Figure 4.10. Distribution of GICw for evolutionary model fitting on 100 trees using 95% of the PCs from the subsetted tetrapodomorph dataset. EB is the best fit model, with GICw ~ 44.9%. However, more than half of the confidence intervals fully overlap with BM (GICw ~ 32.8%), making it unable to be rejected as a best fit model. Vertical bars represent relative frequencies and horizontal axes have box plots of the same relative frequencies.

4.5 Discussion and Conclusions

4.5.1 One Size Fits Most

The occupation of morphospace over time was remarkably consistent across nearly all groups (**Figure 4.3**), matching prior work on jaws that used different trait measures (Anderson et al. 2011, 2013). Lungfishes are an exception, but this may be a geological rather than biological

pattern arising from the exceptional Australian sites of Wee Jasper (Early Devonian) (Young 2011) and Gogo (Late Devonian) (Long and Trinajstic 2010). These localities preserve uncrushed material that can be extracted from rock in three dimensions using acid preparation, thus creating an oversampling of lungfishes in comparison to other groups which may not be found at these sites. Alternatively, some in the literature have asserted that functional saturation and subsequent refilling can also cause morphospaces to remain constricted over long periods (Anderson et al. 2011). Unfortunately, my dataset is too sparse in terms of both major groups examined and stratigraphic coverage to properly assess the effects of any turnover occurring at the stage level, such as the Kellwasser event, which was an extinction localized to the Frasnian-Famennian boundary (Raup and Sepkoski 1982; Friedman and Sallan 2012). Nevertheless, I was able to show that the variation in PC 1 and PC 2 is almost entirely attributable to the either elongated or thick lower jaws of disparate groups of lungfishes due to their feeding ecologies. The upper quadrant (**Figure 4.2**) includes taxa such as *Chirodipterus*, with robust mandibles, an oblong and stout glenoid, and dentine-plating with a large adductor muscle. This combination of characters has been recognized as the earliest evolution of durophagy, marking the beginning of an ecological adaptation that would persist in lungfishes as they transitioned from marine to freshwater environments (Clement 2019; Cui et al. 2022). The lower quadrant includes mostly denticulated forms such as *Griphognathus*, with long, dorsoventrally compressed mandibles, a large glenoid fossa, and small and oblique adductor muscle insertion. Although these characters have often been linked to suction feeding of softer prey, there is some diversity in feeding ecology within the long-snouted lungfishes due to the existence of smooth tooth plated forms that would have coupled suction feeding with crushing (Miles 1977; Westneat 2005; Clement 2012, 2019). These results appear to conform to theoretical expectations of rapid diversification

coupled with disparity due to biotic effects such as innovations in feeding ecology (Schluter 2000; Anderson et al. 2013; Stroud and Losos 2016). Alongside lungfishes, coelacanths were the only other group that occupied their own axis of variation (PC 3, **Figure 4.5**) due to the anteriorly extended adductor fossa, small symphysis, and deeply inset glenoid. This morphology is also associated with suction feeding and, similarly to robust jaws with toothplates in lungfishes, what began in the Devonian remains a key aspect of their modern morphology and feeding ecology (Lund et al. 1985). All remaining groups occupied the average sarcopterygian jaw morphospace through the Devonian, likely indicating success with a generalist predatory lifestyle.

4.5.2 An Early Burst?

My results indicate that the EB case of ACDC is the best-supported model for jaw shape evolution across the early history of lobe-finned fishes and is consistent with theoretical models of trait evolution in an adaptive radiation (Harmon et al. 2010). Because mandibles are closely linked to organismal function through the capture and processing of prey, these shifts in evolutionary rates can be linked to probable patterns of divergence in aspects of ecology, which is central to most conceptualizations of adaptive radiation (Schluter 2000). The recovered beta parameter, capturing the exponential decrease in rates over time in EB models, implied rates were two times lower at the tips than those at the root ($b \sim -0.0226$). This gradual decline in rates is coupled with a rapid accumulation of disparity in shape over time, as shown by the comparable areas of shape space occupied in the Early and Middle Devonian. In contrast to sarcopterygians as a whole, there is weak support for declining rates within the Devonian interval for the major sub-clades of lobe-finned fishes. This indicates the principal feature of

diversification in early sarcopterygians was *between* the major lineages, with more conservative patterns *within* those groups. The sigma covariance measures in the two groups for which BM was the best fit model bear this out (**Figure C10**). Lungfishes had markedly higher average variability and dispersion than porolepiforms. This can be related to visual models of adaptive radiation (e.g., Simpson 1944) and imply the early discovery of adaptive zones within a group's history, a result in line with the aforementioned crushing and suction feeding morphologies. Curiously, the only assemblage for which EB was recovered with even moderate support was tetrapodomorphs, a clade for which diversification is generally associated with terrestrial members of the group rather than the primitively aquatic ones surveyed here (Ruta et al. 2006; Clack 2012). It was also the clade with the weakest support for its model fit while having the largest sample size to draw inferences from.

Failure to recover broad support for declining rates of mandibular evolution for each individual lineage *within* the Devonian is not surprising, since other aspects of phenotypic change appear to show the most pronounced declines *after* the Devonian. Tetrapodomorphs are the exception to this pattern due to the occupation of terrestrial environments that fueled substantial diversification (Ruta et al. 2006; Clack 2012). Qualitatively, primitively aquatic tetrapodomorph fishes show a pattern comparable to lungfishes and coelacanths, with declining taxonomic diversity and increasing environmental restriction over time. The last surviving species of tetrapodomorph fishes in the early Permian were limited to freshwater settings (Janvier 1996; Clack 2012).

On a broader scale, the results of these analyses on the lower jaws of the earliest sarcopterygians can provide additional insight into patterns of phenotypic change displayed by disparate groups. The high early rates of change inferred for "living fossil" groups like

lungfishes and coelacanths based on discrete characters and body shape (Chapter 2 of this Dissertation) can be understood as an extension of the initial evolutionary radiation of sarcopterygians. In fact, it is possible that the distinction between adaptive radiations and "living fossils" is merely about perspective. After all, to a Late Devonian sarcopterygian, a trilobite would have seemed like a "living fossil."

4.6 References

Adams, D.C., Otárola-Castillo, E., 2013. geomorph: an r package for the collection and analysis of geometric morphometric shape data. Methods Ecol. Evol. 4, 393–399. https://doi.org/10.1111/2041-210X.12035

Ahlberg, P.E., Clack, J.A., 1998. Lower jaws, lower tetrapods–a review based on the Devonian genus Acanthostega. Trans. R. Soc. Edinb. Earth Sci. 89, 11–46. https://doi.org/10.1017/S0263593300002340

Alfaro, M.E., Santini, F., Brock, C., Alamillo, H., Dornburg, A., Rabosky, D.L., Carnevale, G., Harmon, L.J., 2009. Nine exceptional radiations plus high turnover explain species diversity in jawed vertebrates. Proc. Natl. Acad. Sci. 106, 13410–13414. https://doi.org/10.1073/pnas.0811087106

Anderson, P.S.L., 2008. Cranial muscle homology across modern gnathostomes. Biol. J. Linn. Soc. 94, 195–216. https://doi.org/10.1111/j.1095-8312.2008.00963.x

Anderson, P.S.L., Friedman, M., Brazeau, M.D., Rayfield, E.J., 2011. Initial radiation of jaws demonstrated stability despite faunal and environmental change. Nature 476, 206–209. https://doi.org/10.1038/nature10207

Anderson, P.S.L., Friedman, M., Ruta, M., 2013. Late to the Table: Diversification of Tetrapod Mandibular Biomechanics Lagged Behind the Evolution of Terrestriality. Integr. Comp. Biol. 53, 197–208. https://doi.org/10.1093/icb/ict006

Andreev, P.S., Sansom, I.J., Li, Q., Zhao, W., Wang, J., Wang, C.-C., Peng, L., Jia, L., Qiao, T., Zhu, M., 2022a. The oldest gnathostome teeth. Nature 609, 964–968. https://doi.org/10.1038/s41586-022-05166-2

Andreev, P.S., Sansom, I.J., Li, Q., Zhao, W., Wang, J., Wang, C.-C., Peng, L., Jia, L., Qiao, T., Zhu, M., 2022b. Spiny chondrichthyan from the lower Silurian of South China. Nature 609, 969–974. https://doi.org/10.1038/s41586-022-05233-8

Baken, E.K., Collyer, M.L., Kaliontzopoulou, A., Adams, D.C., 2021. geomorph v4.0 and gmShiny: Enhanced analytics and a new graphical interface for a comprehensive morphometric experience. Methods Ecol. Evol. 12, 2355–2363. https://doi.org/10.1111/2041-210X.13723

Bapst, D.W., 2012. Paleotree: An R package for paleontological and phylogenetic analyses of evolution. Methods Ecol. Evol. 3, 803–807. https://doi.org/10.1111/j.2041-210X.2012.00223.x

Bellwood, D.R., 2003. Origins and escalation of herbivory in fishes: a functional perspective. Paleobiology 29, 71–83. https://doi.org/10.1666/0094-8373(2003)029<0071:OAEOHI>2.0.CO;2

Botella, H., Blom, H., Dorka, M., Ahlberg, P.E., Janvier, P., 2007. Jaws and teeth of the earliest bony fishes. Nature 448, 583–586. https://doi.org/10.1038/nature05989

Brazeau, M.D., Friedman, M., 2014. The characters of Palaeozoic jawed vertebrates. Zool. J. Linn. Soc. 170, 779–821. https://doi.org/10.1111/zoj.12111

Brinkmann, H., Venkatesh, B., Brenner, S., Meyer, A., 2004. Nuclear protein-coding genes support lungfish and not the coelacanth as the closest living relatives of land vertebrates. Proc. Natl. Acad. Sci. 101, 4900–4905. https://doi.org/10.1073/pnas.0400609101

Brusatte, S.L., 2011. Calculating the Tempo of Morphological Evolution: Rates of Discrete Character Change in a Phylogenetic Context, in: Elewa, A.M.T. (Ed.), Computational

Paleontology. Springer Berlin Heidelberg, Berlin, Heidelberg, pp. 53–74. https://doi.org/10.1007/978-3-642-16271-8_4

Cawley, J.J., Marramà, G., Carnevale, G., Villafaña, J.A., López-Romero, F.A., Kriwet, J., 2021. Rise and fall of †Pycnodontiformes: Diversity, competition and extinction of a successful fish clade. Ecol. Evol. 11, 1769–1796. https://doi.org/10.1002/ece3.7168

Chang, M.-M., 1995. *Diabolepis* and its bearing on the relationships between porolepiforms and dipnoans. Bull. Muséum Natl. Hist. Nat. 4ème Sér. – Sect. C – Sci. Terre Paléontol. Géologie Minéralogie 1–4, 235–268.

Cignoni, P., Callieri, M., Corsini, M., Dellepiane, M., Ganovelli, F., Ranzuglia, G., 2008. MeshLab: an Open-Source Mesh Processing Tool. Eurographics Ital. Chapter Conf. 8 pages. https://doi.org/10.2312/LOCALCHAPTEREVENTS/ITALCHAP/ITALIANCHAPCONF2008/129-136

Cignoni, P., Montani, C., Rocchini, C., Scopigno, R., Tarini, M., 1999. Preserving attribute values on simplified meshes by resampling detail textures. Vis. Comput. 15, 519–539. https://doi.org/10.1007/s003710050197

Clack, J.A., 2012. Gaining Ground: The Origin and Evolution of Tetrapods. Indiana University Press, Bloomington & Indianapolis.

Clavel, J., Aristide, L., Morlon, H., 2019. A Penalized Likelihood Framework for High-Dimensional Phylogenetic Comparative Methods and an Application to New-World Monkeys Brain Evolution. Syst. Biol. 68, 93–116. https://doi.org/10.1093/sysbio/syy045

Clavel, J., Escarguel, G., Merceron, G., 2015. mvMORPH: an R package for fitting multivariate evolutionary models to morphometric data. Methods Ecol. Evol. 6, 1311–1319. https://doi.org/10.1111/2041-210X.12420

Claverie, T., Wainwright, P.C., 2014. A Morphospace for Reef Fishes: Elongation Is the Dominant Axis of Body Shape Evolution. PLoS ONE 9, e112732. https://doi.org/10.1371/journal.pone.0112732

Clement, A.M., 2019. Sarcopterygian Fishes, the "Lobe-Fins," in: Ziermann, J.M., Diaz Jr, R.E., Diogo, R. (Eds.), Heads, Jaws, and Muscles, Fascinating Life Sciences. Springer International Publishing, Cham, pp. 119–142. https://doi.org/10.1007/978-3-319-93560-7_6

Clement, A.M., 2012. A new species of long-snouted lungfish from the Late Devonian of Australia, and its functional and biogeographical implications. Palaeontology 55, 51–71. https://doi.org/10.1111/j.1475-4983.2011.01118.x

Clément, G., Ahlberg, P.E., 2010. The endocranial anatomy of the early sarcopterygian *Powichthys* from Spitsbergen, based on CT scanning, in: Elliott, D.K., Maisey, J.G., Yu, X., Miao, D. (Eds.), Morphology, Phylogeny and Paleobiogeography of Fossil Fishes: Honoring Meemann Chang. Verlag Dr. Friedrich Pfeil, München, pp. 363–377.

Cui, X., Friedman, M., Qiao, T., Yu, Y., Zhu, M., 2022. The rapid evolution of lungfish durophagy. Nat. Commun. 13, 2390. https://doi.org/10.1038/s41467-022-30091-3

Daeschler, E.B., Cressler, W.L., 2011. Late Devonian paleontology and paleoenvironments at Red Hill and other fossil sites in the Catskill Formation of north-central Pennsylvania, in: From the Shield to the Sea: Geological Field Trips from the 2011 Joint Meeting of the

GSA Northeastern and North-Central Sections. Geological Society of America, pp. 1–16. https://doi.org/10.1130/2011.0020(01)

Deakin, W.J., Anderson, P.S.L., Den Boer, W., Smith, T.J., Hill, J.J., Rücklin, M., Donoghue, P.C.J., Rayfield, E.J., 2022. Increasing morphological disparity and decreasing optimality for jaw speed and strength during the radiation of jawed vertebrates. Sci. Adv. 8, eabl3644. https://doi.org/10.1126/sciadv.abl3644

DeVries, R.P., Sereno, P.C., Vidal, D., Baumgart, S.L., 2022. Reproducible Digital Restoration of Fossils Using Blender. Front. Earth Sci. 10, 833379. https://doi.org/10.3389/feart.2022.833379

Fedorov, A., Beichel, R., Kalpathy-Cramer, J., Finet, J., Fillion-Robin, J.-C., Pujol, S., Bauer, C., Jennings, D., Fennessy, F., Sonka, M., Buatti, J., Aylward, S., Miller, J.V., Pieper, S., Kikinis, R., 2012. 3D Slicer as an image computing platform for the Quantitative Imaging Network. Magn. Reson. Imaging 30, 1323–1341. https://doi.org/10.1016/j.mri.2012.05.001

Friedman, M., 2022. Fossils reveal the deep roots of jawed vertebrates. Nature 609, 897–898. https://doi.org/10.1038/d41586-022-02973-5

Friedman, M., 2010. Explosive morphological diversification of spiny-finned teleost fishes in the aftermath of the end-Cretaceous extinction. Proc. R. Soc. B Biol. Sci. 277, 1675–1683. https://doi.org/10.1098/rspb.2009.2177

Friedman, M., Coates, M.I., 2006. A newly recognized fossil coelacanth highlights the early morphological diversification of the clade. Proc. R. Soc. B Biol. Sci. 273, 245–250. https://doi.org/10.1098/rspb.2005.3316

Friedman, M., Sallan, L.C., 2012. Five hundred million years of extinction and recovery: A phanerozoic survey of large-scale diversity patterns in fishes. Palaeontology 55, 707–742. https://doi.org/10.1111/j.1475-4983.2012.01165.x

Garland, M., Heckbert, P.S., 2023. Surface Simplification Using Quadric Error Metrics, in: Whitton, M.C. (Ed.), Seminal Graphics Papers: Pushing the Boundaries, Volume 2. ACM, New York, NY, USA, pp. 131–138. https://doi.org/10.1145/3596711.3596727

Gavrilets, S., Losos, J.B., 2009. Adaptive Radiation: Contrasting Theory with Data. Science 323, 732–737. https://doi.org/10.1126/science.1157966

Givnish, T.J., 2015. Adaptive radiation versus 'radiation' and 'explosive diversification': why conceptual distinctions are fundamental to understanding evolution. New Phytol. 207, 297–303. https://doi.org/10.1111/nph.13482

Gradstein, F.M., Ogg, J.G., Schmitz, M.D., Ogg, G.M., 2020. The Geologic Time Scale 2020. Elsevier, Amsterdam.

Gunz, P., Mitteroecker, P., Bookstein, F.L., 2005. Semilandmarks in Three Dimensions, in: Slice, D.E. (Ed.), Modern Morphometrics in Physical Anthropology, Developments in Primatology: Progress and Prospects. Kluwer Academic Publishers-Plenum Publishers, New York, pp. 73–98. https://doi.org/10.1007/0-387-27614-9_3

Harmon, L.J., Losos, J.B., Jonathan Davies, T., Gillespie, R.G., Gittleman, J.L., Bryan Jennings, W., Kozak, K.H., McPeek, M.A., Moreno-Roark, F., Near, T.J., Purvis, A., Ricklefs, R.E., Schluter, D., Schulte, J.A., Seehausen, O., Sidlauskas, B.L., Torres-Carvajal, O., Weir, J.T., Mooers, A.T., 2010. Early bursts of body size and shape evolution are rare in comparative data. Evolution. https://doi.org/10.1111/j.1558-5646.2010.01025.x

Hill, J.J., Puttick, M.N., Stubbs, T.L., Rayfield, E.J., Donoghue, P.C.J., 2018. Evolution of jaw disparity in fishes. Palaeontology 61, 847–854. https://doi.org/10.1111/pala.12371

Janvier, P., 1996. Early Vertebrates. Oxford University Press, New York.

Johanson, Z., Long, J.A., Talent, J.A., Janvier, P., Warren, J.W., 2006. Oldest coelacanth, from the Early Devonian of Australia. Biol. Lett. 2, 443–446. https://doi.org/10.1098/rsbl.2006.0470

Konishi, S., Kitagawa, G., 2008. Information Criteria and Statistical Modeling, Springer Series in Statistics. Springer New York, New York, NY. https://doi.org/10.1007/978-0-387-71887-3

Konishi, S., Kitagawa, Genshiro, 1996. Generalised information criteria in model selection. Biometrika 83, 875–890. https://doi.org/10.1093/biomet/83.4.875

Lloyd, G.T., Wang, S.C., Brusatte, S.L., 2011. Identifying heterogeneity in rates of morphological evolution: discrete character change in the evolution of lungfish (Sarcopterygii; Dipnoi). Evolution 66, 330–348. https://doi.org/10.1111/j.1558-5646.2011.01460.x

Long, J.A., Trinajstic, K., 2010. The Late Devonian Gogo Formation Lägerstatte of Western Australia: Exceptional Early Vertebrate Preservation and Diversity. Annu. Rev. Earth Planet. Sci. 38, 255–279. https://doi.org/10.1146/annurev-earth-040809-152416

Lu, J., Zhu, M., 2010. An onychodont fish (Osteichthyes, Sarcopterygii) from the Early Devonian of China, and the evolution of the Onychodontiformes. Proc. R. Soc. B Biol. Sci. 277, 293–299. https://doi.org/10.1098/rspb.2009.0708

Lu, J., Zhu, M., Long, J.A., Zhao, W., Senden, T.J., Jia, L., Qiao, T., 2012. The earliest known stem-tetrapod from the Lower Devonian of China. Nat. Commun. 3, 1160. https://doi.org/10.1038/ncomms2170

Lund, W.L., Lund, R., Klein, G.A., 1985. Coelacanth feeding mechanisms and the ecology of the Bear Gulch coelacanths. Compte Rendus Neuvième Congrès Int. Sur Stratigr. Géologie Carbonif. 5, 492–500.

Luo, Y., Cui, X., Qiao, T., Zhu, M., 2021. A new dipnoan genus from the Middle Devonian of Huize, Yunnan, China. J. Syst. Palaeontol. 19, 1303–1315. https://doi.org/10.1080/14772019.2022.2042409

Miles, R.S., 1977. Dipnoan (lungfish) skulls and the relationships of the group: a study based on new species from the Devonian of Australia. Zool. J. Linn. Soc. 61, 1–328. https://doi.org/10.1111/j.1096-3642.1977.tb01031.x

Osborn, H.F., 1902. The Law of Adaptive Radiation. Am. Nat. 36, 353–363.

R Core Team, 2013. R: A language and environment for statistical computing.

Raup, D.M., Sepkoski, J.J., 1982. Mass Extinctions in the Marine Fossil Record. Science 215, 1501–1503. https://doi.org/10.1126/science.215.4539.1501

Rohlf, F.J., Slice, D., 1990. Extensions of the Procrustes Method for the Optimal Superimposition of Landmarks. Syst. Zool. 39, 40. https://doi.org/10.2307/2992207

Rokas, A., Carroll, S.B., 2006. Bushes in the tree of life. PLoS Biol. 4, e352. https://doi.org/10.1371/journal.pbio.0040352

Ruta, M., Wagner, P.J., Coates, M.I., 2006. Evolutionary patterns in early tetrapods. I. Rapid initial diversification followed by decrease in rates of character change. Proc. R. Soc. B Biol. Sci. 273, 2107–2111. https://doi.org/10.1098/rspb.2006.3577

Schluter, D., 2000. The ecology of adaptive radiation, Oxford series in ecology and evolution. Oxford University Press, Oxford.

Schultze, H.-P., 2000. A Porolepiform Rhipidistian from the Lower Devonian of the Canadian Arctic. Foss. Rec. 3, 99–109. https://doi.org/10.5194/fr-3-99-2000

Silvestro, D., Kostikova, A., Litsios, G., Pearman, P.B., Salamin, N., 2015. Measurement errors should always be incorporated in phylogenetic comparative analysis. Methods Ecol. Evol. 6, 340–346. https://doi.org/10.1111/2041-210X.12337

Simões, M., Breitkreuz, L., Alvarado, M., Baca, S., Cooper, J.C., Heins, L., Herzog, K., Lieberman, B.S., 2016. The Evolving Theory of Evolutionary Radiations. Trends Ecol. Evol. 31, 27–34. https://doi.org/10.1016/j.tree.2015.10.007

Simpson, G.G., 1953. The Major Features of Evolution. Columbia University Press. https://doi.org/10.7312/simp93764

Simpson, G.G., 1944. Tempo and Mode in Evolution. Columbia University Press, New York, NY. https://doi.org/10.7312/simp93040

Soulebeau, A., Aubriot, X., Gaudeul, M., Rouhan, G., Hennequin, S., Haevermans, T., Dubuisson, J.-Y., Jabbour, F., 2015. The hypothesis of adaptive radiation in evolutionary biology: hard facts about a hazy concept. Org. Divers. Evol. 15, 747–761. https://doi.org/10.1007/s13127-015-0220-z

Stöver, B.C., Müller, K.F., 2010. TreeGraph 2: Combining and visualizing evidence from different phylogenetic analyses. BMC Bioinformatics 11, 7. https://doi.org/10.1186/1471-2105-11-7

Stroud, J.T., Losos, J.B., 2016. Ecological Opportunity and Adaptive Radiation. Annu. Rev. Ecol. Evol. Syst. 47, 507–532. https://doi.org/10.1146/annurev-ecolsys-121415-032254

Toriño, P., Soto, M., Perea, D., 2021. A comprehensive phylogenetic analysis of coelacanth fishes (Sarcopterygii, Actinistia) with comments on the composition of the Mawsoniidae and Latimeriidae: evaluating old and new methodological challenges and constraints. Hist. Biol. 33, 3423–3443. https://doi.org/10.1080/08912963.2020.1867982

Trewin, N.H., 1986. Palaeoecology and sedimentology of the Achanarras fish bed of the Middle Old Red Sandstone, Scotland. Trans. R. Soc. Edinb. Earth Sci. 77, 21–46. https://doi.org/10.1017/S0263593300010737

Wainwright, P.C., Westneat, M.W., Bellwood, D.R., 2000. Linking feeding behaviour and jaw mechanics in fishes, in: Blake, R.W., Domenici, P. (Eds.), Biomechanics in Animal Behaviour. Garland Science, London, pp. 207–221.

Westneat, M.W., 2005. Skull Biomechanics and Suction Feeding in Fishes, in: Fish Physiology. Elsevier, pp. 29–75. https://doi.org/10.1016/S1546-5098(05)23002-9

Westneat, M.W., 2004. Evolution of Levers and Linkages in the Feeding Mechanisms of Fishes. Integr. Comp. Biol. 44, 378–389. https://doi.org/10.1093/icb/44.5.378

Westneat, M.W., 2003. A biomechanical model for analysis of muscle force, power output and lower jaw motion in fishes. J. Theor. Biol. 223, 269–281. https://doi.org/10.1016/S0022-5193(03)00058-4

Young, G.C., 2011. Wee Jasper-Lake Burrinjuck fossil fish sites: scientific background to national heritage nomination. Proc. Linn. Soc. New South Wales 132.

Young, G.C., 2010. Placoderms (Armored Fish): Dominant Vertebrates of the Devonian Period. Annu. Rev. Earth Planet. Sci. 38, 523–550. https://doi.org/10.1146/annurev-earth-040809-152507

Zhang, C., 2024. SlicerMorphR: Import SlicerMorph data into R.

Zhu, M., Ahlberg, P.E., Zhao, W.-J., Jia, L.-T., 2017. A Devonian tetrapod-like fish reveals substantial parallelism in stem tetrapod evolution. Nat. Ecol. Evol. 1, 1470–1476. https://doi.org/10.1038/s41559-017-0293-5

Zhu, M., Yu, X., 2004. Lower jaw character transitions among major sarcopterygian groups—a survey based on new materials from Yunnan, China, in: Arratia Fuentes, G., Wilson, M.V.H., Cloutier, R., Schultze, H.-P. (Eds.), Recent Advances in the Origin and Early Radiation of Vertebrates: Honoring Hans-Peter Schultze. F. Pfeil, München, pp. 271–286.

Zhu, Y., Li, Q., Lu, J., Chen, Y., Wang, J., Gai, Z., Zhao, W., Wei, G., Yu, Y., Ahlberg, P.E., Zhu, M., 2022. The oldest complete jawed vertebrates from the early Silurian of China. Nature 609, 954–958. https://doi.org/10.1038/s41586-022-05136-8

Chapter 5 – Conclusions

5.1 Where We Stand

This dissertation has interrogated the evolutionary history of sarcopterygians (and other "living fossils") and gleaned significant insights into the macroevolutionary patterns that shaped these vertebrate lineages. It can perhaps best be appreciated by considering each of the chapters as examining phenotypic changes at ever expanding scales, from the stage level to periods and then across eras.

Beginning at the smallest scale, I examined a 'phaneropleurid'-grade lungfish from the Late Devonian (Frasnian) Fram Formation of Ellesmere Island, Canada. Discovered during fieldwork undertaken by the same Nunavut Paleontological Expeditions that unearthed the transitional "fishapod" *Tiktaalik* (Daeschler et al. 2006), this lungfish also has an anatomy that highlights a key transitional moment in the history of the clade. Its cranial ribs and elongated parasphenoid stalk, which aid in air gulping, links it to derived lungfishes. Further, the elongation of the base of the second dorsal fin, a characteristic which began to appear in lungfishes by the Middle Devonian, places it with other members of the 'phaneropleurid' grade (Cloutier and Ahlberg 1996; Friedman 2010; Challands and den Blaauwen 2017). The large body and differences in the skull roof also set it apart from *Scaumenacia*, which is notably missing from the faunal assemblage preserved in the Fram Formation where this lungfish may occupy a similar role in the ecosystem. Taken together, the transitional anatomy identified in this lungfish

represents a set of characters that may be useful in anchoring the unstable early backbone of the lungfish phylogeny if integrated into morphological matrices in the future.

Scaling up to the late Silurian–Late Devonian, I explored the diversity in mandible geometry in early sarcopterygians during one of the first supposed episodes of adaptive radiation. I found that the clade as a whole is best fit by a model of exponentially declining rates of evolution, while more diffusive evolution was the best fit in other assemblages within the group (tetrapodomorphs, porolepiforms, and lungfishes). Even tetrapodomorphs, the only group where declining rates were the best fit in our tests, recovered rates near zero, adding to prior work suggesting diffusive evolution in the clade using different metrics (Anderson et al. 2011). I even failed to find support for variation among sarcopterygians relating to stratigraphic age across the entire timescale examined. However, I did find that the early diversification in this clade can best be described as occurring between the major lineages explored rather than within the groups. The implication of these results was the variability in magnitude of the phenotypic adaptations to novel environments by early bony fishes that emerged before large-scale turnover events at the end of the Devonian. Additionally, although the best fit model for sarcopterygians was declining rates, it was possible that the reason the estimated decay was low was because the sampling of this analysis was capturing the peak of their diversity but only the beginnings of their decline.

To allow for the largest perspective possible, I then expanded the scale from the Devonian to the recent and explored the rate of morphological evolution in the iconic coelacanth, lungfish, and holostean "living fossil" lineages. While coelacanths and lungfishes exhibit declining rates of discrete character evolution over time, holosteans show comparatively constant rates of evolution. Body shape evolution showed similar nuanced patterns, with strong support for declining rates in coelacanths, and conflicting support in lungfishes and holosteans. These

results add broader context to the jaws analyses. At this scale, the decline in phenotypic rates of evolution in two of the groups (coelacanths and lungfishes) after the Devonian are clear. This offers a compelling narrative through-line capturing the full breadth of the initial adaptive radiation due to ecomorphological change followed by ecological restriction and sustained low rates of morphological evolution—it may be a continuum.

5.2 The Paths Ahead

No analyses are ever perfect, but there are several ways in which they can be improved or expanded upon in future work. I'll discuss descriptive work generally in the following section, but an equally important facet of morphological character work is incorporating the data into available matrices to estimate phylogenies. In lungfishes, the reason this was not included in the third chapter was due to the difficulty of working with the disparate datasets available. However, with the description finished, future workers are now freed to focus instead on translating it into coded characters, combining the latest datasets (with special attention paid to the Devonian backbone), and running phylogenetic analyses. Both of the other datasets, the 2D body and 3D jaw shape, could be improved with additional sampling and methods that can estimate missing data. Sometimes, the limits of the available samples can be reached, which is what happened with the 3D jaws in chapter 4. In those cases, it may be possible to use statistical methods to impute missing landmarks. Although I think estimation of missing landmarks is a valuable tool, I am cautious with its usage due to mixed evidence in the literature (Brown et al. 2012; Arbour and Brown 2014) and the potential biases it could introduce into smaller datasets, though I have not tested it myself. For phylogenetic inference, I believe I was very successful at implementing stratigraphic and horizon-scale age data into the analyses. I am an early adopter of these

techniques in a Bayesian framework and they resulted in very detailed rate estimation throughout the history of the clades I was investigating. The next step would be to perform a total evidence analysis with all of the aforementioned techniques incorporated, but it may take a while given the state of the morphological matrices available. Finally, using multivariate datasets (in 2D or 3D) with methods that complement each other (like chapter 2 and 4) could be enhanced by performing true cross-clade comparisons with lineages like horseshoe crabs or the tuatara (i.e., other "living fossils"). Only by stepping out of the fish world can these large-scale macroevolutionary patterns truly be appreciated.

5.3 A Reflection

The findings in this dissertation underscore the importance of bringing paleontological data to bear on macroevolutionary questions. This is especially relevant for neontologists, who frequently use fossils just to time-calibrate trees instead of using them for what they represent—a morphological time capsule. Of course they can generally help to calibrate trees, but they can also be used as informative tips and coupled with their biostratigraphic context to more precisely estimate divergence times during phylogenetic inference (King and Rücklin 2020). Perhaps more importantly to this work, they can also be used as a direct measurement of evolutionary rate at a time in the past, rather than inferring rates exclusively from molecular phylogenies. Even in the worst of times (e.g., missing data, sampling biases, the entire concept of taphonomy, etc.), there are still techniques to permit robust analytical incorporation of the morphological and stratigraphic information into most analyses (Dávalos et al. 2014; Silvestro et al. 2014; Lloyd and Slater 2021; Mongiardino Koch et al. 2021).

I also cannot completely discount that most inferences are improved by better sampling. However, with paleontological work it is possible to simply run out of usable specimens, making the task of increasing sampling difficult or impossible at the outset like with my fourth chapter. In those cases, apart from imputing missing data, it would be useful to expand to cross-clade, comparative datasets. Multiple discussions of my work in the second chapter have involved a mention about broadening the dataset to include specifically non-fish groups and highlight any patterns. Although I believe that is outside of the current scope of my chapter, I agree it would be a powerful way to broaden this work into the future analyses. Another way to improve the analyses is resolved trees for the component clades. Although I used the most recently published datasets (second chapter) and trees (fourth chapter), certain problem clades continue to negatively affect phylogenetic inference. Whether it is the lack of resolution of the phylogenetic backbone in lungfishes (Lloyd et al. 2011) or rapid divergences in Devonian sarcopterygians creating short internodes, well-known issues continue to impact modern analyses. Now that at least some lungfish genomes are available, it falls on paleontologists to consolidate the dozen or so disparate morphological datasets into one standardized and comprehensive one for Dipnoi specifically.

One of the first steps towards accomplishing those goals requires assessing morphological characters and redescribing specimens. As my third chapter illustrates, transitional lungfishes during the dreaded Devonian backbone of the tree can be a source of excitement and frustration. It was my first description (a difficult but ultimately rewarding experience) and exemplified why this specialized research is foundational to the broader work being done by evolutionary (paleo)biologists. Examining the material extensively to confirm whether or not the dorsal fin preserved a basal plate while surrounded by millions of other

specimens in an old institution is truly humbling and makes the endeavor seem impossible. However, it is precisely this methodical work that is needed to slowly chip away at nuanced evolutionary questions. I may not have been able to integrate my fossil into a more comprehensive dataset, but my examination of this specimen should help inform analyses incorporating ‘phaneropleurids’ in the future.

With this dissertation, I have done my part in unraveling the intricate evolutionary history of sarcopterygians (and others), from describing a new species to the interrogation of putative episodes of adaptive radiation in deep time. It is my hope that these findings not only enhance our understanding of ancient vertebrate lineages but also pave the way for further investigations into the mechanisms driving morphological innovation in extinct lineages, living fossils (no scare quotes this time), and beyond.

5.4 References

Anderson, P.S.L., Friedman, M., Brazeau, M.D., Rayfield, E.J., 2011. Initial radiation of jaws demonstrated stability despite faunal and environmental change. Nature 476, 206–209. https://doi.org/10.1038/nature10207

Arbour, J.H., Brown, C.M., 2014. Incomplete specimens in geometric morphometric analyses. Methods Ecol. Evol. 5, 16–26. https://doi.org/10.1111/2041-210X.12128

Brown, C.M., Arbour, J.H., Jackson, D.A., 2012. Testing of the Effect of Missing Data Estimation and Distribution in Morphometric Multivariate Data Analyses. Syst. Biol. 61, 941–954. https://doi.org/10.1093/sysbio/sys047

Challands, T., den Blaauwen, J., 2017. A redescription of the Middle Devonian dipnoan *Pentlandia macroptera* Traquair, 1889, and an assessment of the Phaneropleuridae. Zool. J. Linn. Soc. 180, 414–460. https://doi.org/10.1111/zoj.12491

Cloutier, R., Ahlberg, P.E., 1996. Morphology, characters, and the interrelationships of basal sarcopterygians, in: Stiassny, M.L.J., Parenti, L.R., Johnson, G.D. (Eds.), Interrelationships of Fishes. Academic Press, Inc., New York, pp. 445–479. https://doi.org/10.1016/B978-012670950-6/50018-7

Daeschler, E.B., Shubin, N.H., Jenkins Jr, F.A., 2006. A Devonian tetrapod-like fish and the evolution of the tetrapod body plan. Nature 440, 757–763. https://doi.org/10.1038/nature04639

Dávalos, L.M., Velazco, P.M., Warsi, O.M., Smits, P.D., Simmons, N.B., 2014. Integrating Incomplete Fossils by Isolating Conflicting Signal in Saturated and Non-Independent Morphological Characters. Syst. Biol. 63, 582–600. https://doi.org/10.1093/sysbio/syu022

Friedman, M., 2010. Postcranial evolution in early lungfishes (Dipnoi: Sarcopterygii): new insights from *Soederberghia groenlandica*, in: Elliott, D.K., Maisey, J.G., Yu, X., Miao, D. (Eds.), Morphology, Phylogeny and Paleobiogeography of Fossil Fishes: Honoring Meemann Chang. Verlag Dr. Friedrich Pfeil, München, Germany, pp. 299–324.

King, B., Rücklin, M., 2020. Tip dating with fossil sites and stratigraphic sequences. PeerJ 8, e9368. https://doi.org/10.7717/peerj.9368

Lloyd, G.T., Slater, G.J., 2021. A Total-Group Phylogenetic Metatree for Cetacea and the Importance of Fossil Data in Diversification Analyses. Syst. Biol. 70, 922–939. https://doi.org/10.1093/sysbio/syab002

Lloyd, G.T., Wang, S.C., Brusatte, S.L., 2011. Identifying heterogeneity in rates of morphological evolution: discrete character change in the evolution of lungfish (Sarcopterygii; Dipnoi). Evolution 66, 330–348. https://doi.org/10.1111/j.1558-5646.2011.01460.x

Mongiardino Koch, N., Garwood, R.J., Parry, L.A., 2021. Fossils improve phylogenetic analyses of morphological characters. Proc. R. Soc. B Biol. Sci. 288, 20210044. https://doi.org/10.1098/rspb.2021.0044

Silvestro, D., Schnitzler, J., Liow, L.H., Antonelli, A., Salamin, N., 2014. Bayesian Estimation of Speciation and Extinction from Incomplete Fossil Occurrence Data. Syst. Biol. 63, 349–367. https://doi.org/10.1093/sysbio/syu006

Appendices

Note: Data for all chapters in this dissertation are available via the University of Michigan Deep Blue archive.

Appendix A: Supplement to Chapter 2

A.1 Phylogenetic Reconstruction

Coelacanths

The Devonian *Gavinia* + *Styloichthys* were the earliest diverging actinistian clade (90.4% posterior support), followed by *Miguashaia* (45.4%) (**Figure A1**). This is opposite to the arrangement found by Toriño et al. [1], though the earliest portion of their tree had lower bootstrap values than our posterior support (17% – 22%). Our constrained monophyly of *Allenypterus* + *Holopterygius* resulted in *Euporosteus* + *Diplocercides* forming a low-support clade (13%), as opposed to a polytomy. The Carboniferous backbone of our tree, including *Lochmocercus*, *Hadronector*, *Polysteorhynchus*, *Caridosuctor*, and *Rhabdoderma*, was recovered in a different arrangement but with higher support (60% – 92.6%) than Toriño et al. [1]. The Permian lineages also differed in arrangement to those found by Toriño et al. [1], but with comparably low levels of support, which has the hallmarks of a rapid diversification event. Apart from causing issues when inferring relationships, this uncertainty has been identified by previous studies, which have noted its effects alongside issues caused by taxa that have been historically difficult to code [1,2]. *Heptanema* and *Dobrogeria* were recovered within Latimerioidei, with *Whiteia* as sister group to the clade. Within Latimerioidei, the mawsoniid and latimerid relationships had much higher support than in Toriño et al. ([1]: figures 3, 5) (**Figure A1**). *Chinela* and *Diplurus*were were aligned with the mawsoniids and *Garnbergia* was the immediate sister lineage to the latimerids. The earliest diverging latimeriid clade was *Foreyia* +

Ticinepomis (97.5%), with *Libys* + *Megalocoelacanthus* (87.9% posterior support) found closer to the crown, a reversal of the relationships recovered in Toriño et al. [1]. The Late Cretaceous *Macropoma* is the immediate sister lineage of the extant *Latimeria* (70.5%), with Late Jurassic *Swenzia* the closest relative to this pair, reflecting one [3] of two [1] competing hypotheses of relationships among these lineages. Given the overall higher support coupled with the stratigraphic uncertainty included in our analyses, these results are the most consistent and rigorous for this clade.

Lungfishes

There was extremely low support within and between the majority of Devonian and Permian clades (**Figure A2**), representing the majority of taxa. This resulted in broad differences between the trees estimated in our analyses, and those in Lloyd et al. [4]. Most of the sister-group relationships that had the highest support (>50% posterior support) in our analyses were also found in the original publication (e.g., *Dipnorhynchus spp.*, *Barwickia downunda* + *Dipterus valenciennesi*, *Rhinodipterus spp.*, *Holodipterus spp.*, and *Griphognathus spp.*); however, some relationships with high support differed (e.g., *Palaeodaphus insignis* + [*Jarvickia arctica* + *Sunwapta grandiceps*], [*Rhynchodipterus elginensis* + *Soederberghia groenlandica*] + *Griphognathus spp.*, and *Delatitia breviceps* + *Parasagenodus sibiricus*). The highest backbone support was recovered between the Carboniferous and post-Permian clades (>50%). All these nodes differed from Lloyd et al. [4] except for *Arganodus atlantis* + *Ferganoceratodus jurassicus* (51%). This low support result is likely representative of the quality and construction of these lungfish character datasets over time, as has been noted in prior publications (e.g., [5]).

Holosteans

The topology of the tree was broadly consistent with that in López-Arbarello and Sferco [6], including modest overall support across the tree (**Figure A3**). Here, we will only discuss differences as they pertain to holosteans to the exclusion of any outgroups. Although the three species of *Dapedium* were recovered as stem Holostei on the MCC tree in agreement with recent studies [6,7], they had <50% posterior support, and shorter runs frequently recovered them within Ginglymodi. Because of this, we cannot rule out the group being stem Ginglymodi [8,9] nor any other placement about the holostean stem (e.g., [10]). They are therefore considered early branching holosteans with uncertain phylogenetic placement. Other differences from López-Arbarello and Sferco [6] included *Caturus furcatus* recovered as sister to the Amiiformes rather than to the ionoscopids (58.2%), *Kyphosichthys grandei* nested within *Sangiorgioichthys* (83%), and better resolution within the Semionotiformes and Cretaceous and Paleogene Lepisosteiformes (66% – 100%).

A.2 Landmarking and Shape Data

Coelacanths

11 fixed landmarks for coelacanths from Friedman and Coates [11] (1-10, 12) with 3 added in this analysis (11, 13-14) (**Figure A4**): (1) tip of snout, (2) posterior margin of postparietals, (3) anterior insertion of first dorsal fin, (4) posterior insertion of first dorsal fin, (5) posterior insertion of second dorsal fin, (6) anterior insertion of epichordal lobe, (7) posterior tip of accessory lobe, (8) anterior insertion of hypochordal lobe, (9) posterior insertion of anal fin, (10)

base of pelvic fin, (11) posterior ventral edge of interpalate, (12) quadrate/articular joint, (13) central, ventral surface of orbit, and (14) central, dorsal surface of orbit.

Lungfishes

11 landmarks were created for lungfishes in this analysis (**Figure A5**): (1) anterior tip of the upper jaw (premaxilla), (2) posteriormost edge of skull roof (posterior to A bone), (3) anterior insertion of dorsal fin, (4) posterior tip of epichordal lobe, (5) anterior insertion of anal fin, (6) anterior insertion of pelvic fin, (7) anterior insertion of the pectoral fin, (8) posterior ventral edge of interpalate, (9) lower jaw joint, (10) central, ventral surface of the orbit, and (11) central, dorsal surface of the orbit. These landmarks were specifically tailored to complement the ones derived from previous analyses for coelacanths and holosteans.

Holosteans

12 fixed landmarks for holosteans from Clarke and Friedman [12] (1-8, 10, 12-14) with two added in this analysis (9, 11) (**Figure A6**): (1) anterior tip of the upper jaw (premaxilla), (2) postero-dorsal tip of braincase, (3) anterior insertion of dorsal fin, (4) posterior insertion of dorsal fin, (5) dorsal surface representation of the last vertebral centra, (6) ventral surface representation of the last vertebral centra, (7) posterior insertion of anal fin, (8) anterior insertion of anal fin, (9) base of pelvic fin, (10) anterior insertion of the pectoral fin, (11) posterior ventral edge of interpalate, (12) lower jaw, joint, (13) the central, ventral surface of the orbit, and (14) the central, dorsal surface of the orbit. Landmark #2 from Clarke and Friedman [12] is not included in this analysis

A.3 Figures

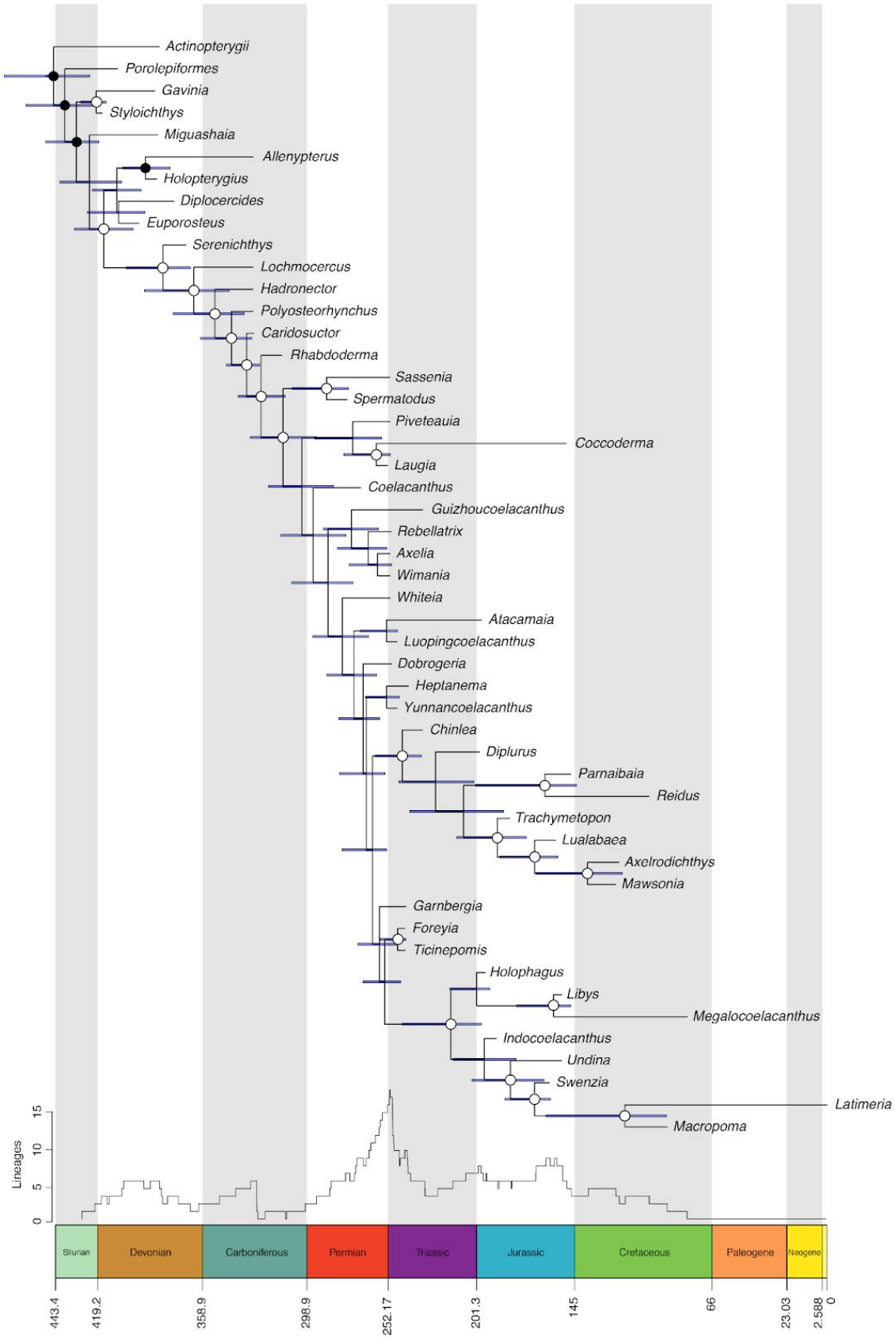
Actinopterygii
Porolepiformes
Gavinia
Styloichthys
Miguashaia
Allenypterus
Holopterygius
Diplocercides
Euporosteus
Serenichthys
Lochmocercus
Hadronector
Polyosteorhynchus
Caridosuctor
Rhabdoderma
Sassenia
Spermatodus
Piveteauia
Coccoderma
Laugia
Coelacanthus
Guizhoucoelacanthus
Rebellatrix
Axelia
Wimania
Whiteia
Atacamaia
Luopingcoelacanthus
Dobrogeria
Heptanema
Yunnancoelacanthus
Chinlea
Diplurus
Parnaibaia
Reidus
Trachymetopon
Lualabaea
Axelrodichthys
Mawsonia
Garnbergia
Foreyia
Ticinepomis
Holophagus
Libys
Megalocoelacanthus
Indocoelacanthus
Undina
Swenzia
Latimeria
Macropoma
Lineages
0
5
10
15
Silurian
Devonian
Carboniferous
Permian
Triassic
Jurassic
Cretaceous
Paleogene
Neogene
443.4
419.2
358.9
298.9
252.17
201.3
145
66
23.03
2.588
0

Figure A1. Time-scaled maximum clade credibility tree for coelacanths. Phylogeny inferred using morphological data in BEAST v2.6.5 with the Fossilized Birth-Death model. Nodes marked in black represent clade constraints, nodes marked in black circling white represent clades with >50% posterior probability, and blue bars on nodes represent 95% posterior probability distribution. The graph above the timescale is a Lineages Through Time plot of taxa belonging to the coelacanth clade calculated from the MCC tree.

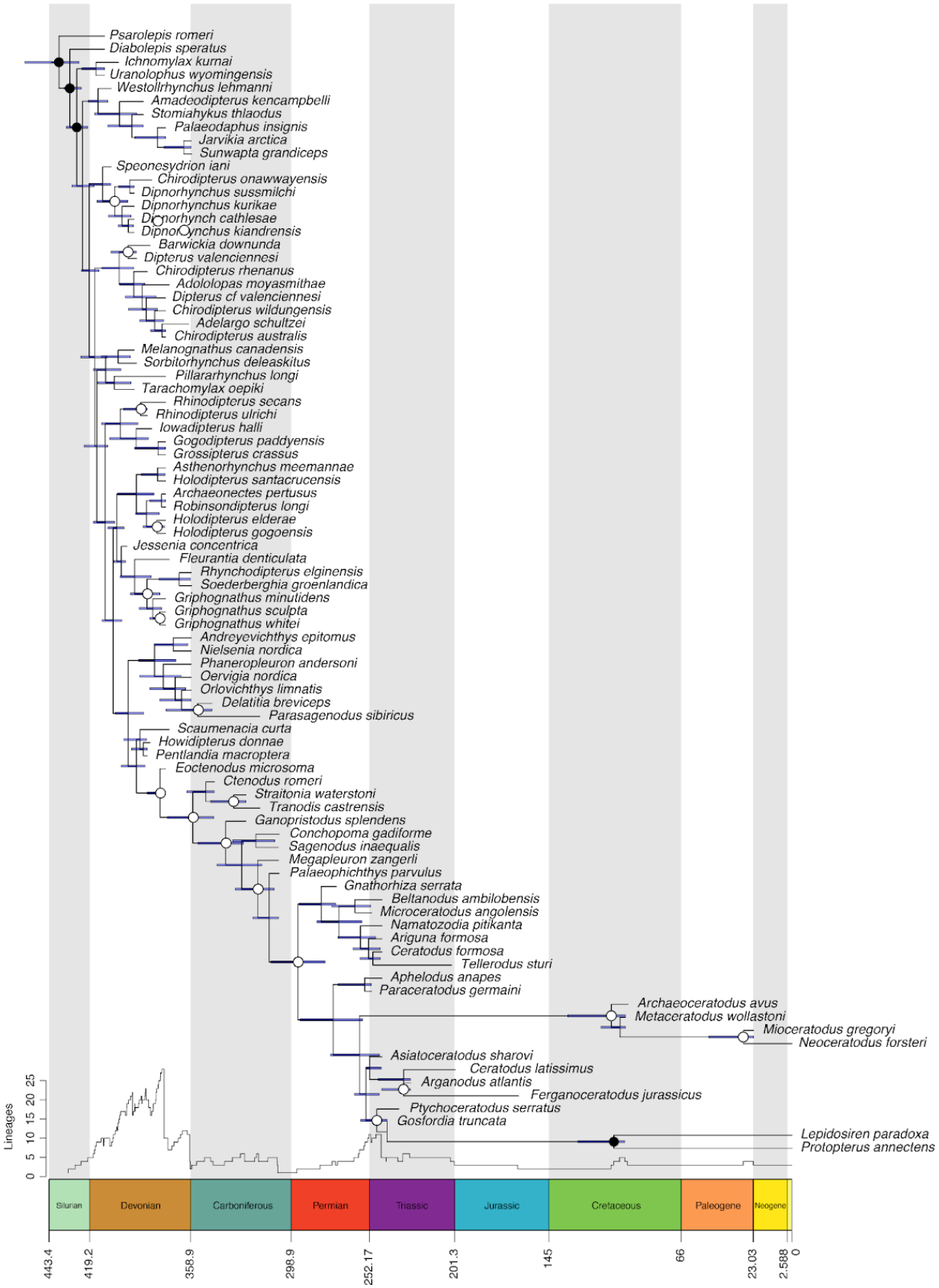
Psarolepis romeri
Diabolepis speratus
Ichnomylax kurnai
Uranolophus wyomingensis
Westollrhynchus lehmanni
Amadeodipterus kencampbelli
Stomiahykus thlaodus
Palaeodaphus insignis
Jarvikia arctica
Sunwapta grandiceps
Speonesydrion iani
Chirodipterus onawwayensis
Dipnorhynchus sussmilchi
Dipnorhynchus kurikae
Dipnorhynch cathlesae
Dipnorhynchus kiandrensis
Barwickia downunda
Dipterus valenciennesi
Chirodipterus rhenanus
Adololopas moyasmithae
Dipterus cf valenciennesi
Chirodipterus wildungensis
Adelargo schultzei
Chirodipterus australis
Melanognathus canadensis
Sorbitorhynchus deleaskitus
Pillararhynchus longi
Tarachomylax oepiki
Rhinodipterus secans
Rhinodipterus ulrichi
Iowadipterus halli
Gogodipterus paddyensis
Grossipterus crassus
Asthenorhynchus meemannae
Holodipterus santacrucensis
Archaeonectes pertusus
Robinsondipterus longi
Holodipterus elderae
Holodipterus gogoensis
Jessenia concentrica
Fleurantia denticulata
Rhynchodipterus elginensis
Soederberghia groenlandica
Griphognathus minutidens
Griphognathus sculpta
Griphognathus whitei
Andreyevichthys epitomus
Nielsenia nordica
Phaneropleuron andersoni
Oervigia nordica
Orlovichthys limnatis
Delatitia breviceps
Parasagenodus sibiricus
Scaumenacia curta
Howidipterus donnae
Pentlandia macroptera
Eoctenodus microsoma
Ctenodus romeri
Straitonia waterstoni
Tranodis castrensis
Ganopristodus splendens
Conchopoma gadiforme
Sagenodus inaequalis
Megapleuron zangerli
Palaeophichthys parvulus
Gnathorhiza serrata
Beltanodus ambilobensis
Microceratodus angolensis
Namatozodia pitikanta
Ariguna formosa
Ceratodus formosa
Tellerodus sturi
Aphelodus anapes
Paraceratodus germaini
Archaeoceratodus avus
Metaceratodus wollastoni
Mioceratodus gregoryi
Neoceratodus forsteri
Asiatoceratodus sharovi
Ceratodus latissimus
Arganodus atlantis
Ferganoceratodus jurassicus
Ptychoceratodus serratus
Gosfordia truncata
Lepidosiren paradoxa
Protopterus annectens
Lineages
0 5 10 15 20 25
Silurian
Devonian
Carboniferous
Permian
Triassic
Jurassic
Cretaceous
Paleogene
Neogene
443.4
419.2
358.9
298.9
252.17
201.3
145
66
23.03
2.588
0

Figure A2. Time-scaled maximum clade credibility tree for lungfishes. Phylogeny inferred using morphological data in BEAST v2.6.5 with the Fossilized Birth-Death model. Nodes marked in black represent clade constraints, nodes marked in black circling white represent clades with >50% posterior probability, and blue bars on nodes represent 95% posterior probability distribution. The graph above the timescale is a Lineages Through Time plot of taxa belonging to the lungfish clade calculated from the MCC tree.

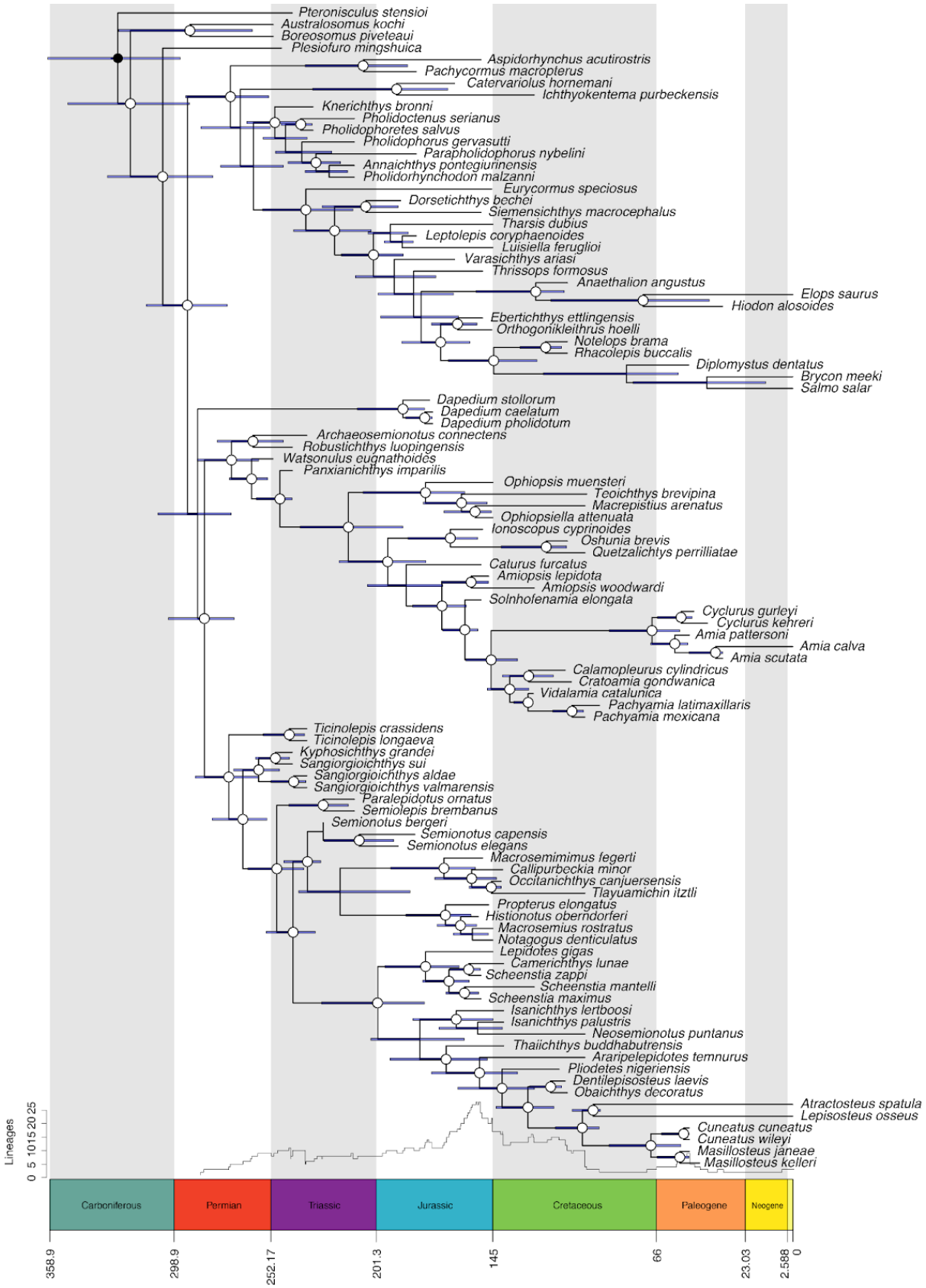
Pteronisculus stensioi
Australosomus kochi
Boreosomus piveteaui
Plesiofuro mingshuica
Aspidorhynchus acutirostris
Pachycormus macropterus
Catervariolus hornemani
Ichthyokentema purbeckensis
Knerichthys bronni
Pholidoctenus serianus
Pholidophoretes salvus
Pholidophorus gervasutti
Parapholidophorus nybelini
Annaichthys pontegiurinensis
Pholidorhynchodon malzanni
Eurycormus speciosus
Dorsetichthys bechei
Siemensichthys macrocephalus
Tharsis dubius
Leptolepis coryphaenoides
Luisiella feruglioi
Varasichthys ariasi
Thrissops formosus
Anaethalion angustus
Elops saurus
Hiodon alosoides
Ebertichthys ettlingensis
Orthogonikleithrus hoelli
Notelops brama
Rhacolepis buccalis
Diplomystus dentatus
Brycon meeki
Salmo salar
Dapedium stollorum
Dapedium caelatum
Dapedium pholidotum
Archaeosemionotus connectens
Robustichthys luopingensis
Watsonulus eugnathoides
Panxianichthys imparilis
Ophiopsis muensteri
Teoichthys brevipina
Macrepistius arenatus
Ophiopsiella attenuata
Ionoscopus cyprinoides
Oshunia brevis
Quetzalichtys perrilliatae
Caturus furcatus
Amiopsis lepidota
Amiopsis woodwardi
Solnhofenamia elongata
Cyclurus gurleyi
Cyclurus kehreri
Amia patterson
Amia calva
Amia scutata
Calamopleurus cylindricus
Cratoamia gondwanica
Vidalamia catalunica
Pachyamia latimaxillaris
Pachyamia mexicana
Ticinolepis crassidens
Ticinolepis longaeva
Kyphosichthys grandei
Sangiorgioichthys sui
Sangiorgioichthys aldae
Sangiorgioichthys valmarensis
Paralepidotus ornatus
Semiolepis brembanus
Semionotus bergeri
Semionotus capensis
Semionotus elegans
Macrosemimimus legerti
Callipurbeckia minor
Occitanichthys canjuersensis
Tlayuamichin itztli
Propterus elongatus
Histionotus oberndorferi
Macrosemius rostratus
Notagogus denticulatus
Lepidotes gigas
Camerichthys lunae
Scheenstia zappi
Scheenstia mantelli
Scheenstia maximus
Isanichthys lertboosi
Isanichthys palustris
Neosemionotus puntanus
Thaiichthys buddhabutrensis
Araripelepidotes temnurus
Pliodetes nigeriensis
Dentilepisosteus laevis
Obaichthys decoratus
Atractosteus spatula
Lepisosteus osseus
Cuneatus cuneatus
Cuneatus wileyi
Masillosteus janeae
Masillosteus kelleri
Lineages
0 5 10 15 20 25
Carboniferous
Permian
Triassic
Jurassic
Cretaceous
Paleogene
Neogene
358.9
298.9
252.17
201.3
145
66
23.03
2.588
0

Figure A3. Time-scaled maximum clade credibility tree for holosteans. Phylogeny inferred using morphological data in BEAST v2.6.5 with the Fossilized Birth-Death model. Nodes marked in black represent clade constraints, nodes marked in black circling white represent clades with >50% posterior probability, and blue bars on nodes represent 95% posterior probability distribution. The graph above the timescale is a Lineages Through Time plot of taxa belonging to the holostean clade calculated from the MCC tree.

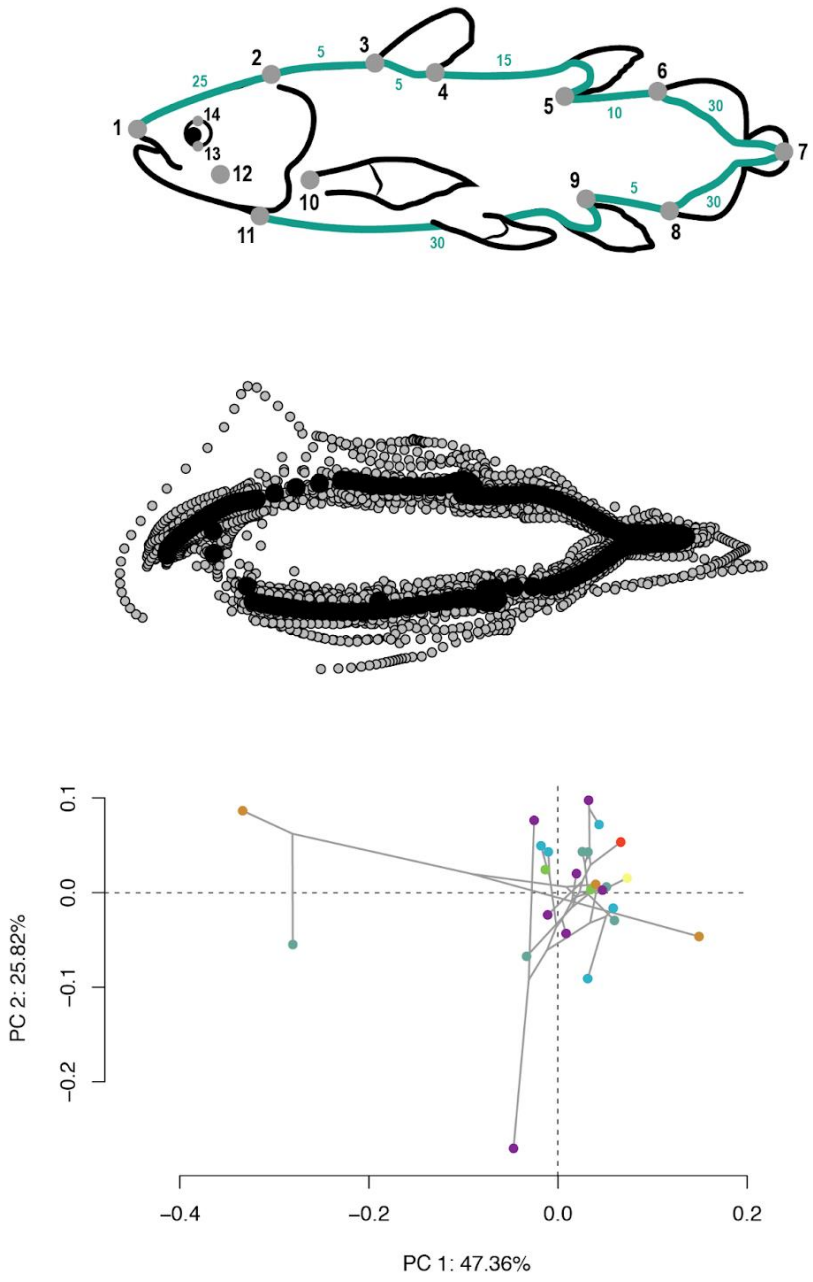

Figure A4. Landmarking scheme and shape space for coelacanths. The landmarking scheme (top) used to create coordinate data (center) for morphometric analyses (bottom). The scheme is described in detail in the Landmarking & Shape Data section. Colors representing the last appearance datum of each taxon standardized to the International Commission on Stratigraphy.

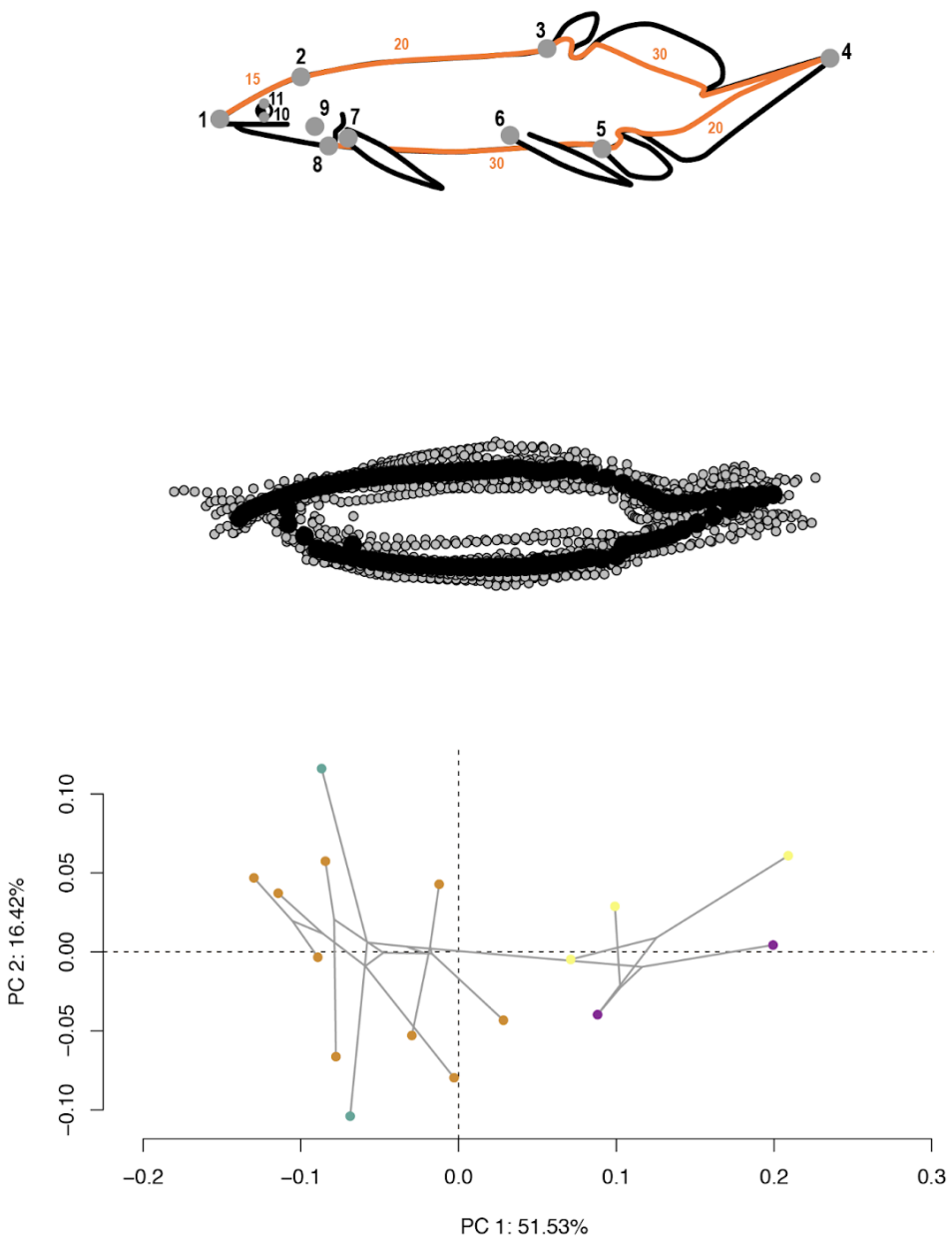

Figure A5. Landmarking scheme and shape space for lungfishes. The landmarking scheme (top) used to create coordinate data (center) for morphometric analyses (bottom). The scheme is described in detail in the Landmarking & Shape Data section. Colors representing the last appearance datum of each taxon standardized to the International Commission on Stratigraphy.

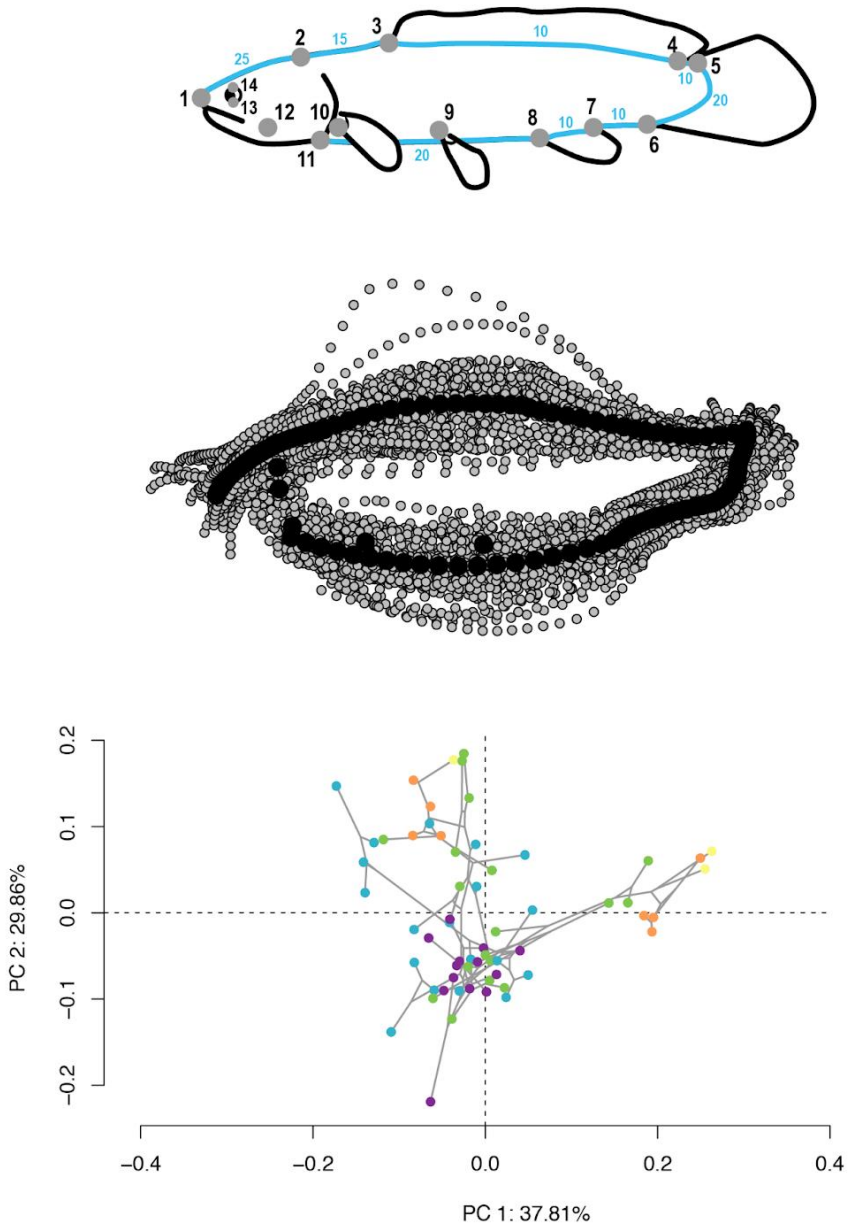

Figure A6. Landmarking scheme and shape space for holosteans. The landmarking scheme (top) used to create coordinate data (centre) for morphometric analyses (bottom). The scheme is described in detail in the Landmarking & Shape Data section. Colours representing the last appearance datum of each taxon standardised to the International Commission on Stratigraphy.

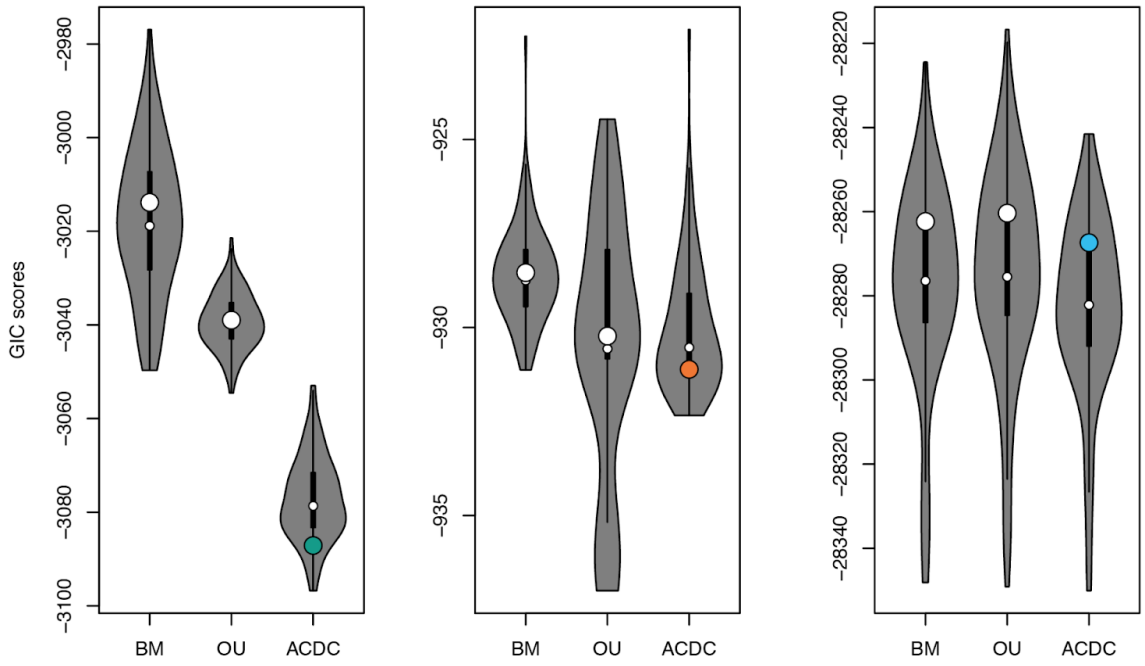

Figure A7. GIC scores for each living fossil clade. We calculated GIC scores for coelacanths (left), lungfishes (centre), and holosteans (right). Model fitting was performed via *mvMORPH* and the PC axes that summarised 100% of the variability for each clade using the MCC tree (circles) and 100 trees randomly sampled from the posterior (violin plot distribution).

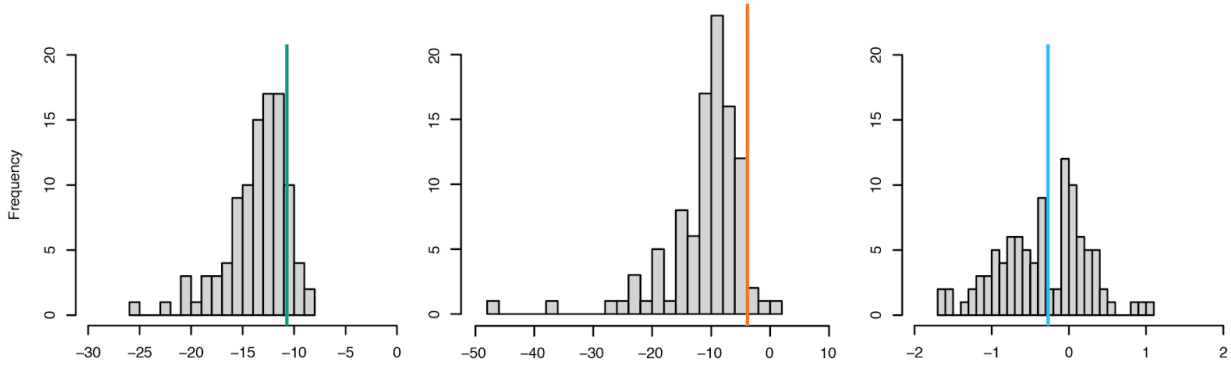

Figure A8. Bootstrapped beta parameter estimates for each living fossil clade. We performed 100 bootstrap replicates for coelacanths (left), lungfishes (centre), and holosteans (right) using the estimates from the empirical model fitting. Vertical coloured bars indicate the MCC-derived parameter estimate for each group (-10.7, -3.85, and -0.27 for coelacanths, lungfishes, and holosteans, respectively).

A.4 Tables

Table A1. Verbal summaries of results arising from analyses of three living fossil lineages.

	coelacanths	**lungfishes**	**holosteans**
discrete character rates through time	strongly declining rates, with peak in the middle of clade history	strongly declining rates, with peak early in clade history	moderately declining rates, with relatively constant rates for much of clade history
discrete character saturation	minor saturation	strong saturation	moderate saturation
body shape evolution	overwhelming support for EB case of ACDC, with strongly declining rates over time	weak support for EB case of ACDC, with moderately declining rates over time	strong support for EB case of ACDC, with negligible decline in rates over time

Table A2. *mvgls* model-fit GIC results for coelacanths using the MCC tree and the PC axes that summarised 100% of the variability. Models listed in the text. Fit = GIC scores, delta = change from highest-ranked score, w = GIC weights.

	fit	delta	w
ACDC	-3,087.114	0	1
BM	-3,013.844	73.270	0
OU	-3,038.983	48.132	0

Table A3. *mvgls* model-fit GIC results for lungfishes using the MCC tree and the PC axes that summarised 100% of the variability. Models listed in the text. Fit = GIC scores, delta = change from highest-ranked score, w = GIC weights.

	fit	delta	w
ACDC	-931.112	0	0.521
BM	-928.540	2.572	0.144
OU	-930.226	0.886	0.335

Table A4. *mvgls* model-fit GIC results for holosteans using the MCC tree and the PC axes that summarised 100% of the variability. Models listed in the text. Fit = GIC scores, delta = change from highest-ranked score, w = GIC weights.

	fit	delta	w
ACDC	-28, 267.370	0	0.900
BM	-28, 262.350	5.023	0.073
OU	-28, 260.350	7.017	0.027

A.5 References

1. Toriño P, Soto M, Perea D. 2021 A comprehensive phylogenetic analysis of coelacanth fishes (Sarcopterygii, Actinistia) with comments on the composition of the Mawsoniidae and Latimeriidae: evaluating old and new methodological challenges and constraints. *Hist. Biol.* **33**, 3423–3443. (doi:10.1080/08912963.2020.1867982)
2. Forey PL. 1998 *History of the Coelacanth Fishes*. Chapman & Hall.
3. Cavin L, Mennecart B, Obrist C, Costeur L, Furrer H. 2017 Heterochronic evolution explains novel body shape in a Triassic coelacanth from Switzerland. *Sci. Rep.* **7**, 13695. (doi:10.1038/s41598-017-13796-0)
4. Lloyd GT, Wang SC, Brusatte SL. 2011 Identifying heterogeneity in rates of morphological evolution: discrete character change in the evolution of lungfish (Sarcopterygii; Dipnoi). *Evolution* **66**, 330–348. (doi:10.1111/j.1558-5646.2011.01460.x)
5. Challands TJ, Smithson TR, Clack JA, Bennett CE, Marshall JEA, Wallace-Johnson SM, Hill H. 2019 A lungfish survivor of the end-Devonian extinction and an Early Carboniferous dipnoan radiation. *J. Syst. Palaeontol.* **17**, 1825–1846. (doi:10.1080/14772019.2019.1572234)
6. López-Arbarello A, Sferco E. 2018 Neopterygian phylogeny: the merger assay. *R. Soc. Open Sci.* **5**, 172337. (doi:10.1098/rsos.172337)
7. Latimer AE, Giles S. 2018 A giant dapediid from the Late Triassic of Switzerland and insights into neopterygian phylogeny. *R. Soc. Open Sci.* **5**, 180497. (doi:10.1098/rsos.180497)
8. Thies D, Waschkewitz J. 2016 Redescription of *Dapedium pholidotum* (Agassiz, 1832) (Actinopterygii, Neopterygii) from the Lower Jurassic Posidonia Shale, with comments on the phylogenetic position of *Dapedium* Leach, 1822. *J. Syst. Palaeontol.* **14**, 339–364. (doi:10.1080/14772019.2015.1043361)
9. Gibson SZ. 2016 Redescription and Phylogenetic Placement of †*Hemicalypterus weiri* Schaeffer, 1967 (Actinopterygii, Neopterygii) from the Triassic Chinle Formation, Southwestern United States: New Insights into Morphology, Ecological Niche, and Phylogeny. *PLOS ONE* **11**, e0163657. (doi:10.1371/journal.pone.0163657)

10. Xu G-H, Zhao L-J, Coates MI. 2014 The oldest ionoscopiform from China sheds new light on the early evolution of halecomorph fishes. *Biol. Lett.* **10**, 20140204. (doi:10.1098/rsbl.2014.0204)
11. Friedman M, Coates MI. 2006 A newly recognized fossil coelacanth highlights the early morphological diversification of the clade. *Proc. R. Soc. B Biol. Sci.* **273**, 245–250. (doi:10.1098/rspb.2005.3316)
12. Clarke JT, Friedman M. 2018 Body-shape diversity in Triassic–Early Cretaceous neopterygian fishes: sustained holostean disparity and predominantly gradual increases in teleost phenotypic variety. *Paleobiology* **44**, 402–433. (doi:10.1017/pab.2018.8)

Appendix B: Supplement to Chapter 3

B.1 Geological Context

The Canadian Arctic Archipelago is composed of three successions of Phanerozoic sedimentary rocks. The oldest of these is the Cambrian to Upper Devonian Franklinian wedge, which transitions from carbonates and evaporites to the clastic terrestrial sediments of the Okse Bay Group. This group was formed when Laurussia (Euramerica) was positioned along the equator and comprises five formations deposited by orogenic erosion events into a foreland basin (from oldest to youngest): Strathcona Fiord (Eifelian), Hecla Bay (Eifelian-Givetian), Fram (Frasnian), Hell Gate (Frasnian), and Nordstrand Point (Frasnian) (Embry and Klovan, 1976). The Late Devonian (Frasnian) Fram Formation, found in the middle of the Okse Bay Group on Ellesmere Island consists of an alternating series of siltstones and sandstones (10 – 20 m, fining upwards). The siltstones encompass the thicker but less resistant sections whereas the sandstones are thinner, more resistant to weathering, form cliffs, and have erosive bottoms (Embry and Klovan, 1976; Embry, 1991). Because of these sequences, the sandstones have been interpreted as meandering streams and point bar deposits with the siltstones representing alternating overbank floodplain deposits (Embry and Klovan, 1976).

The NV2K17 locality (N77°09.895′ W86°16.157′) is an approximately 15–20 cm-thick fossiliferous zone within a 30m-thick siltstone in the southward dipping extent of the Schei Syncline near the eastern limb of Bird Fiord (Daeschler et al., 2006; Downs et al., 2011, 2019). Palynomorph biostratigraphic data indicate an early to middle Frasnian age (*medius* and

maclarenii zones) (Chi and Hills, 1976; Embry and Klovan, 1976). Within the fossiliferous zone, specimens are found as either articulated, partially crushed, three-dimensionally preserved fossils or scattered, isolated skeletal elements. They do not show any sorting nor preferred orientation except for those fragments with their longest dimension perpendicular to the bedding. This, in addition to the presence of carbonate nodules and intraformational clasts, has been interpreted as evidence that it was deposited during a single channel avulsion event that moved the vertebrate remains out of the channel and into the floodplain, where they were rapidly deposited with the suspended load (Miller et al., 2007). 60 cm of siltstone grading into a paleosol with root traces and additional carbonate nodules overlies NV2K17. This locality has recently produced porolepiforms (*Laccognathus sp*.) (Downs et al., 2011), antiarch placoderms (Asterolepis sp.) (Downs et al., 2019), tetrapodomorphs (*Tiktaalik roseae*) (Daeschler et al., 2006; Shubin et al., 2006), and this new phaneropleurid lungfish.

Material collected from this locality is subject to an agreement with the Territory of Nunavut; as such, the entire collection has been housed at the Academy of Natural Sciences in Philadelphia, Pennsylvania, U.S.A. since 2004, but will eventually be transferred to the Canadian Museum of Nature, Ottawa, Ontario, Canada to form the Nunavut Fossil Vertebrate Collection (Shubin et al., 2014).

B.2 References

Chi, B.I., Hills, L.V., 1976. Biostratigraphy and Taxonomy of Devonian Megaspores, Arctic Canada. Bull. Can. Pet. Geol. 24, 640–818. https://doi.org/10.35767/gscpgbull.24.4.640

Daeschler, E.B., Shubin, N.H., Jenkins Jr, F.A., 2006. A Devonian tetrapod-like fish and the evolution of the tetrapod body plan. Nature 440, 757–763. https://doi.org/10.1038/nature04639

Downs, J.P., Daeschler, E.B., Jenkins, F.A., Shubin, N.H., 2011. A new species of Laccognathus (Sarcopterygii, Porolepiformes) from the Late Devonian of Ellesmere Island, Nunavut, Canada. J. Vertebr. Paleontol. 31, 981–996. https://doi.org/10.1080/02724634.2011.599462

Downs, J.P., Daeschler, E.B., Lo, N., Carey, E.N., Shubin, N.H., 2019. *Asterolepis alticristata* n. sp. (Antiarchi) from the Upper Devonian (Frasnian) of Nunavut, Canada, and a report on the antiarch diversity of the Fram Formation. Geodiversitas 41, 679. https://doi.org/10.5252/geodiversitas2019v41a19

Embry, A.F., 1991. Middle-Upper Devonian Clastic Wedge of the Arctic Islands, in: Trettin, H.P. (Ed.), Geology of the Innuitian Orogen and Arctic Platform of Canada and Greenland. Geological Survey of Canada, Ottawa and Calgary, Canada, pp. 263–279.

Embry, A.F., Klovan, J.E., 1976. The Middle-Upper Devonian Clastic Wedge of the Franklinian Geosyncline. Bull. Can. Pet. Geol. 24, 485–639. https://doi.org/10.35767/gscpgbull.24.4.485

Miller, J.H., Shubin, N., Daeschler, E., Downs, J., 2007. Stratigraphic context of Tiktaalik roseae (Late Devonian): paleoenvironment of the fish-tetrapod transition. Geol. Soc. Am. Meet. Denver Colo. 28-31 Oct. 2007 Abstr. Programs 39.

Shubin, N.H., Daeschler, E.B., Jenkins, F.A., 2014. Pelvic girdle and fin of *Tiktaalik roseae*. Proc. Natl. Acad. Sci. 111, 893–899. https://doi.org/10.1073/pnas.1322559111

Shubin, N.H., Daeschler, E.B., Jenkins, F.A., 2006. The pectoral fin of Tiktaalik roseae and the origin of the tetrapod limb. Nature 440, 764–771. https://doi.org/10.1038/nature04637

Appendix C: Supplement to Chapter 4

C.1 Figures

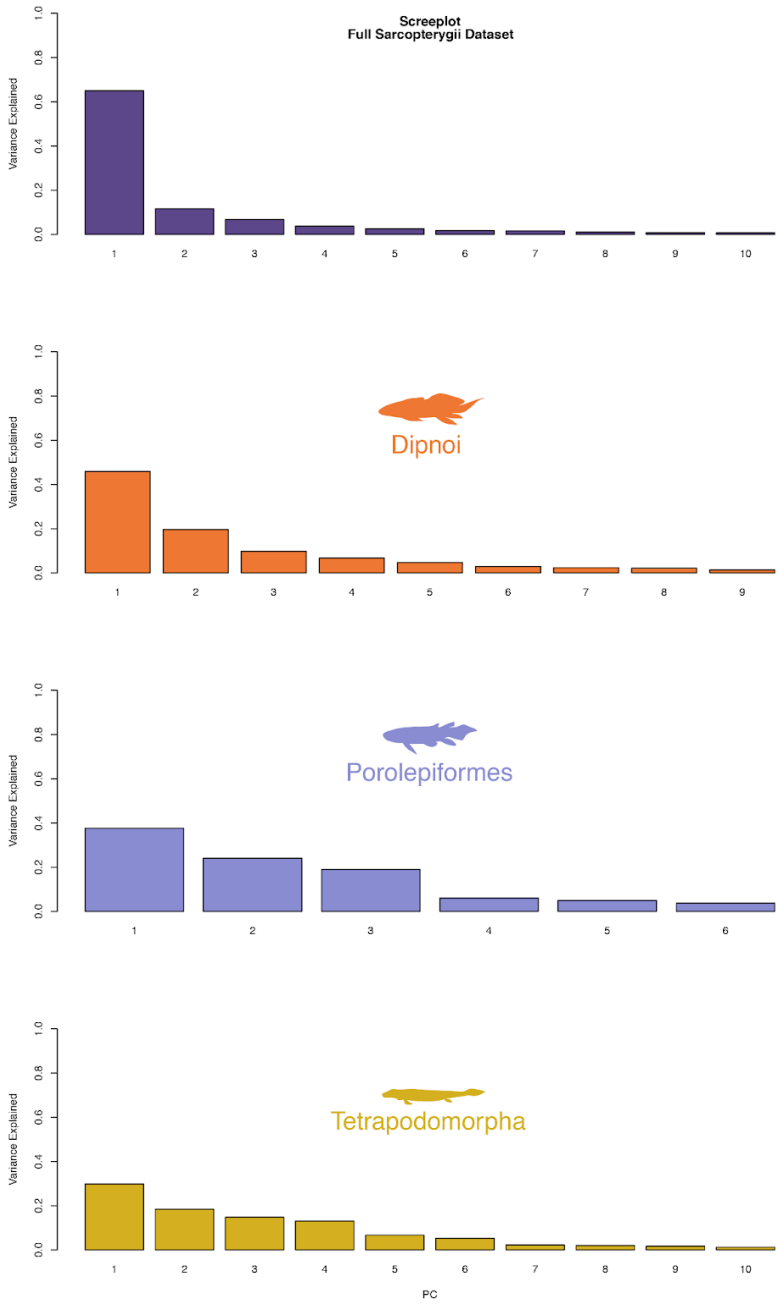

Figure C9. Scree plots showing the proportional contribution of each principal component axis to the overall variation for each of the clades up to 95%. Plots colored according to each group: porolepiforms, dipnoans, and tetrapodomorphs. 10 axes summarized the variability in the full sarcopterygian dataset, 9 in the lungfish dataset, 6 in the porolepiform dataset, and 10 in the tetrapodomorph dataset. Silhouettes from PhyloPic, *Tiktaalik* silhouette by *Nobu Tamura* (CC BY-SA 3.0).

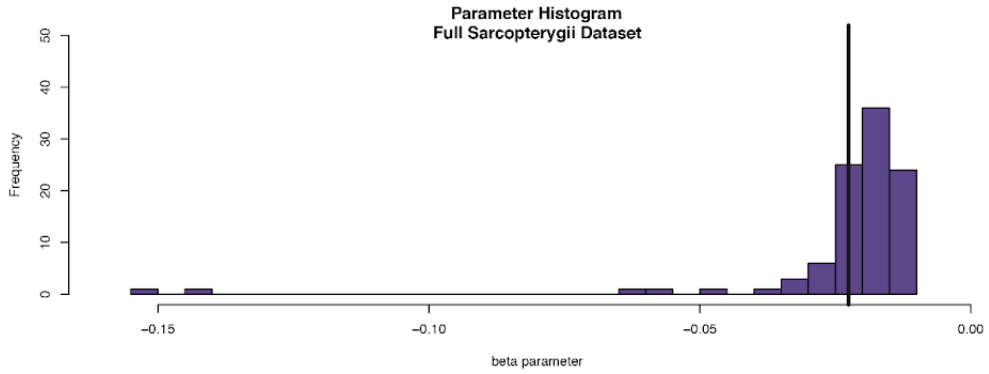
Parameter Histogram
Full Sarcopterygii Dataset
Frequency
0
10
20
30
40
50
−0.15
−0.10
−0.05
0.00
beta parameter

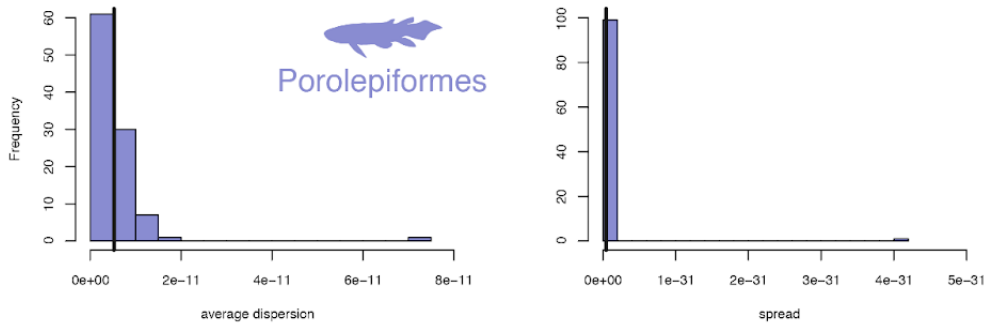
Porolepiformes
Frequency
0
10
20
30
40
50
60
0e+00
2e−11
4e−11
6e−11
8e−11
average dispersion
0
20
40
60
80
100
0e+00
1e−31
2e−31
3e−31
4e−31
5e−31
spread

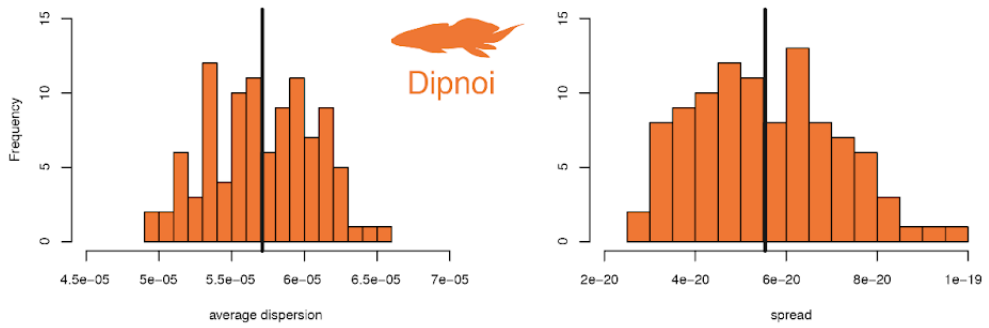
Dipnoi
Frequency
0
5
10
15
4.5e−05
5e−05
5.5e−05
6e−05
6.5e−05
7e−05
average dispersion
0
5
10
15
2e−20
4e−20
6e−20
8e−20
1e−19
spread

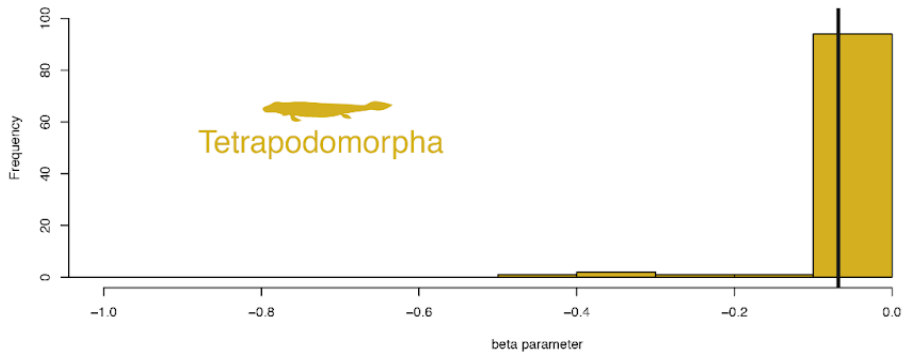
Tetrapodomorpha
Frequency
0
20
40
60
80
100
−1.0
−0.8
−0.6
−0.4
−0.2
0.0
beta parameter

Figure C10. Histograms showing the distribution of parameter estimates for the best fit model per clade across the 100 sampled trees. Plots colored according to each group: porolepiforms, dipnoans, and tetrapodomorphs. Sarcopterygian beta (EB) was negative (b ~ -0.0226; 95% CI: -0.046, 0.011); porolepiform average dispersion and spread (sigma from BM) were low (7.04 x 10^{-12}; 95% CI: 1.11 x 10^{-17}, 1.28 x 10^{-11}) and very low (5.21 x 10^{-20}; 95% CI: 2.87 x 10^{-20}, 8.16 x 10^{-20}), respectively; dipnoan average dispersion and spread (sigma from BM) were high (5.67 x 10^{-5}; 95% CI: : 5.05 x 10^{-5}, 6.34 x 10^{-5}) and low (5.21 x 10^{-20}; 95% CI: 2.87 x 10^{-20}, 8.16 x 10^{-20}), respectively; tetrapodomorph beta was slightly negative (-0.068; 95% CI: -0.2635448, 0) and, in comparison to sarcopterygians as a whole, was closer to or at 0 (i.e., not declining) in over half of all trees. Silhouettes from PhyloPic, *Tiktaalik* silhouette by *Nobu Tamura* (CC BY-SA 3.0).